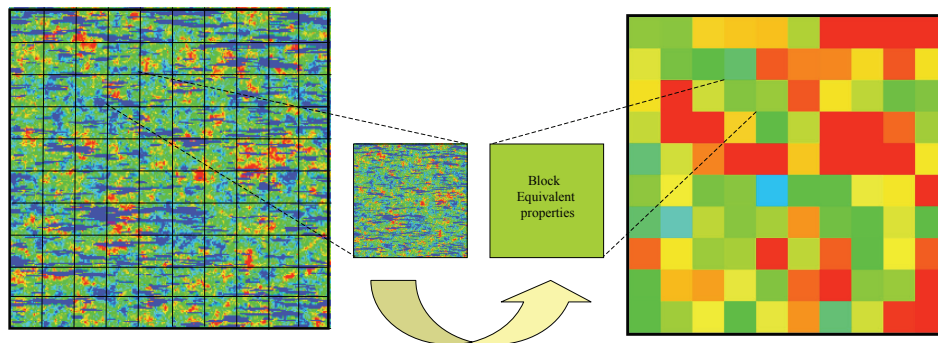


Upscaling non-reactive solute transport



PhD Thesis submitted by
Gerónimo Llerar-Meza

Advisors:
J. Jaime Gómez-Hernández
Daniel Fernàndez-Garcia



UNIVERSIDAD
POLITECNICA
DE VALÈNCIA

grupo de
HIDROGEOLOGIA

Upscaling non-reactive solute transport

PhD Thesis submitted by
Gerónimo Llerar-Meza

Advisors:

J. Jaime Gómez-Hernández
Daniel Fernàndez-Garcia

**Departamento de Ingeniería Hidráulica y Medio
Ambiente
Universidad Politécnica de Valencia
Valencia, Spain**

March 2009

A Liz

Abstract

This thesis focuses on upscaling solute transport. Upscaling of solute transport is usually required to obtain computationally efficient numerical models in many field applications such as, remediation of aquifers, environmental risk to groundwater resources or the design of underground repositories of nuclear waste. The usual observation of non-Fickian transport observed in the field, manifested by peaked concentration profiles with pronounced tailing, has questioned the use of the classical advection-dispersion equation to simulate solute transport at the computational scale of a numerical model. In this context, we have investigated the use of upscaled mass transfer models as a tool for upscaling solute transport in a general numerical modeling framework.

Solute transport by groundwater is very affected by the presence of high and low water velocity zones, where the contaminant can be channelized or stagnant. These contrasting water velocity zones disappear in the upscaled model as soon as the scale discretization is larger than the size of these zones. We propose for modeling solute transport at large scale a phenomenological model based on the concept of memory functions that are used to represent the unresolved process taking place within each homogenized block of the numerical models.

We propose a new method to estimate equivalent block transport and mass transfer parameters. The new upscaling technique consists in replacing each block with heterogeneous transmissivities by a homogeneous block in which the parameters associated to a memory functions are used to represent the unresolved mass exchange between highly mobile and less mobile zones occurring within each block. Upscaling of the transmissivity is based on the *Simple Laplacian with skin*, whereas block transport parameters are estimated through the interpretation of the residence time distribution of particles passing through a given block using fine-scale simulations.

The methodology proposed is applied to a Monte Carlo simulations of solute transport in several two-dimensional synthetic aquifers. The results are compared to a reference Monte Carlo analysis implemented at a smaller scale. Transport phenomena at the computational scale were described by means of a multirate mass transfer model. Several formulations of the multi-rate mass

transfer model, which differ in the type of memory function, were used as constitutive transport equation.

The performance of the upscaled models was evaluated from two different perspectives. First, we analyzed the reproduction of the ensemble mean behavior of the main features associated with the simulated breakthrough curves (BTCs). We examined the effect of upscaling on model uncertainty and the spatial distribution of the solute mass plume. The results showed that an appropriate description of the residence time distribution for all blocks of the numerical model provides an upscaled transport model that is capable to reproduce the ensemble mean behavior of the BTCs. In addition, results showed that the reproduction of uncertainty and dilution of plume was not good enough by any of the upscaled transport models.

Resumen

El objeto de la presente tesis es el estudio del escalado del transporte de solutos no reactivos. El escalado es usualmente aplicado para obtener modelos numéricos de acuífero, que son una herramienta alternativa altamente eficiente, para establecer estrategias en problemas tales como, la remediación de suelos y aguas subterráneas contaminadas, el diseño de almacenamientos de residuos reactivos, o la evaluación del riesgo ambiental para las aguas subterráneas.

El comportamiento anómalo (en la literatura anglosajona *non-Fickian*) observado en los resultados de ensayos de trazadores ejecutados en campo o en laboratorio, tales como los perfiles de concentración con un alto pico y una larga cola, cuestionan el uso de la clásica ecuación de advección-dispersión, para simular el transporte a escala computacional. En este contexto, se presentan las investigaciones en el uso de los modelos escalados de transferencia de masa como una herramienta alternativa para el escalado del transporte, bajo el enfoque de la modelación aplicada.

El desplazamiento de un contaminante en las aguas subterráneas es afectado por la presencia de zonas de altas y de bajas velocidades del flujo, donde el contaminante puede viajar libremente o bien puede ser retenido. Ese contraste de velocidades tiende a desaparecer en los modelos escalados, a medida que la escala de la malla de modelación sea más grande que el tamaño de esas zonas. En dichas circunstancias, para reproducir el comportamiento del transporte observado con un modelo escalado, es necesario considerar un proceso adicional de transferencia de masa entre las zonas más y menos conductivas en la ecuación de advección-dispersión.

Así, se propone como alternativa, un modelo fenomenológico basado en concepto de que el transporte puede ser simulado a gran escala usando a una malla de modelación con bloque homogéneos de gran tamaño, donde los parámetros de transporte asociado consideran alguna memoria vinculada a la heterogeneidad de las propiedades hidrogeológicas, a cuales son sometidas las partículas de contaminante a lo largo de su viaje por el medio.

De este modo, se presenta una metodología para estimar los valores equivalentes de bloque asociados a la ecuación alternativa de transporte. La nueva técnica de escalado consiste en que cada bloque con valores heterogéneos de transmisividad es reemplazado por un bloque homogéneo. A cada uno de esto

bloques se le asigna un valor equivalente de transmisividad y de los coeficientes de transferencia de masa y de dispersión, para representar los mecanismos de transporte que tienen lugar en cada uno a escala fina. Estos valores son asignados en función de los mismos en las celdas que contiene cada bloque. El valor equivalente de la transmisividad se obtiene aplicando la técnica de escalado conocida como *Simple Laplaciano con piel*. Por su parte, los coeficientes de transferencia de masa y de dispersión asociados a una función de memoria, son derivados de la interpretación de la distribución de los tiempos de residencia de las partículas que atraviesan el área delimitada por cada bloque a escala fina.

La metodología propuesta ha sido evaluada mediante simulaciones de Monte Carlo de transporte, aplicada en diversos casos sintéticos de acuíferos bidimensionales, y en cada caso usando diferentes formulaciones de transferencia de masa. Los resultados de los modelos escalados son comparados con una solución de referencia derivada a una escala fina.

El comportamiento de los modelos escalados fue evaluado desde dos perspectivas diferentes: De un lado, se analiza la reproducción del comportamiento medio de las principales características del conjunto de curvas de llegada (BTCs). Además, se determina el efecto que causa el escalado sobre la reproducción de la incertidumbre, así como en la reproducción de la distribución espacial del penacho de contaminante de referencia. Los resultados derivados del análisis estocástico indican, que una apropiada reproducción de la distribución de los tiempos de residencia en cada uno de los bloques del modelo numérico a escala gruesa, asegura que el modelo escalado es capaz de reproducir el comportamiento medio del conjunto de BTCs. Por otro lado, se muestra que los modelos escalados poseen un bajo poder predictivo para reproducir el nivel de incertidumbre y el grado de dilución del penacho de la solución de referencia.

Resum

L'objectiu de la presente tesi és l'estudi de l'escalat del transport de soluts no reactius. L'escalat és usualment aplicat per a obtenir models numèrics d'aqüífer, que són una eina alternativa altament eficient, per establir estratègies en problemes com ara, la remediació de sòls i aigües subterrànies contaminades, el disseny d'emmagatzematges de residus reactius, o l'evaluació del risc ambiental per a les aigües subterrànies.

El comportament anòmal (referit en la literatura anglosaxona com *non-Fickian*) observat en els resultats d'assaigs de traçadors executats en camp o en laboratori, tals com els perfils de concentració amb un alt pic i una llarga cua, qüestionen l'ús de la clàssica equació d'advecció-dispersió, per simular el transport a escala computacional. En aquest context, es presenten les investigacions en l'ús dels models escalats de transferència de massa com una eina alternativa per l'escalat del transport, baix l'enfocament de la modelació aplicada.

El desplaçament d'un contaminant a les aigües subterrànies és afectat per la presència de zones d'altas i de baixes velocitats del flux, on el contaminant pot viatjar lliurement o bé pot ser retingut. Aquest contrast de velocitats tendeix a desaparèixer en els models escalats, a mesura que l'escala de la malla de modelació sigui més gran que la mida d'aquestes zones. En aquestes circumstàncies, per reproduir el comportament del transport observat amb un model escalat, cal considerar un procés addicional de transferència de massa entre les zones més i menys conductives en l'equació d'advecció-dispersió. Es proposa ací com a alternativa, un model fenomenològic basat en el concepte de que el transport pot ser simulat a gran escala utilitzant una malla de modelació amb bloc homogenis de grans dimensions, on els paràmetres de transport associats consideren alguna memòria vinculada a l'heterogeneïtat de les propietats hidrogeològiques, a quals són sotmeses les partícules de contaminant al llarg del seu viatge pel mig.

D'aquesta manera, es presenta una metodologia per estimar els valors equivalents de bloc associats a l'equació alternativa de transport. La nova tècnica d'escalat consisteix en que cada bloc amb valors heterogenis de transmissivitat és reemplaçat per un bloc homogeni. A cadascun dels blocs se li assigna un valor equivalent de transmissivitat i dels coeficients de trans-

ferència de massa i de dispersió, per representar els mecanismes de transport que tenen lloc a cada un a escala fina. Aquests valors són assignats en funció dels mateixos en les cel·les que conté cada bloc. El valor equivalent de la transmissivitat s’obté aplicant la tècnica d’escalat coneguda com *Laplaci ^ simple amb pell*. Per la seva banda, els coeficients de transferència de massa i de dispersió associats a una funció de memòria, són derivats de la interpretació de la distribució dels temps de residència de les partícules que travessen l’àrea delimitada per cada bloc a escala fina.

La metodologia proposada ha sigut avaluada mitjançant simulacions de Monte Carlo de transport, aplicada a diversos casos sintètics d’aqüífers bidimensionals, i en cada cas usant diferents formulacions de transferència de massa. Els resultats dels models escalats són comparats amb una solució de referència derivada a una escala fina.

El comportament dels models escalats va ser valorat des de dues perspectives diferents: D’una banda, s’analitza la reproducció del comportament mitjà de les principals característiques del conjunt de corbes d’arribada (BTCs). A més, es determina l’efecte que causa l’escalat sobre la reproducció de la incertesa, així com en la reproducció de la distribució espacial del plomall de contaminant de referència. Els resultats derivats de l’anàlisi estocàstic indiquen que una apropiada reproducció de la distribució dels temps de residència a cadascun dels blocs del model numèric a escala gruixuda, assegura que el model escalat és capaç de reproduir el comportament mitjà del conjunt de BTCs. D’altra banda, es mostra que els models escalats tenen un baix poder predictiu per reproduir el nivell d’incertesa i el grau de dilució del plomell de la solució de referència.

Contents

Abstract	iii
Resumen	v
Resum	vii
Agradecimientos	ix
1 Introduction	1
1.1 Motivation and Objectives	1
1.2 Thesis structure	2
2 Review of upscaling methodologies	5
2.1 Introduction	5
2.2 Advection Dispersion model (ADE)	6
2.3 Time-Depend Macrodispersive Model (TDM)	9
2.4 Multi-rate mass transfer model (MRMT)	10
2.5 Continuous time random walk (CTRW)	13
2.6 Fractional Advection-Dispersion Transport Models (FADTM) .	14
2.7 Summary and Conclusions	15
3 Upscaling Transport with Mass Transfer Model	21
3.1 Introduction	22
3.2 Transport Models	24
3.2.1 The Local Transport Model	24
3.2.2 The Upscaled Mass Transfer Model	25
3.3 Monte Carlo Transport Simulations	27
3.3.1 Setup	27
3.3.2 Reference Transmissivity Fields	28
3.3.3 Flow and Transport Solution	30
3.4 Estimation of Block Equivalent Properties	31
3.4.1 Methodology	31
3.4.2 Implementation Details	34

3.5	Numerical Results and Discussion	35
3.5.1	Ensemble Average Behavior	36
3.5.2	Propagation of Uncertainty	40
3.6	Summary and Conclusions	48
	Bibliography	51
4	Modeling solute transport at large scale in heterogeneous me-	57
	dias	
4.1	Introduction	58
4.2	Solute transport experiments	61
4.2.1	Experimental Design	61
4.2.2	Reference transmissivity field	62
4.2.3	Flow and transport solution	70
4.2.4	Flow and transport parameters	71
4.3	Results and discussion	72
4.3.1	Overview of plume behavior	72
4.3.2	Longitudinal distribution mass profile	77
4.3.3	Dilution Index	77
4.4	Summary and conclusions	82
5	Conclusions and future research	91
5.1	General Conclusion	91
5.2	Future researches	93
	Appendix	97
A	Calibration of Mass Transfer Parameters	97

List of Figures

2.1	Representation of mass transfer conceptual model.	12
3.1	Illustration of the upscaling process: (a) Map of transmissivities for a given realization superposed with the discretization of the upscaled model (black lines); (b) Map of equivalent transmissivities (T_{xx}^v).	28
3.2	Illustration of the steps involved in the stochastic generation of the composite transmissivity field, $Y(\mathbf{x}) = (1 - I(\mathbf{x}))Y_1(\mathbf{x}) + I(\mathbf{x})Y_2$. Blue and red pixels in the $I(\mathbf{x})$ -map indicates materials M_1 and M_2 , respectively.	29
3.3	Comparison of the cumulative mass flux breakthrough curves obtained at a given x -control plane ($x = 143.3$ units) using one realization of the transmissivity field $Y_1(\mathbf{x})$ and its associated composite medium $Y(\mathbf{x})$	30
3.4	Map of hydraulic heads superposed with particle paths obtained from a transport simulation (only 100 particles) in an individual realization of the composite random field.	32
3.5	Calculation of residence times in a given block of the numerical model.	34
3.6	Evolution of the effective longitudinal dispersivity with travel distance	37
3.7	Evolution with travel distance of the mean sum of square error associated with the calibrated model obtained curve-fitting f_τ with a theoretical model.	37
3.8	Evolution of the ensemble average first arrival of the BTC T_{05} with travel distance.	38
3.9	Evolution of the ensemble average slope $T_{60} - T_{80}$ with travel distance.	39
3.10	Evolution of the ensemble average slope $T_{80} - T_{95}$ with travel distance.	40
3.11	Evolution of the mean concentration peak with travel distance.	41

3.12	Ensemble of breakthrough curves obtained at $x = 34$ units for the different upscaled models contrasted against the reference solution. The 95% confidence interval refer to the ensemble of 50 realizations.	42
3.13	Ensemble of breakthrough curves obtained at $x = 110.8$ units for the different upscaled models contrasted against the reference solution. The 95% confidence interval refer to the ensemble of 50 realizations.	43
3.14	Propagation of uncertainty: Comparison of the reference confidence interval with those obtained using the upscaled models at two different control planes.	44
3.15	Cumulative frequency distribution of the late-time slope of BTCs for the different upscaled models. The late-time slope corresponds to the region of the BTCs comprised between the 60% and 80% of the BTC total mass obtained at $x = 34.9$ units. . .	45
3.16	Cumulative frequency distribution of the late-time slope of BTCs for the different upscaled models. The late-time slope corresponds to the region of the BTCs comprised between the 60% and 80% of the BTC total mass obtained at $x = 110.8$ units. .	46
3.17	Cumulative frequency distribution of the early arrival time (T_{05}) of BTCs for the different upscaled models.	47
3.18	Comparison of the simulated ensemble of BTCs obtained with and without transverse macrodispersivity.	48
4.1	Representation of the steps involved in the stochastic generation of composite transmissivity field.	63
4.2	Illustration of the realization of the reference natural log of transmissivity $G_1(\mathbf{x})$ of M_1 of the first environment	64
4.3	Illustration of the realization of the reference natural log of transmissivity $G_1(\mathbf{x})$ of M_1 of the second environment	65
4.4	Transmissivity structure and histogram for the first composite field.	65
4.5	Experimental variogram and model variogram as inferred from to realization of the first scenario for the x and y directions. . .	66
4.6	Cumulative mass flux breakthrough curves obtained at a given x-control plane ($x = 159.9$ units) using the realization of the transmissivity field $\mathbf{G}_1(\mathbf{x})$ and its associated composite medium $\mathbf{G}(\mathbf{x})$	67
4.7	Transmissivity structure and histogram for the second composite field.	67

LIST OF FIGURES

4.8	Experimental variogram and model variogram as inferred from to realization of the second composite field for the x and y directions.	68
4.9	Cumulative mass flux breakthrough curves obtained at a given x-control plane ($x = 159.9$ units) using the realization of the transmissivity field $G_1(\mathbf{x})$ and its associated second composite medium $G(\mathbf{x})$ for field 2.	68
4.10	Transmissivity structure and histogram for the third composite field.	68
4.11	Cumulative mass flux breakthrough curves obtained at a given x-control plane ($x = 159.9$ units) using the realization of the transmissivity composite field 2 and its associated composite field 3.	69
4.12	Different size of blocks used to change of scale of the reference $G(\mathbf{x})$ field	70
4.13	Plan view of the location of source and a transverse cross section. Cross-section indicate the location used to display temporal evolution of mass profiles at x-distance 75 units from injection point.	71
4.14	Solute log concentration plume simulated for different upscaled models at $t = 300$ using a size of block 5 cells and corresponding the reference solution for the three cases of composite field. (a) case of the first scenario, (b) case of the second scenario and (c) case of the third scenario.	73
4.15	Solute log concentration plume simulated for different upscaled models at $t = 300$ using a size of block 15 cells and corresponding the reference solution for the three cases of composite field. (a) case of the first scenario, (b) case of the second scenario and (c) case of the third scenario	74
4.16	Comparison of the temporal evolution of relative entropy of double rate and macrodispersion models for the three cases test.	76
4.17	Longitudinal mass distribution profiles of the reference solution and predictions using double rate with those associated with macrodispersive models corresponding at time $t = 300$ (left column) and $t = 600$ (right column). Row a), b) and c) corresponding to the 5 x 5 upscaled case 1, case 2 and case 3 of the scenarios of composite field test, respectively. Injection point at $x = 60$ units	78

4.18	Longitudinal mass distribution profiles of the reference solution and predictions using double rate with those associated with macrodispersive models corresponding at time $t = 300$ (left column) and $t = 600$ (right column). Row a), b) and c) corresponding to the 15 x 15 upscaled case 1, case 2 and case 3 of the scenarios of composite field test, respectively. Injection point at $x = 60$ units	79
4.19	Comparison of the temporal evolution of normalized mass at a given location downstream from the injection point $x = 75$ units for double rate with those associated with macrodispersive models versus the reference solution: (a) case of the first scenario, (b) case of the second scenario, and (c) case of the third scenario of composite field test.	80
4.20	Comparison of the temporal evolution of the dilution index . .	81

List of Tables

2.1	Density Functions $f^v(\alpha)$ corresponding Memory Functions $g^v(t)$ (after <i>Haggerty et al.</i> , 2000)	12
3.1	Parameters to be estimated for each constitutive upscaled mass transfer model.	26

1

Introduction

1.1 Motivation and Objectives

Solute transport models can be used to predict the response of an aquifer to planned remediation or for assessing environmental risk groundwater resources. The development of theories and methodologies in the last decades have achieve higher levels of predictive models, allowing a greater use of them. However, the question is how to represent heterogeneity of transport parameters into numerical models.

Hydrogeologic properties in aquifer vary in space, which means the characterization of the spatial variation of the properties are needed to predict the behaviour of flow and solute transport. Geostatistics provides the ability to characterize the spatial variation of the hydrogeologic properties of porous media with a high resolution. Although high resolution are mandatory to adequately describe the underlying physical processes, modeling groundwater flow and solute transport with such resolution is most frequently unfeasible, especially when dealing with geochemical systems. the problems stems from the proper depiction of subgrid heterogeneity in numerical transport models without compromising the computational cost.

Upscaling can be used to incorporate subgrid heterogeneity at the same time that simplifies the system to overcome computational burden. Yet, it is based on a constitutive upscaled transport model which highly controls the final solution.

Solute transport in an aquifer is traditionally simulated using the classical advection-dispersion equation. Unfortunately, the classical advection-dispersion equation has been shown not to be adequate to model solute transport at scales larger than the scale of heterogeneity. For instance, the classical formulation of solute transport significantly underestimates the late-time behavior of breakthrough curves at observation locations. Alternative models have been proposed in the literature for modeling solute transport at the computational scale. Continuous time random walks, fractional derivatives, and multirate mass transfer models constitute the most promising alternatives.

The objectives of this thesis are to review basic concepts of alternatives transport models to simulate solute transport at the computational scale, to present its scope and difference of these approaches, to present a new methodology to performance a upscaling mass transfer process based on the concept of memory function; and to evaluate the use of upscaled mass transfer models as a tool for upscaling solute transport. In this dissertation, upscaling mass transport is restricted to non-reactive solute, that is to say, contaminants that dissolve completely into the groundwater and do not react with any chemical components of aquifer, nor degrade or chemically change over time.

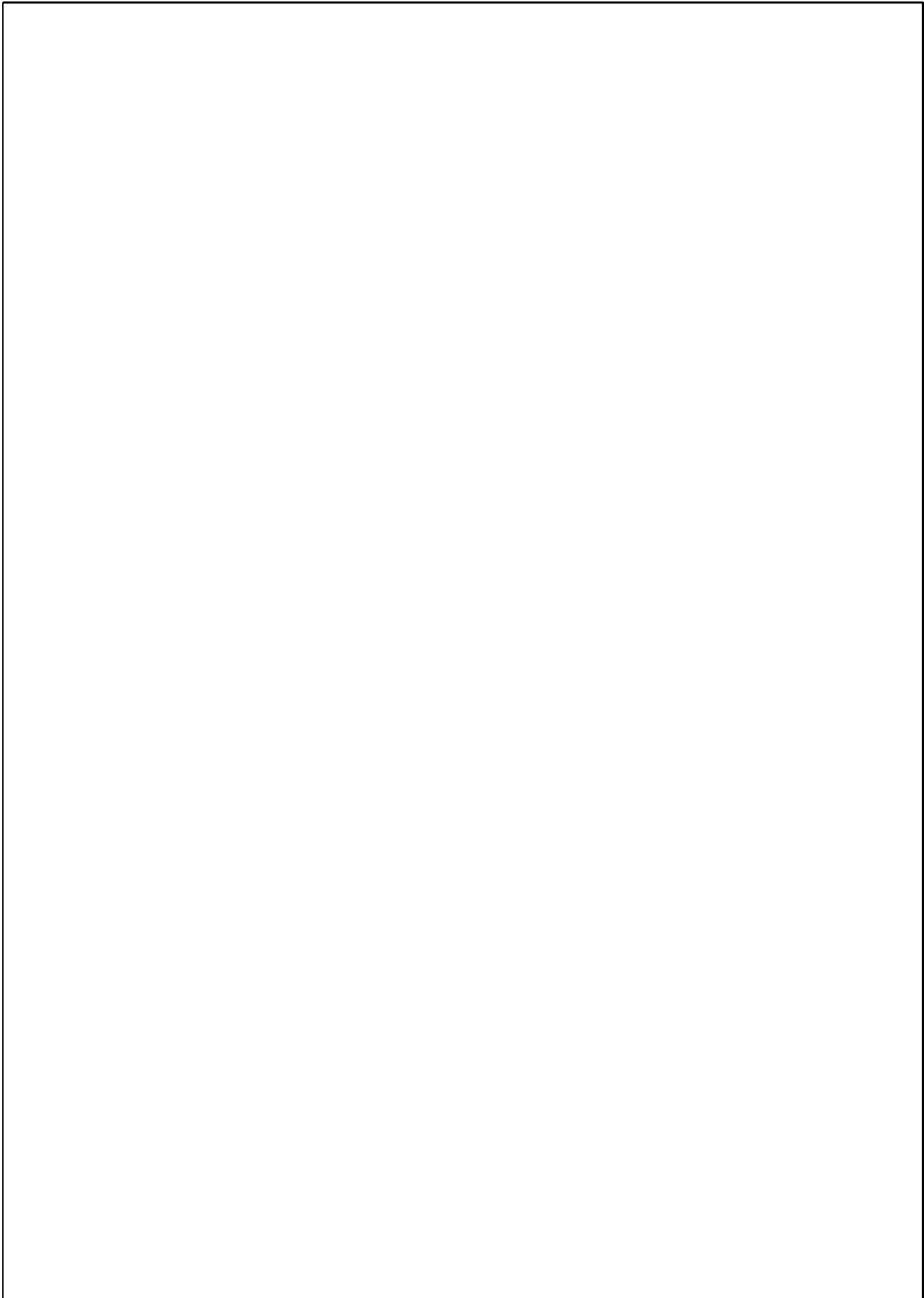
1.2 Thesis structure

This dissertation is organized as follows. The first chapter of this dissertation is the introduction. It is intended to present the issues motivating this research and its organization. Chapter 2 provides an extensive review of alternative models that have been proposed in the literature for modeling solute transport at the computational scale. We focus our attention on alternative models have been proposed in the literature for modeling solute transport at the computational scale. Continuous time random walks, fractional derivatives, and multirate mass transfer models constitute the most promising alternative. We examine the underlying assumptions, scope and differences of these approaches.

Chapter 3 illustrates the use of upscaled mass transfer models as a tool for upscaling solute transport in a general numerical modeling framework. This was achieved by comparing Monte Carlo simulations at different support scales. The performance of upscaled models was evaluated analyzing the reproduction of ensemble mean behaviour of the main features associated with simulated breakthrough curves and propagation of uncertainty. Furthermore, we describe how the upscaling process based on the concept of memory function is performed. Each block with heterogeneous transmissivity, is replaced by a homogeneous block in which the unresolved processes are represented by the parameter values associated with the memory function. The parameter

values are computed blockwise in order to reproduce, within each block, the residence time and spread observed at the small scale.

Chapter 4 presents some transport simulations designed to investigate the ability of upscaled models to reproduce solute transport for different type of heterogeneous fields. We quantify the predictive power of upscaled models analyzing the reproduction of dilution index and relative entropy associated each solute plume. It also evaluates longitudinal mass distribution profiles under different support scale. Finally, in chapter 5 we close with general conclusions from this thesis. We also suggest several potential avenues of future research as well as questions raised during this work that need further investigation.



2

Review of upscaling methodologies

Abstract

The evolution and characterization in the space and time of mass solute plume in aquifers needs the use of tools such as solute transport models. Non-reactive transport of solute through porous media has been simulated using the classical advection dispersion equation (ADE). The anomalous behaviour transport observed in test field, exhibited by asymmetric shape of breakthrough curves, has questioned the use of ADE to simulate transport at a scale high than scale heterogeneity. In this framework have been proposed alternatives transport models to treat solute transport. This chapter presents a review of four approaches that give rise to representations of transport process (advection and dispersion) of nonreactive tracer in heterogeneous porous media.

2.1 Introduction

The quantification of solute transport through aquifers has been focus of research over several decades in hydrogeology. Traditionally, transport solute in aquifers is represent using the ADE framework at computational scale. However, it is well documented in the literature and known from field test that ADE can not reproduce anomalous transport observed. Contaminant transport is very affected by the presence of high and low water velocity zones,

where solute can be channelized or stagnant. For this reason, trying to reproduce the same transport behaviour observed in field requires alternative transport approaches. We focus our attention on four such approaches: Multirate mass transfer (MRMT), Time-Depend Macrodispersive (TMDM), Continuous time random walk (CTRW) and Fractional Advection-Dispersion Transport (FADT). We start present the theoretical framework of ADE.

2.2 Advection Dispersion model (ADE)

The mass conservation equation constitutes the basis for describing the flow and solute transport in the subsurface. It is basically a mass balance equation which expresses that the net mass entering a control volume must be equal to the accumulate mass. For nonreactive solute it is written as,

$$\frac{\partial \rho(\mathbf{x}, t)}{\partial t} = -\nabla \cdot \mathbf{J}(\mathbf{x}, t) + r(\mathbf{x}, t) \quad (2.1)$$

where $\rho(\mathbf{x}, t)$ is the solute mass per unit volume, $\mathbf{J}(\mathbf{x}, t)$ is the total mass flux vector whose magnitude gives the mass per unit time crossing a unit surface perpendicular to the vector direction, and $r(\mathbf{x}, t)$ is a solute mass source/sink term. This equation is written in differential form but it is also valid for any fixed control volume in the system, which is the general context in porous media where most properties area determined over difference support volumes. In this case, defining a volume average operator of an aquifer property π as,

$$\pi^v(\mathbf{x}) = \frac{1}{v} \int_{v(\mathbf{x})} \pi dV$$

being \mathbf{x} the centroid of the control volume, the mass conservation equation can be written as,

$$\phi \frac{\partial C^v(\mathbf{x}, t)}{\partial t} = -\nabla \cdot \mathbf{J}^v(\mathbf{x}, t) + r^v(\mathbf{x}, t) \quad (2.2)$$

where ϕ is the porosity of the medium, and C is the solute concentration. The control volume denotes any given support scale, ranging from scale of measurement to the computational scale.

The mass flux is usually written in relative terms with respect to the advective contribution of mass fluxes, $\mathbf{J}_a^v(\mathbf{x}, t)$, which is defined as $\mathbf{J}_a^v(\mathbf{x}, t) = \mathbf{q}^v(\mathbf{x}, t)C^v(\mathbf{x}, t)$. The residual contribution to mass flux with respect to \mathbf{J}_a^v is denoted as $\mathbf{J}_d^v(\mathbf{x}, t)$ and accounts for dispersive processes, i.e., the effect of velocity fluctuations about some average value,

$$\mathbf{J}_d^v(\mathbf{x}, t) = \mathbf{J}^v(\mathbf{x}, t) - \mathbf{J}_a^v(\mathbf{x}, t) \quad (2.3)$$

At the laboratory scale (the scale of core sample), denoted herein as $v = \ell$, the groundwater flux \mathbf{q}^ℓ is given by Darcy’s law

$$\mathbf{q}^\ell(\mathbf{x}, t) = -\mathbf{K}^\ell(\mathbf{x})\nabla h^\ell(\mathbf{x}, t) \quad (2.4)$$

and the dispersive mass fluxes $\mathbf{J}_d^\ell(\mathbf{x}, t)$ are typically express through the Fickian constitutive theory, which maintains that the dispersive fluxes at a given location are proportional to the gradient of solute concentrations at the location,

$$\mathbf{J}_d^\ell(\mathbf{x}, t) = -\phi\mathbf{D}^\ell(\mathbf{x})\nabla C^\ell(\mathbf{x}, t) \quad (2.5)$$

where \mathbf{D}^ℓ is the local hydrodynamic dispersion tensor, which is typically defined in two or three dimensions by the eigenvalues associated with principal axes parallel and perpendicular to the directional flow through

$$\phi D_i^\ell = \phi D_d \tau + \alpha_i |\mathbf{q}| \quad (2.6)$$

where D_d is the molecular diffusion coefficient (assumed isotropic), τ is the tortuosity, D_i^ℓ are the eigenvalues of D^ℓ , and α_i are the local dispersivity coefficients. Components parallel and transverse to the flow direction are usually denoted as longitudinal and transverse dispersivities, α_L and α_T .

Substituting the definitions of the advective and Fickian Dispersive mass fluxes(2.5) in the mass conservation equations (2.2), it is obtained the classical advection-dispersion equation presumably valid at the laboratory scale,

$$\phi \frac{\partial C^\ell(\mathbf{x}, t)}{\partial t} = -\nabla \cdot (\mathbf{q}^\ell(\mathbf{x}, t)C^\ell(\mathbf{x}, t)) + \nabla \cdot (\phi\mathbf{D}^\ell(\mathbf{x})\nabla C^\ell(\mathbf{x}, t)) + r^\ell(\mathbf{x}, t) \quad (2.7)$$

Most frequently, numerical models that are used to make solute transport predictions utilize the Fickian assumption. Unfortunately, the computational scale typically used in numerical models is significantly larger than the laboratory scale and the Fickian constitutive theory in no longer valid.

Available alternative transport models generalize the Fickian constitutive theory by taking into account that total mass fluxes should in general depend on the past history of mass fluxes in space and time. This has been demonstrated by stochastic theory [Deng *et al.* (1993)] as well as by the volume averaging method [Wood *et al.* (2003)]. This spatialtemporal dependency is sometimes described by a convolution integral,

$$\mathbf{J}_d^v(\mathbf{x}, t) = - \int_0^t \int_{\mathbb{R}^3} \phi \mathbf{M}^v(s, \tau; \mathbf{x}) \nabla C^v(\mathbf{x} - s, t - \tau) ds d\tau \quad (2.8)$$

where $\mathbf{M}^v(s, t; \mathbf{x})$ is the spatial-temporal kernel memory function, which can be seen as a weighting function of the concentration gradients. In this way

the macrodispersive flux depends on the concentration gradients throughout the space-time domain and thereby it exhibits a nonlocal dependence on the concentration gradients [*Cushman and Ginn* (2000)].

In general, the function $\mathbf{M}^v(s, t; \mathbf{x})$ is block specific (conditioned to the \mathbf{x} location of the control volume centroid), not depending only on the underlying heterogeneity but also on the numerical discretization of the domain and the size/shape of the solute plume. Hence, substituting the generalized Fickian equation (2.8) in the mass conservation equation (2.1), the alternative transport model reads.

$$\begin{aligned} \phi \frac{\partial C^v(\mathbf{x}, t)}{\partial t} = & -\nabla \cdot (\mathbf{q}^v(\mathbf{x}, t)C^v(\mathbf{x}, t)) + \\ & + \nabla \cdot \left\{ \int_0^t \int_{\mathbb{R}^3} \phi \mathbf{M}^v(s, \tau; \mathbf{x}) \nabla C^v(\mathbf{x} - s, t - \tau) ds d\tau \right\} + r^v(\mathbf{x}, t) \end{aligned} \quad (2.9)$$

Considering that for large travel distance ($t \rightarrow \infty$) concentration gradients inside the integral are approximately constant at some point, the advection-dispersion equation is recovered with an equivalent dispersion coefficient given by

$$\phi \mathbf{D}^v(\mathbf{x}) = \int_0^t \int_{\mathbb{R}^3} \phi \mathbf{M}^v(s, \tau; \mathbf{x}) ds d\tau \quad (2.10)$$

This expression is sometimes written in relative terms with respect to local Fickian dispersive contribution as,

$$\phi \mathbf{D}^v(\mathbf{x}) = \phi \mathbf{D}^\ell(\mathbf{x}) + \int_0^t \int_{\mathbb{R}^3} \phi \mathbf{M}_m^v(s, \tau; \mathbf{x}) ds d\tau \quad (2.11)$$

where $\phi \mathbf{M}_m^v(s, \tau; \mathbf{x}) = \phi \mathbf{M}(s, \tau; \mathbf{x}) - \phi \mathbf{D}^\ell(\mathbf{x}) \delta(x - s, t - \tau)$. The subscript m refers to the macrodispersive kernel memory function. The first term explains the contribution of dispersive flux at local scale (assumed Fickian), whereas the second term represents an additional dispersive contribution duo to heterogeneity embedded into the fixed volume v . Using small perturbation stochastic theories, *Gelhar and Axness* (1983) obtained the same expression in the probability space. They found that for an infinite domain, large plume, and steady-state uniform flow conditions the memory function should be expressed as

$$\phi \mathbf{M}_m^\infty(s, t) = G_0(s, t) C_{\mathbf{q}\mathbf{q}}(s) \quad (2.12)$$

where $G_0(s, t)$ is the Gaussian homogeneous solution to the advection-dispersion equation and $C_{\mathbf{q}\mathbf{q}}$ is the covariance function of the velocity field. following this

reasoning, modelers that used commercial transport codes based on advection-dispersion equation, normally need to enhance the values of dispersivity coefficients to account for the unresolved heterogeneity not described by the model. In this context, block equivalent dispersion tensor of a numerical transport code, \mathbf{D}^b , can be formally expressed as

$$\phi D_i^b = \phi \tau D_d + (\alpha_i + A_a^b |\mathbf{q}|) \quad (2.13)$$

D_i^b are the eigenvalues of \mathbf{D}^b , and A_i^b is the increase in block dispersivities. Here, we used the notation that $v = b$ when referring to grid-blocks or elements of a numerical transport code. For most model discretizations, the increase in longitudinal dispersivity, A_L^b , is the dominant parameter having values much larger than α_L ; A_L^b ranges from meters to kilometers [e.g. *Gelhar et al. (1992)*] whereas α_L is in order of millimeters [e.g. *Fernàndez-Garcia et al. (2004)*].

Standard macrodispersion models are those that employ enhanced block dispersivity coefficients to compensate for the homogenization on the basis of the aforementioned discussion. However, further research has shown that these conditions hardly occur in reality. General conditions are not Fickian. In this case, the Fickian theory tends to largely underestimates the tail of concentration breakthrough curves even for moderate field heterogeneities and ”well-behaving” multiGaussian random fields [*Fernàndez-Garcia et al. (2007)*].

2.3 Time-Depend Macrodispersive Model (TDM)

Another approach is Time-Depend Macrodispersive Models. This approach is based on the localization of nonlocal Fickian Theory presented in the previous section (equation 2.8). The nonlocal Fickian flux is localized about the plume center of mass. In the case that the memory kernel $\mathbf{M}_m(s, \tau; \mathbf{x})$ dies out as $|s|$ and $|\tau|$ increases, the macrodispersive flux strongly depends on the concentration gradient at the current time and position and one can approximate the macrodispersive flux simply as,

$$\mathbf{J}_d^v(\mathbf{x}, t) \approx -\phi \mathbf{D}^v(\mathbf{x}, t) \nabla C^v(\mathbf{x}, t) \quad (2.14)$$

being,

$$\phi \mathbf{D}^v(\mathbf{x}, t) = \phi \mathbf{D}^\ell(\mathbf{x}) + \int_0^t \int_{\mathbb{R}^3} \phi \mathbf{M}^v(s, \tau; \mathbf{x}) ds d\tau \quad (2.15)$$

Now, using the mass conservation equation with the localized version of the macrodispersive flux (equation 2.14), the solute transport equation is written as,

$$\phi \frac{\partial C^v(\mathbf{x}, t)}{\partial t} = -\nabla \cdot (\mathbf{q}^v(\mathbf{x}, t) C^v(\mathbf{x}, t)) + \nabla \cdot (\phi \mathbf{D}^v(\mathbf{x}, t) \nabla C^v(\mathbf{x}, t)) + r^v(\mathbf{x}, t) \quad (2.16)$$

Note that this equation differs from the classical advection-dispersion equation (2.7) in the tensor of dispersion $\mathbf{D}(\mathbf{x}, t)$ not only depends on the spatial location but it also changes with time. Transport models that follow this approach are referred to as time-dependent macrodispersive models.

Basically, two similar approaches have been suggested to use effective time-dependent macrodispersion tensors derived from stochastic theories for small plumes [*Dagan (1991); Rajaram and Gelhar (1993); Dentz et al. (2000)*]. In this case, the time-dependent macrodispersion tensors in (2.16) correspond to a solute plume with shape equal to the grid-block of the numerical model. Likewise, *Rubin et al. (1999, 2003)* have determined effective time-dependent macrodispersion tensor by removing the frequency spectra of velocity fluctuations in small-perturbation expression of macrodispersion.

Although the theoretical framework in (2.16) is general and not restricted to small perturbations, on practice, there is still not an algorithm to estimate time-dependent dispersion tensor specific to grid-blocks of a numerical model. Moreover, close-form analytical stochastic solutions provide time-dependent dispersion coefficients that vary with time but do not change from one grid-blocks to another.

2.4 Multi-rate mass transfer model (MRMT)

Other equations for modeling the solute transport at computational scales larger than the characteristic length is an advection-dispersion equation (ADE) with an additional source/ sink term, which accounts for exchange between high and low conductivity zones. In other words, the domain is decomposed into a mobile zone with pore spaces filled with mobile water, transport process in this zone include advection, dispersion, and chemical reactions; and an immobile zone with pore spaces filled with stagnant water where advective transport is negligible. Figure 2.1 shows a diagram schematic of conceptual model of mass transfer model. The rate at which solute moves between these two domains is controlled by a mass transfer coefficient α . One defines C_m and C_{im} , the concentrations in mobile and immobile zones respectively. The ADE, as it includes advection and dispersion, is used to describe C_m . The source sink term represents the mass transfer exchange between a mobile zone and a continuous or discrete distribution of immobile zones leading to the non-Fickian solute mass fluxes at the computational scale,

$$\begin{aligned} \theta_m \frac{\partial C_m^v(\mathbf{x}, t)}{\partial t} + \theta_{im} \int_0^\infty f^v(\alpha) \frac{\partial C_{im}^v(\mathbf{x}, t; \alpha)}{\partial t} d\alpha \\ = -\nabla(\mathbf{q}^v(\mathbf{x}, t)C_m^v(\mathbf{x}, t)) + \nabla \cdot (\theta_m \mathbf{D}^v(\mathbf{x}) \nabla C_m^v(\mathbf{x}, t)) + r^v(\mathbf{x}, t) \end{aligned} \quad (2.17)$$

The mass flux between mobile and immobile zones is driven by the concentration difference between zones as,

$$\theta_{im} \frac{\partial C_{im}^v(\mathbf{x}, t; \alpha)}{\partial t} = \alpha(C_m^v(\mathbf{x}, t) - C_{im}^v(\mathbf{x}, t; \alpha)) \quad \forall \alpha \quad (2.18)$$

where α is the mass transfer coefficient, $f^v(\alpha)$ is the density function of mass transfer rates, θ_m and θ_{im} are the volume fractions of the mobile and immobile zones, C_m is the concentration in mobile zones and C_{im} is the concentration immobile zones.

Integrating the mass transfer equation (2.18) and then substituting $C_{im}^v(\mathbf{x}, t; \alpha)$ into (2.17), one obtains a transport equation simply depending on one variable, the mobile concentration,

$$\begin{aligned} \theta_m \frac{\partial C_m^v(\mathbf{x}, t)}{\partial t} + \theta_m \cdot \beta_{tot}^v \int_0^t g^v(\tau) \frac{\partial C_m^v(\mathbf{x}, t - \tau)}{\partial t} d\tau \\ = -\nabla(\mathbf{q}^v(\mathbf{x}, t)C_m^v(\mathbf{x}, t)) + \nabla \cdot (\theta_m \mathbf{D}^v(\mathbf{x}) \nabla C_m^v(\mathbf{x}, t)) + r^v(\mathbf{x}, t) \end{aligned} \quad (2.19)$$

where β_{tot}^v is the total maximum capacity to retain particles in the immobile zones, $g^v(t)$ is known as the (temporal) memory function,

$$g^v(t) = \int_0^\infty \alpha f^v(\alpha) e^{-\alpha t} d\alpha \quad (2.20)$$

The memory function can be interpreted as the particle resident time distribution function in the immobile zone. In other words the memory function represents the mass flux to the immobile zones per unit volume of aquifer, for a unit change in concentration in the mobile zones [(Haggerty *et al.*, 2000); (Carrera *et al.*, 1998)]. The formulation of this term depends on the geometry of immobile zones and on the variability of mass transfer or diffusion rates (Haggerty *et al.*, 2000). Table 2.1 shows the density functions $f^v(\alpha)$ for the models of mass transfer used in this dissertation.

Various researches [e.g. Zinn and Harvey (2003)] have demonstrated that nonreactive solute transport through heterogeneous medium is often better simulated when an advection-dispersive model is used in conjunction with a mass transfer equation. Conceptually, this artificial mass term does not represent local kinetic reactions but it rather accounts for solute mass exchange

between high and low velocity areas occurring at the Darcy-scale within each grid block. Although straightforward relationships between memory functions and physical properties of the aquifer are not established yet, the meaning of the memory function has been seen to strongly depend on heterogeneity. The formulation of the memory function depends on the geometry of immobile zones and on the variability of mass transfer or diffusion rates (*Haggerty et al.*, 2000).

Model	$f^v(\alpha)$	$g^v(t)$
First-order	$\beta_{tot}\delta(\alpha - \alpha_f)$	$\alpha_f\beta_{tot}e^{-\alpha_f t}$
Multirate Series	$f^v(\alpha)$	$\int_0^\infty \alpha f^v(\alpha)e^{-\alpha t} d\alpha$
Power Law Distribution ^a	$\frac{\beta_{tot}(k-2)}{\alpha_{max}^{k-2} - \alpha_{min}^{k-2}} \alpha^{k-3}$	$\int_{\alpha_{min}}^{\alpha_{max}} \alpha f^v(\alpha)e^{-\alpha t} d\alpha$

^a A truncated power law density function with $k > 0, k \neq 2$, and $\alpha_{min} \leq \alpha \leq \alpha_{max}$. α_{max} is the maximum rate coefficient, α_{min} is the minimum rate coefficient, and k is the exponent.

Table 2.1: Density Functions $f^v(\alpha)$ corresponding Memory Functions $g^v(t)$ (after *Haggerty et al.*, 2000)

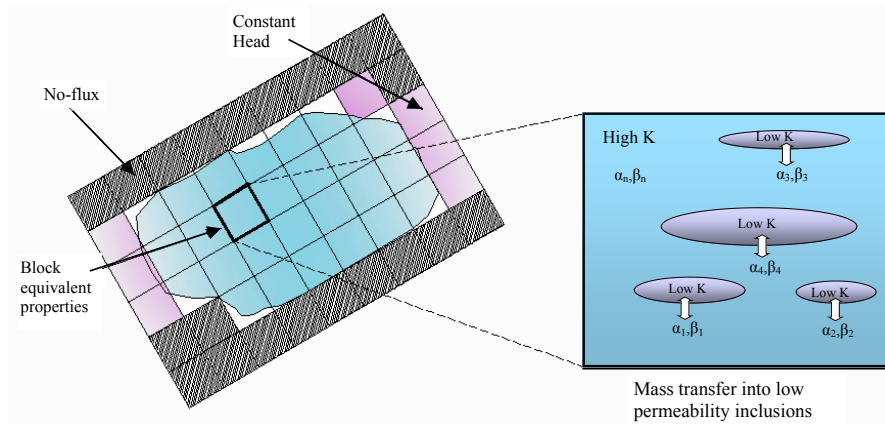


Figure 2.1: Representation of mass transfer conceptual model.

2.5 Continuous time random walk (CTRW)

The continuous time random walk (CTRW) is a generalization of the standard (discrete) random walk. It is based on the idea that not only the length of a particle jump is random (not necessarily following a Gaussian distribution as the standard random walk) but also the particle undergoes a random waiting time between two successive jump. The length of a given jump and the waiting time are drawn from a joint pdf $\psi(\mathbf{x}, t)$, which is known as the jump pdf. From $\psi(\mathbf{x}, t)$, the jump length pdf and the waiting time pdf can be derived as marginal distribution,

$$\lambda(\mathbf{x}) = \int_0^\infty \psi(\mathbf{x}, t) dt \quad (2.21)$$

and

$$\omega(t) = \int_{-\infty}^\infty \psi(\mathbf{x}, t) d\mathbf{x} \quad (2.22)$$

Following *Metzler and Klafter* (2000), different types of CTRW processes can be categorized by the characteristic waiting time and jump length second moment,

$$T = \int_0^\infty t\omega(t) dt \quad (2.23)$$

$$\Sigma_{ij}^2 = \int_{-\infty}^\infty x_i x_j \lambda(\mathbf{x}) d\mathbf{x} \quad (2.24)$$

Anomalous dispersion takes place when either the characteristic waiting time or characteristic jump length are not finite. The continuous time random walk method provides a general framework in the sense that both the fractional-dispersion transport models and mass transfer models haven demonstrated to be particular cases of the CRTW formalism (*Dentz and Berkowitz*, 2003; *Cushman and Ginn*, 2000). Most frequently, for simplicity, the CTRW formalism is simplified by considering the waiting time and jump length mutually independent. In this case, assuming a finite characteristic jump length but undefined characteristic waiting time, the transport equation governing the movement of particles under steady state flow condition is (*Dentz and Berkowitz*, 2003)

$$\phi \frac{\partial C_m^v(\mathbf{x}, t)}{\partial t} = -\nabla \cdot \left[\int_0^t M^v(t) \mathbf{q}^v(\mathbf{x}) C^v(\mathbf{x}, t) - M^t(v) \mathbf{D}^v(\mathbf{x}) \nabla C^v(\mathbf{x}, t) dt \right] + r^v(\mathbf{x}) \quad (2.25)$$

being $M(t)$ the memory function which is typically expressed in the Laplace domain as

$$M(p) = Tp \frac{\psi(p)}{1 - \psi(p)} \quad (2.26)$$

p is the Laplace variable. The memory function serves to capture the non-Fickian transport induce by the heterogeneity not represented by the model.

2.6 Fractional Advection-Dispersion Transport Models (FADTM)

Fractional advection-dispersion transport models have been used in recent years [e.g. *Metzler and Klafter (2000)*; *Schumer et al. (2003)*; *Benson et al. (2000)*] as a way to generalize the advection-dispersion equation with the objective to better describe the power-law scaling behavior in the spread of solute plume observed in the field. Mathematically, fractional dispersion can be viewed as a specific case of continuous time random walk in which the transition displacement distribution of particles $p(\mathbf{s})$ is described by a Lévy distribution. A Lévy distribution is a generalization of the Gaussian distribution. It is defined in the Fourier space as

$$f(\mathbf{k}) = e^{(|\sigma k|)^\alpha} \quad (2.27)$$

where k is the Fourier variable, α is the magnitude of the Lévy flight and α is the Lévy index. For $\alpha < 2$ the variance of the distribution function is undefined, for $\alpha < 1$ the mean of the distribution function is also undefined. For $\alpha = 1$ we recover the standard Gaussian distribution and the inverse of The Fourier Transform has an explicit expression.

The transport equation is defined as

$$\phi \frac{\partial C_m^v(\mathbf{x}, t)}{\partial t} = -\nabla \cdot (\mathbf{q}^v(\mathbf{x}, t) C^v(\mathbf{x}, t)) + \nabla \cdot (\phi \mathbf{D}_{\alpha-1}^v(\mathbf{x}) \nabla^{\alpha-1} C^v(\mathbf{x}, t)) + r^v(\mathbf{x}, t) \quad (2.28)$$

where the term $\mathbf{D}_{\alpha-1}^v(\mathbf{x}) \nabla^{\alpha-1} C^v(\mathbf{x}, t)$ is defined in the Fourier space as

$$\mathfrak{F}[\mathbf{D}_\alpha^v(\mathbf{x}) \nabla^\alpha C^v(\mathbf{x}, t)] = -\mathbf{D}_\alpha^v(\mathbf{x}) |\mathbf{k}|^\alpha C^v(\mathbf{k}, t) \quad (2.29)$$

Note that this expression is a generalization of the Fourier Transform of a derivative for noninteger numbers. In order to emphasize the relationship between this model and the previous discussion, we will use the convenient result that the fractional advection-dispersion equation can be obtained as a

special case of the nonlocal Fickian transport equation (2.8). That is, *Cushman and Ginn* (2000) demonstrated that the fractional advection-dispersion equation is recovered from CTRW when the kernel memory term is given by the following specific form, which in one-dimension reads as,

$$M(s, \tau) = \frac{D_{\alpha-1}^v \delta(\tau) H(s)}{\Gamma(2 - \alpha) s^{\alpha-1}} \quad (2.30)$$

where $D_{\alpha-1}^v$ is constant, $\delta(\tau)$ is the Dirac delta, and $H(s)$ is Heaviside function on $(0, \infty)$. The important point here is to note that the Dirac delta function serves to localize the flux in time, so that the fractional advection dispersion equation only nonlocal in space (*Cushman and Ginn*, 2000). Also, the Heaviside function serves to restrict the nonlocality in space to positive s values, which corresponds to an upstream weighting memory function.

2.7 Summary and Conclusions

A review of recent transport approaches to simulate solute transport using numerical models has been presented. The emphasis of this review has been place on the theoretical framework of each approach. These models provide new ways to quantify contaminant transport. However, transport problem generally require a great detail of heterogeneity than the flow problems. The issues important to represented solute transport is the capture of aquifer heterogeneity.

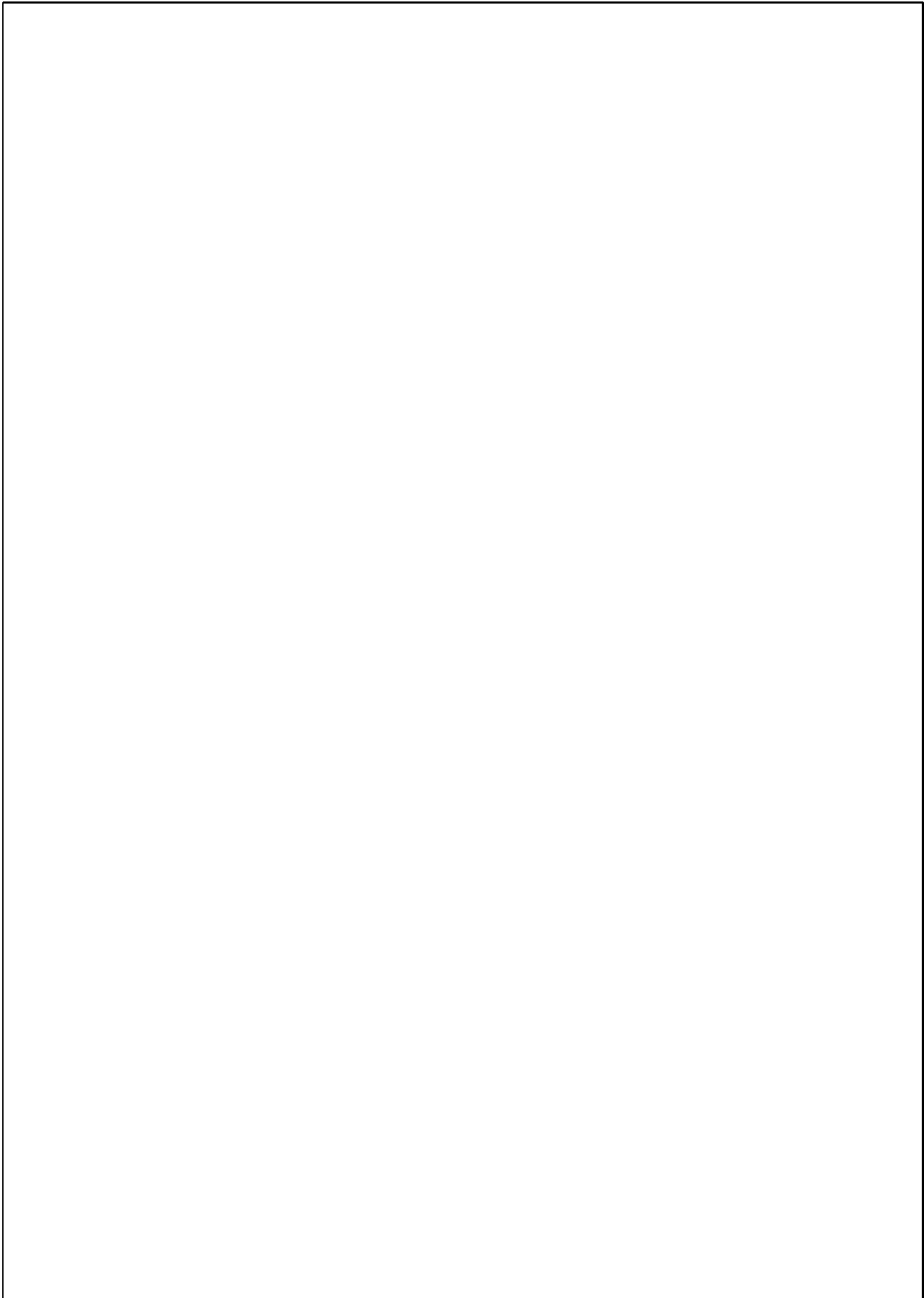
The question of how to assign appropriate transport parameter values to each element or block in the numerical model has been not completely resolved. A way to resolve this issue is to use upscaling. In this context, the next chapters of this dissertation will investigate and propose a methodology to upscale solute transport, since upscaling of transport is usually required to obtain computationally efficient numerical models in many field applications.

Bibliography

- Benson, D. A., S. W. Wheatcraft, and M. M. Meerschaer (2000), The fractional-order governing equation of Lévy motion, *Water Resources Research*, 36(6), 1413–1424.
- Carrera, J., X. Sánchez-Vila, I. Benet, A. Medina, G. Galarza, and J. Guimerà (1998), On matrix diffusion: formulations, solution methods and qualitative effects, *Hydrogeology Journal*, 6, 178–190.
- Cushman, J. H., and T. R. Ginn (2000), Fractional advection-dispersion equation: A classical mass balance with convolution-Fickian flux, *Water Resources Research*, 36(12):3763–3766.
- Dagan, G. (1991), Dispersion of a passive solute in non-ergodic transport by steady velocity fields in heterogeneous formation, *J. Fluid Mech.*, 233, 197–210
- Deng, F. W., J. H. Chusman, and J.W. Delleur (1993), A fast fourier transform stochastic analysis of the contaminant transport problem , *Water Resources Research*, 29(9), 3421–3247.
- Dentz, M., Kinzelbach H., Attringer S., Kinzelbach (2000), Temporal behavior of a solute cloud in a heterogeneous porous medium 1. Point-like injection, *Water Resources Research*, 39(12),3591–3604
- Dentz, M., and B. Berkowitz (2003), Transport behavior of a passive solute in continuous time random walks and multirate mass transfer, *Water Resources Research*, 39(5), 1111, doi:10.1029/2001WR001163.
- Gelhar, L. W., and C. L. Axness (1983), Three-dimensional stochastic analysis of macrodispersion in aquifer, *Water Resources Research*, 19(1), 161–180.
- Gelhar, L. W., C. Welty, and K. Rehfeld (1992), A critical review of data on field-scale dispersion aquifers, *Water Resources Research*, 28(7), 1955–1974.
- Fernàndez-Garcia, D., T. H. Illangasekare, and H. Rajaram (2004), Conservative and sorptive forced-gradient and uniform flow tracer test in a three-

- dimensional laboratory test aquifer, *Water Resources Research*, 40, W10103, doi:10.1029/2004WR003112.
- Fernàndez-Garcia and Gómez-Hernández (2007), Impact of upscaling on solute transport: travel times, scale-dependence of dispersivity and uncertainty, *Water Resources Research*, VOL. 43, W02423, doi:10.1029/2005WR004727, 2007.
- Guswa, A. J., and D. L. Freyberg (2000), Slow advection and diffusion through low permeability inclusions, *Journal of Contaminant Hydrology*, 46, 205–232.
- Haggerty, R., S.A. McKenna, and L. C. Meigs (2000), On the late-time behaviour of tracer test breakthrough curves, *Water Resources Research*, 36(12), 3467–3479.
- Metzler, R. and J. Klafter (2000), The random walk’s guide to anomalous diffusion: A fractional dynamics approach, *Physical reports*, 339, 1–77.
- Neuman, S. P., D. M. Tartakovsky (2008), Perspective on theories of non-Fickian transport in heterogeneous media, *Advances Water Resources*, in press.
- Rajaram, H., and L. W. Gelhar (1993), Plume scale-dependent dispersion in heterogeneous aquifers 2. Eulerian analysis and three-dimensional aquifers, *Water Resources Research*, 29(9), 3261–3276
- Rubin, Y., A. Sun, Maxwell, and A. Bellin (1993), The concept of block effective macrodispersivity and a unified approach for grid-scale- and plume-scale-dependent transport, *J. Fluid Mech.*, 395, 161–180
- Rubin, Y., A. Bellin, and L. E. Lawrence (2003), On the use of block-effective macrodispersion for numerical simulations of transport in heterogeneous formations, *Water Resources Research*, 39(9), 1242, doi:10.1029/2002WR001727.
- Schumer, R., D. A. Benson, M. M. Meerschaert, and B. Baeumer (2003), Fractal mobile/immobile solute transport, *Water Resources Research*, 39(10), 1–12, doi:10.1029/2003WRR002141.
- Wood, B. D., F. Cherblan, M. Quintard, and S. Whitaker (2003), Volume averaging for determining the effective dispersion tensor: Closure using periodic unit cells and comparison with ensemble averaging, *Water Resources Research*, 39(8), 1210, doi:10.1029/2002WR001729.

Zinn, B., and C. F. Harvey (2003), When good statistical models of aquifer heterogeneity go bad: A comparison of flow, dispersion, and mass transfer in connected and multivariate Gaussian hydraulic conductivity fields, *Water Resources Research*, 39(3), 1051, doi:10.1029/2001WR0



3

Upscaling Transport with Mass Transfer Model

Abstract

The ambiguity associated with the choice of an adequate conceptual transport model constitutes a major challenge associated with the upscaling of solute transport. Among the different alternatives to the classical advection-dispersion model, the (multirate) mass transfer model has been proposed as a valuable and convenient alternative to model the large-scale behavior of solute transport. Here, we evaluate the use of mass transfer models as a constitutive equation for upscaling solute transport. To achieve this, we compare Monte Carlo simulations of solute transport at two different support scales. Transport simulations performed at the smallest scale represent a set of reference transport solutions, which are contrasted against transport simulations obtained using an upscaled model. Several formulations of the multi-rate mass transfer model, which differ in the type of memory function, are used as a constitutive transport equation. The large scale scenario represents an operational model obtained by partially homogenizing the reference solution. Results show that, albeit the double-rate and the truncated power-law mass transfer models were capable to properly describe the ensemble average behavior of the main features associated with the integrated breakthrough curves, the uncertainty associated with the upscaled mass transfer models was still substantially smaller than that attributed to the reference solution. Importantly, the corresponding cumulative distribution function of concentrations (CDF) associated with the

upscaled model follows a distribution similar to the reference solution but with smaller dispersion. The reason is that while appropriate memory functions can be used to preserve the residence time distribution of mass particles during upscaling, the lack of memory in space prevents the model from reproducing mass fluxes in all directions. Specifically, the reproduction of mass fluxes taking place at the interface between two homogenized blocks of the upscaled model are not satisfied, thus providing a poor description of the spatial distribution of mass particles.

3.1 Introduction

Albeit different approaches can be used to generate high-resolution maps of aquifer attributes by means of geostatistics or related tools, still, in practice, due to computational efficiencies, some sort of upscaling (i.e., transfer of small-scale information into a larger support volume) is usually necessary to construct a numerical transport model. In subsurface hydrology, the large spatial variability observed in aquifer attributes, being the hydraulic conductivity an attribute that varies several orders of magnitude within an aquifer, largely influences solute transport predictions and drastically complicates the upscaling of solute transport.

Among the effects of heterogeneity, the usual observation of anomalous (non-Fickian) transport, manifested in the field by peaked concentration profiles having long back-tails, has questioned the use of the classical advection-dispersion equation (ADE) to model transport phenomena at the usual computational scale of a numerical model (*Mackay et al.*, 1986; *Adams and Gelhar*, 1992; *Riva et al.*, 2008; *Gouze et al.*, 2008; *Haggerty et al.*, 2000). These field observations are supported by laboratory experiments (*Levy and Berkowitz*, 2003; *Fernández-García et al.*, 2005c), numerical simulations of solute transport in heterogeneous media (*Zinn and Harvey*, 2003; *Feehley et al.*, 2000; *Fernández-García et al.*, 2005a, 2007; *Salamon et al.*, 2007), and fundamental statistical theory.

By modeling hydraulic conductivity (defined at a small support scale) as a correlated random space function, stochastic theories have succeeded in demonstrating that mean mass fluxes at the \mathbf{x} location and time t should not in general be exclusively dependent on the mean concentration gradients at that location and time, as it is expressed by Fick’s law. Instead, dispersive mass fluxes should depend on the past values of the mean concentration gradients over the entire space-time domain (*Hu et al.*, 1995; *Morales-Casique et al.*, 2006), thus rendering memory to the transport equation.

In response to this lack of Fickianity, several alternative transport models have been proposed in the literature to properly describe transport phenomena

at a large support scale. Promising alternatives contemplate continuous time random walks (CTRW) (*Berkowitz and Scher, 1998*), fractional derivatives (*Benson et al., 2000*), and multirate mass transfer models (MRMT) (*Haggerty and Gorelick, 1995; Carrera et al., 1998*) among others. Comprehensive reviews of the theories of anomalous transport in heterogeneous media are provided by *Berkowitz et al. (2006)* and *Neuman and Tartakovsky (2008)*. Interestingly, the CTRW formalism supposes a more general framework, but simplifies to the MRMT model in its most common adopted form (*Dentz and Berkowitz, 2003*). Still, the MRMT model has the advantage that its formulation and physical interpretation is well-known by practitioners, and many numerical transport codes based on the MRMT model are already available for field applications (*Zheng and Wang, 1999; Carrera et al., 1998; Salamon et al., 2006; Willmann et al., 2008*). Alternatively, the stochastic ADE equation, defined over a small support volume, can be used to directly provide the conditional low-order moments (mean and covariance) of concentrations and solute fluxes (*Morales-Casique et al., 2006*). Interestingly, upon considering no statistical interdependence of the velocity field, the mean transport equation reduces to the CTRW model (*Neuman and Tartakovsky, 2008*).

Here, we focus on the use of MRMT models as a constitutive equation for upscaling solute transport. Various researches (e.g., *Guswa and Freyberg, 2002; Carrera et al., 1998; Harvey and Gorelick, 2000; Zinn and Harvey, 2003; Liu et al., 2004; Riva et al., 2008; Willmann et al., 2008*) have shown that large-scale non-reactive solute transport phenomena observed in a heterogeneous medium is often better represented when a mass transfer equation is coupled with the ADE.

Conceptually, this artificial mass transfer equation does not represent local kinetic reactions or diffusive mass transfer processes but it rather accounts for subgrid heterogeneity (*Zinn and Harvey, 2003; Willmann et al., 2008*). In this context, we compare Monte Carlo simulations of solute transport obtained at two different support scales with the aim to evaluate the adequacy of MRMT models as a tool for upscaling. Transport simulations performed at the smallest scale represent a set of reference solutions defined on the basis of a local ADE. At the large scale, several formulations of the MRMT model are evaluated as potential constitutive transport equations.

The upscaled model scenario represents an operational or a functional model obtained by partially "homogenizing" the reference geological system (defined over a fine-scale) so that it ultimately consists of various homogeneous regions. We emphasize the word "partial homogenization" to be in contrast with most previous analysis of upscaling of solute transport (e.g., *Harvey and Gorelick, 2000; Zinn and Harvey, 2003; Willmann et al., 2008*) in which the system is completely homogenized. The distinctive aim of this work is that: (1) we look at the process of transferring subgrid information to finite blocks

or homogeneous regions of a numerical model by means of MRMT models; (2) we seek for a more comprehensive understanding of the interplay between the (homogenized) regions of an upscaled transport model; and (3) we evaluate how uncertainty is affected by the change of the support scale when the MRMT model is selected for upscaling.

3.2 Transport Models

3.2.1 The Local Transport Model

At the local scale, denoted herein as ω , we considered solute transport to be governed by the advective-dispersion equation (ADE). Neglecting the changes in porosity with time and disregarding the source/sink term, this is written as

$$\theta^\omega \frac{\partial c^\omega}{\partial t} = -\nabla \cdot (\mathbf{q}^\omega c^\omega - \theta^\omega \mathbf{D}^\omega \nabla c^\omega), \quad (3.1)$$

where the first term in the divergence operator is the advective mass flux and the second term accounts for dispersive fluxes. c^ω is the volume average concentration of solute in ω , and \mathbf{q}^ω is the Darcy flux. This equation is based on the mass conservation principle and assumes that the dispersive mass fluxes can be described by Fick’s law at some small scale ω , i.e., mass fluxes at point \mathbf{x} and time t are proportional to concentration gradients at point \mathbf{x} and time t ,

$$\mathbf{J}_d^\omega(\mathbf{x}, t) = -\theta^\omega \mathbf{D}_d^\omega \nabla c^\omega(\mathbf{x}, t). \quad (3.2)$$

This assumption has been challenged by several authors. In general, in the absence of dead-end-pores, Fick’s law can be argued to be valid for sufficiently small support volumes (*Neuman and Tartakovsky, 2008*). In any case, from a practical point of view, our analysis is based on the fact that the non-Fickian transport behavior observed at the Lauswiesen site (*Riva et al., 2008*) and at the MADE site (*Salamon et al., 2007*) has been adequately modeled using an ADE (defined over a small support volume) in conjunction with a high-resolution description of heterogeneity. This is precisely the situation we consider here.

The local dispersion tensor, \mathbf{D}_d^ω , is the sum of the effective molecular diffusion tensor, \mathbf{D}_{diff}^ω , and the mechanical dispersion tensor, \mathbf{D}_{disp}^ω . The latter accounts for residual fluxes at the local scale ω , and is typically defined with eigenvectors oriented parallel and perpendicular to the direction of flow, and eigenvalues defined as

$$D_{disp,i}^\omega = \alpha_i \frac{|\mathbf{q}^\omega|}{\theta^\omega}, \quad (3.3)$$

where α_i are the local dispersivity coefficients. The α_i components parallel and transverse to the flow direction are usually denoted as longitudinal and transverse dispersivities, α_L and α_T .

3.2.2 The Upscaled Mass Transfer Model

At the computational scale, denoted here as v ($v \gg \omega$), transport phenomena is represented by means of the MRMT model (*Haggerty and Gorelick, 1995; Carrera et al., 1998; Haggerty et al., 2000*). The MRMT model allows to represent a large variety of mass transfer processes taking place simultaneously over a wide range of scales, i.e., processes ranging from pore diffusion at the grain scale to matrix diffusion into fractured rocks can be simultaneously represented. This model considers an overlapped continuum media formed by a mobile domain, where advection-dispersion takes place, and many immobile domains, where mass can be transferred to and temporarily be trapped.

Here, the MRMT model is not used in strict sense to represent a variety of diffusive processes. Instead, the mobile and immobile zones are viewed as to represent areas of relatively fast and relatively slow solute movement (inside v). Similar representations of a heterogeneous media have been considered by *Zinn and Harvey (2003)* and *Willmann et al. (2008)*. Formally, the MRMT equation is essentially an ADE with a source/sink term,

$$\theta^v \frac{\partial c^v}{\partial t} = -\nabla \cdot (\mathbf{q}^v c^v - \theta^v \mathbf{D}_d^v \nabla c^v) + \theta^v \Gamma^v(\mathbf{x}, t), \quad (3.4)$$

where

$$D_{d,i}^v = D_{diff,i}^\omega + (\alpha_i + A_i) \frac{|\mathbf{q}^v|}{\theta^v} \quad (3.5)$$

$$\Gamma^v(\mathbf{x}, t) = \beta(\mathbf{x}) \int_0^t g(\mathbf{x}, \tau) \frac{\partial c^v}{\partial t}(\mathbf{x}, t - \tau) d\tau \quad (3.6)$$

The additional dispersive contribution term in (3.5), A_i , accounts for processes that can actually be represented with a Fickian model, whereas processes associated with anomalous transport are represented through the memory function $g(\mathbf{x}, \tau)$.

As time evolves, the memory function emphasizes the different past values of the concentration derivatives with time, thus rendering memory to solute transport. The coefficient $\beta(\mathbf{x})$ defines the magnitude of memory effects and is known as the capacity coefficient.

Several forms of the MRMT model are found in the literature (e.g., *Carrera et al., 1998; Haggerty et al., 2000*). Among them, the single-rate model, the gamma model, the log-normal model, the power-law model, and the diffusion

model (with spherical, layered and cylindrical geometries) are the most commonly used. Each one of these conceptual models have been successfully employed to model field and laboratory experiments. Remarkably, the single-rate mass transfer model was successfully utilized to reproduce the tracer experiment at the Macrodispersion Experiment (MADE) site using either (partially homogenized) numerical models (*Fehley et al.*, 2000) or (completely homogenized) analytical solutions (*Harvey and Gorelick*, 2000). Importantly, the quantities associated with these mass transfer models at the MADE site were shown to be mostly related to Darcy-scale heterogeneity (*Salamon et al.*, 2007).

Here, we selected three potential upscaled constitutive equations based on a different form of the memory function: the single-rate model, a discrete multirate model with two immobile domains (double-rate), and the truncated power-law memory function. The mathematical expression of the memory function $g(\mathbf{x}, t)$ can be generally written as

$$g(\mathbf{x}, t) = \int_0^\infty \alpha f(\mathbf{x}, \alpha) e^{-\alpha t} d\alpha \quad (3.7)$$

where $f(\mathbf{x}, \alpha)$ is a function that can be physically interpreted as the probability distribution function of mass transfer rates associated with distinct domains of the overlapped continuum. Detail description of the three selected upscaled mass transfer models are provided in Table 3.1. We note that because our upscaled model considers a domain formed by various homogeneous regions, the mass transfer parameters in (3.6) depend also on the space location accordingly.

Table 3.1: Parameters to be estimated for each constitutive upscaled mass transfer model.

Model	Memory function	Parameters
First-order Mass Transfer	$\alpha_1 e^{-\alpha_1 t}$	$\beta, \alpha_1, v_m, A_L$
Double rate Mass Transfer ^a	$\alpha_1 \frac{\beta_1}{\beta} e^{-\alpha_1 t} + \alpha_2 \frac{\beta_2}{\beta} e^{-\alpha_2 t}$	$\beta_{j=1,2}, \alpha_{j=1,2}, v_m, A_L$
Power Law Mass Transfer ^b	$\sim t^{1-k}$	$\beta, \alpha_{max}, \alpha_{min}, k, v_m, A_L$

^a $\beta = \beta_1 + \beta_2$

^b The power law model is only defined over the interval $\alpha_{min} \leq \alpha \leq \alpha_{max}$

In a randomly heterogeneous aquifer, stochastic theories predict that the mean dispersive flux should in general depend on the past mean concentration gradients throughout the entire space-time domain (*Neuman*, 1993; *Morales-Casique et al.*, 2006; *Neuman and Tartakovsky*, 2008). In a similar manner, the memory function in the MRMT model operates as a weighting function that penalizes past concentration derivatives in time (but not in space). In

this context, the MRMT model should be seen as a model with a space-localized memory kernel. This is in contrast with the time-localized memory kernel associated with the fractional advection-dispersion model (*Cushman and Ginn, 2000*). In anyway, we note that the intend here is not to question the validity of the theoretical premises underlying the upscaled MRMT model but to directly assess the applicability of a well established model.

3.3 Monte Carlo Transport Simulations

3.3.1 Setup

We consider a confined two-dimensional aquifer whose domain consists in a square area of 240×240 units. Flow is driven by a mean hydraulic gradient oriented parallel to the x -direction ($J_x = 0.01$, $J_y = 0$) under steady-state flow conditions. Boundary conditions were no-flux for boundaries parallel to the mean flow and constant-head otherwise. Thus, groundwater flow is moving from left to right.

Aquifer heterogeneity is represented by considering the natural log of transmissivity, $Y(\mathbf{x})$, as a spatially varying attribute. All other properties are assumed spatially constant. A total of 50 different transport solutions were obtained by generating multiple equally likely realizations of $Y(\mathbf{x})$. $Y(\mathbf{x})$ is assumed isotropic at the small support scale and is represented by uniformly discretizing the entire domain into 240×240 square pixels of 1 unit size.

Each upscaled mas transfer model was obtained by transferring the fine-scale pixel information into a numerical model formed by 10×10 regular homogeneous blocks. Thus, the size of each block was of 24×24 units. Figure 3.1 shows an individual reference transmissivity field, $Y(\mathbf{x})$, contrasted against the corresponding depiction of the transmissivity field in the upscaled model.

To simplified the problem, at the local scale, transport is assumed purely advective so that $\mathbf{D}_d^\omega = 0$. The transport problem setup considers a solute plume initially distributed over a long transverse line located upgradient and having a constant concentration. This line was centered in the transverse dimension of the domain and takes up 140 units. To avoid boundary effects, the plume source was separated 21 units from the upgradient head boundary and 50 units from the impermeable boundaries.

Transport simulations were designed to efficiently calculate the global mass flux breakthrough curves observed at 14 x -control planes equally distributed within the entire domain. The simulated breakthrough curves constituted the reference transport solution used to subsequently analyze the performance of upscaling by the different upscaled models.

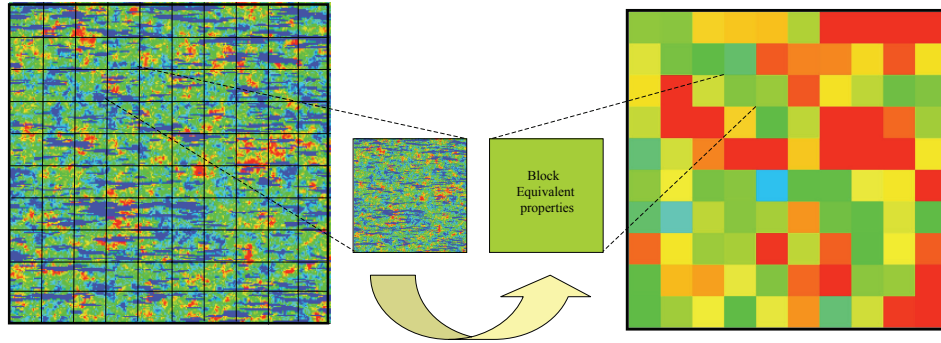


Figure 3.1: Illustration of the upscaling process: (a) Map of transmissivities for a given realization superposed with the discretization of the upscaled model (black lines); (b) Map of equivalent transmissivities (T_{xx}^v).

3.3.2 Reference Transmissivity Fields

The reference transmissivity fields were conceptualized as an stochastic bimodal composite medium. The objective here was to test the upscaled models in a complex geological system formed by highly conductive conduits embedded in an otherwise well behaving Gaussian heterogeneous medium. Thus, we assumed that the aquifer is composed of two coexisting materials or facies (M_1 and M_2), each represented by a different random function model of the spatial distribution of the natural log of transmissivity, $Y_1(\mathbf{x})$ and $Y_2(\mathbf{x})$,

$$Y(\mathbf{x}) = (1 - I(\mathbf{x}))Y_1(\mathbf{x}) + I(\mathbf{x})Y_2(\mathbf{x}) \quad (3.8)$$

where $I(\mathbf{x})$ is an indicator spatial random variable,

$$I(\mathbf{x}) = \begin{cases} 1 & \mathbf{x} \in M_2 \\ 0 & \text{otherwise} \end{cases} \quad (3.9)$$

The natural log of transmissivity $Y_1(\mathbf{x})$ of the first material, M_1 , follows a multiGaussian random function with a geometric mean of $T_g=1$ and an anisotropic exponential covariance function,

$$C_{Y_1}(|\mathbf{r}|) = \sigma_{Y_1}^2 \exp \left(-\sqrt{\left(\frac{r_x}{\lambda_x^{Y_1}}\right)^2 + \left(\frac{r_y}{\lambda_y^{Y_1}}\right)^2} \right) \quad (3.10)$$

where $\mathbf{r} = (r_x, r_y)$ is the separation vector between two points of the aquifer, $\sigma_{Y_1}^2$ is the variance of $Y_1(\mathbf{x}) = \ln T_1(\mathbf{x})$ assumed as 9, and $\lambda_x^{Y_1}$ and $\lambda_y^{Y_1}$ are the longitudinal and transverse correlation scales set to 40 and 4 units, respectively. The second material, M_2 , represents a family of highly conductive

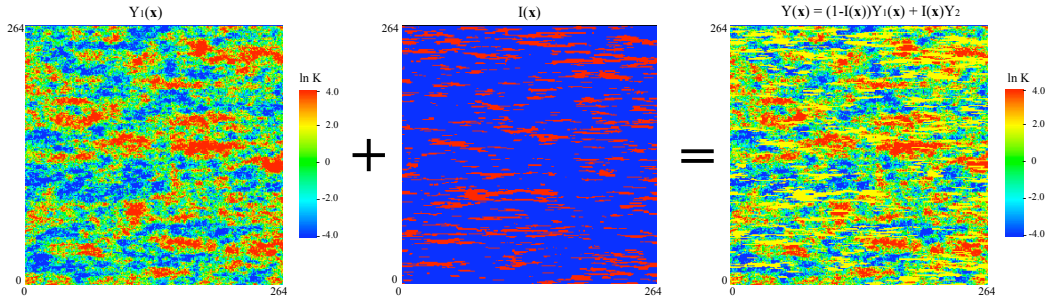


Figure 3.2: Illustration of the steps involved in the stochastic generation of the composite transmissivity field, $Y(\mathbf{x}) = (1 - I(\mathbf{x}))Y_1(\mathbf{x}) + I(\mathbf{x})Y_2$. Blue and red pixels in the $I(\mathbf{x})$ -map indicates materials M_1 and M_2 , respectively.

conduits. We considered that the variation of $Y_2(\mathbf{x})$ is of minor importance compared with $Y_1(\mathbf{x})$, and we therefore assigned a deterministic constant transmissivity value to $Y_2(\mathbf{x})$, i.e., $Y_2(\mathbf{x}) = Y_2 = 2.0$. Figure 3.2 illustrates the steps involved in the stochastic generation of the composite random field for a given realization of $Y(\mathbf{x})$.

In a bimodal media, the volumetric proportion of material M_2 , denoted as p_2 , defines the mean and variance of the indicator random variable, respectively written as $\langle I(\mathbf{x}) \rangle = p_2$ and $\sigma_I^2 = p_2 p_1$, where p_1 is the volumetric proportion of M_1 ($p_1 = 1 - p_2$). We consider that the family of highly conductive conduits (material M_2) occupies 20% of the domain, i.e., $p_2 = 0.2$ and $p_1 = 0.8$. This choice allowed us to obtain transmissivity fields leading to breakthrough curves with long back-tailing during transport simulations. Figure 3.3 compares the cumulative mass flux breakthrough curves obtained at a given x -control plane using one realization of $Y_1(\mathbf{x})$ and its associated composite medium, $Y(\mathbf{x})$. Note that the slope of the late-time behavior observed for $Y_1(\mathbf{x})$ is substantially more elongated than that observed for $Y(\mathbf{x})$. The indicator variable was further characterized with an anisotropic covariance function,

$$C_I(|\mathbf{r}|) = \sigma_I^2 \exp \left(-\sqrt{\left(\frac{r_x}{\lambda_x^I}\right)^2 + \left(\frac{r_y}{\lambda_y^I}\right)^2} \right) \quad (3.11)$$

where λ_x^I and λ_y^I are the longitudinal and transverse correlation scales of the indicator variable set to 16 units and 1 unit, respectively. Following (*Rubin and Journel*, 1991; *Rubin*, 1995), we assumed that the spatial distribution of $Y_1(\mathbf{x})$ and $I(\mathbf{x})$ are mutually uncorrelated. Based on this and according to *Rubin* (1995) and *Lu and Zhang* (2002), the resulting composite random field, $Y(\mathbf{x})$, displays a theoretical mean, variance and covariance function given by,

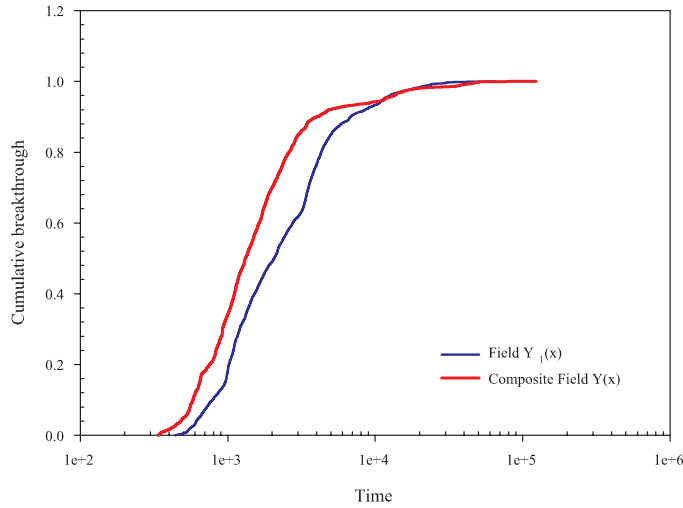


Figure 3.3: Comparison of the cumulative mass flux breakthrough curves obtained at a given x -control plane ($x = 143.3$ units) using one realization of the transmissivity field $Y_1(\mathbf{x})$ and its associated composite medium $Y(\mathbf{x})$.

$$\langle Y(\mathbf{x}) \rangle = p_1 \langle Y_1 \rangle + p_2 Y_2 \quad (3.12)$$

$$C_Y(|\mathbf{r}|) = [C_I(|\mathbf{r}|) + p_1^2] C_{Y_1}(|\mathbf{r}|) + (\langle Y_1 \rangle - Y_2)^2 C_I(|\mathbf{r}|) \quad (3.13)$$

$$\sigma_Y^2 = [p_1 p_2 + p_1^2] \sigma_{Y_1}^2 + (\langle Y_1 \rangle - Y_2)^2 p_1 p_2 \quad (3.14)$$

Thus, the statistical properties of the final composite media are $\langle Y(\mathbf{x}) \rangle = 0.4$ and $\sigma_Y^2 = 7.84$, having integral scales in the x and y directions of $\lambda_x^Y = 32.8$ units and $\lambda_y^Y = 3.2$ units. Because $Y_1(\mathbf{x})$ and $I(\mathbf{x})$ are not correlated, the stochastic generation of $Y_1(\mathbf{x})$ and $I(\mathbf{x})$ was performed independently. Thus, for each realization of $Y(\mathbf{x})$, we separately generated $I(\mathbf{x})$ using an indicator sequential simulation program, ISIM3D (*Gómez-Hernández and Srivastava, 1990*), and $Y_1(\mathbf{x})$ using a sequential gaussian simulation program, GCOSIM3D (*Gómez-Hernández and Journel, 1993*). The composite media is finally obtained from $Y(\mathbf{x}) = (1 - I(\mathbf{x}))Y_1(\mathbf{x}) + I(\mathbf{x})Y_2$.

3.3.3 Flow and Transport Solution

A finite difference ground-water flow model, MODFLOW2000 (*Harbaugh et al., 2000*), was used to solve the flow problem at both scales. The discretization

of the numerical grid was given by the discretization of the spatial distribution of transmissivities. The model calculates the flow rates at grid interfaces. These velocity fields were then used in a transport code based on the Random Walk Particle Method, RW3D (*Fernández-García et al.*, 2005a,b), to simulate either conservative solute transport needed to obtain fine-scale transport solutions or solute transport coupled with multirate mass transfer to obtain the corresponding upscaled model solutions (coarse-scale).

The particle tracking methodology presented by *Salamon et al.* (2006) was employed to simulate multirate mass transfer processes. Essentially, transport is simulated by injecting a large number of mass particles into the system; each particle representing a small portion of the solute plume. Advection is simulated by moving particles along flowlines, whereas dispersion is emulated by a Brownian motion. Mass-transfer processes are efficiently incorporated by switching the state of the particle between mobile/immobile states according to appropriate transition probabilities.

Transport simulations start by injecting a large number of particles (10,000) equidistantly distributed in a line transverse to the mean flow direction with size 140 units. For each movement, the time step was adapted based on a grid Courant number of 0.01 (*Wen and Gómez-Hernández*, 1996). A unit mass was assigned to each particle. The first arrival time and the position of particles passing through 14 control planes transverse to the mean flow direction and located at several distances away from the source were tracked until particles exited the last control plane. Figure 3.4 shows the map of hydraulic heads superposed with the pathlines of particles obtained in an individual realization of $Y(\mathbf{x})$. Only the movement of 100 particles are depicted so that the figure can be easily understood.

3.4 Estimation of Block Equivalent Properties

3.4.1 Methodology

In the upscaled model, flow is still driven by Darcy’s law but we use an equivalent anisotropic transmissivity tensor, \mathbf{T}^v , to represent the heterogeneous medium inside v . For each block, \mathbf{T}^v , was calculated based on the simple Laplacian method with skin (*Gómez-Hernández*, 1991; *Wen and Gómez-Hernández*, 1996) as

$$T_{ii}^v = \frac{\int_v q_i^\omega(\mathbf{u})d\mathbf{u}}{-\int_v \partial h^\omega / \partial x_i(\mathbf{u})d\mathbf{u}}. \quad (3.15)$$

This methodology yields flow fluxes in the upscaled model, $\mathbf{q}^v(\mathbf{x})$, that represent block spatial average quantities,

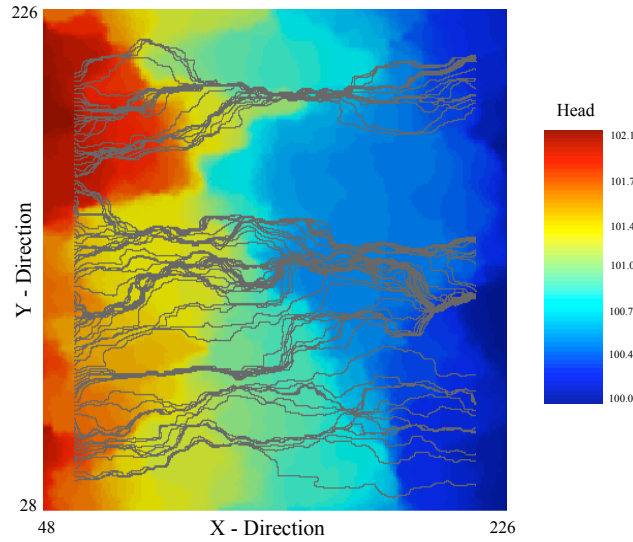


Figure 3.4: Map of hydraulic heads superposed with particle paths obtained from a transport simulation (only 100 particles) in an individual realization of the composite random field.

$$\mathbf{q}^v = \frac{1}{v} \int_v \mathbf{q}^\omega(\mathbf{u}) d\mathbf{u}. \quad (3.16)$$

Then, we estimated the appropriate mass transfer parameters of the up-scaled transport model by using a methodology conducive to preserve the residence time distribution of solute mass particles in each block. This seems a natural approach when using the up-scaled MRMT model because the memory function, which plays a central role, can be physically interpreted as the residence time distribution of solute mass in the immobile domains (slow velocity areas) (Haggerty *et al.*, 2000). Essentially, the up-scaled parameters were estimated by curve-fitting the residence time distribution (numerically obtained from fine-scale transport simulations) with a theoretical MRMT model. When transport takes place according to the MRMT model in an equivalent homogeneous medium (i.e., a block of the up-scaled model), the cumulative residence time distribution, $F_\tau(\tau)$, can be approximately written in Laplace space as

$$\widehat{F}_\tau(p) \approx \frac{1}{p} \exp \left[L_b \left(\frac{1}{2A_\ell} - \sqrt{\frac{1}{4A_\ell^2} + \frac{\psi(p)}{A_\ell v_m}} \right) \right] \quad (3.17)$$

$$\psi(p) = p + \beta \int_0^\infty f(\alpha) \frac{p\alpha}{p + \alpha} d\alpha \quad (3.18)$$

where A_ℓ is the effective longitudinal dispersivity coefficient, L_b is the mean travel displacement of solute mass particles in v , and v_m is the mobile velocity. Here, we have assumed that F_τ is not significantly influenced by transverse dispersion since we are measuring integrated mass fluxes over a surface.

The effective velocity of the solute inside v moving through the mobile domain (preferential channels) is the mobile velocity, v_m . This is an important concept here because the solute plume is not necessarily sampling the entire region of a given block. Moreover, θ^v does not represent the void ratio of the entire aquifer (θ^ω), but only defines the pore volume fraction associated with the mobile domain. The parameters obtained from curve-fitting are: v_m , β and those characterizing $f(\alpha)$ (see Table 3.1). From them, we estimated θ^v so that the mean residence time, $\bar{\tau}$, is preserved during upscaling,

$$\theta^v = \frac{\theta^\omega}{1 + \beta} C_\tau, \quad (3.19)$$

where C_τ is

$$C_\tau = \frac{\bar{\tau}}{\tau^v}, \quad \tau^v = \frac{\theta^\omega L_b}{|\mathbf{q}^v|}, \quad (3.20)$$

and $\bar{\tau}$ is the mean residence time

$$\bar{\tau} = \int \tau f_\tau(\tau) d\tau, \quad f_\tau = \frac{dF_\tau}{d\tau}, \quad (3.21)$$

being f_τ the frequency distribution function of residence times. The parameter C_τ takes into consideration that the mean residence time, $\bar{\tau}$, is not necessary given by the averaged spatial velocity inside v . This term can be also related to the noncontributing capacity coefficient (β_{nc}) introduced by *Zinn and Harvey* (2003) as

$$C_\tau = \frac{1 + \beta_{nc} + \beta}{1 + \beta}. \quad (3.22)$$

A block equivalent transverse macrodispersivity value associated with the MRMT model was estimated using the method of moments as

$$A_t = \frac{\sigma_y^2}{2L_b} \quad (3.23)$$

where σ_y^2 is the variance of transverse displacements of the particles moving through v .

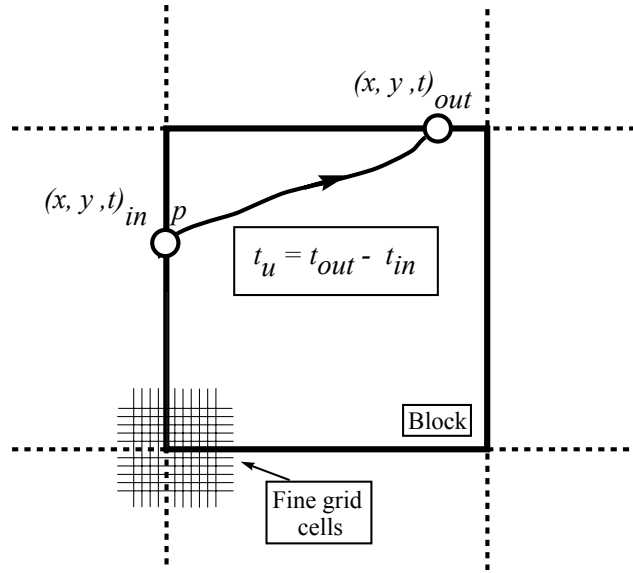


Figure 3.5: Calculation of residence times in a given block of the numerical model.

3.4.2 Implementation Details

Numerically, the residence time distributions, $f_\tau(\tau)$ and $F_\tau(\tau)$, were obtained by recording the first passage time (t_{in}) and the exiting time (t_{out}) of a particle passing through a given block during fine-scale simulations (see Figure 3.5). The distribution of residence times was estimated by reconstructing the (cumulative) frequency distribution of residence times $\{\tau_i, i = 1, \dots, N_p\}$, where N_p is the number of particles traveling through the block, and $\tau_i = t_{out} - t_{in}$ is the residence time of the i -th mass particle. The mean residence time $\bar{\tau}$ was estimated as

$$\bar{\tau} = \int \tau f_\tau(\tau) d\tau \approx \frac{1}{N_p} \sum_{i=1}^{N_p} \tau_i \quad (3.24)$$

The time-domain solution of (3.17) was calculated using the STAMMT-L code (*Haggerty and Reeves, 2002*). An optimization program, PEST (*Doherty, 2004*), was utilized to calibrate the mass transfer parameters associated with $F_\tau(\tau)$. The minimized objective function by PEST included the estimates of the cumulative distribution function obtained at different times as well as the low-order temporal moments of $f_\tau(\tau)$ (see appendix).

The fact that the residence time distribution at each block is preserved during upscaling renders the upscaled mass transfer model a promising tool to

couple solute transport with chemical reactions controlled by residence times. Yet, from a practical point of view, we recognize that the proposed upscaling methodology can be computationally expensive because it requires to solve flow and transport at a small-scale. This is only justifiable when the upscaled model is used afterwards to solve a more computationally demanding problem (e.g., reactive transport involving many species and reactions). Nevertheless, several approaches to reduce the computational burden can be considered. Similar to what is known for upscaling hydraulic conductivity (*Sánchez-Vila et al.*, 1995; *Wen and Gómez-Hernández*, 1996; *Sánchez-Vila et al.*, 2006), instead of solving the flow and transport problem over the entire domain, the equations can be iteratively solved over smaller support volumes, which contain v plus a “skin” region.

The skin ensures a more realistic flow and transport boundary condition associated with each block. Importantly, in this case, we note that the injection of solute should be placed in the skin region so that enough memory effects are retained. Anyhow, noticing that the objective of this paper is not to present an upscaling methodology but to evaluate the adequacy of an alternative constitutive transport model, we employed the most exact version of the upscaling methodology, which is to resolve f_τ and F_τ directly from global fine-scale simulations.

3.5 Numerical Results and Discussion

The evaluation of each constitutive upscaled transport model was performed by contrasting the Monte Carlo simulated BTCs obtained using the upscaled models against the reference BTCs solution. In addition to the upscaled mass transfer models, we further compare the results with the well-known macrodispersive model and the purely advective upscaled model. The purely advective model does not account for macrodispersive fluxes and memory effects, and serves to illustrate the effects of smoothing the heterogeneous $Y(\mathbf{x})$ -field by upscaling.

The macrodispersive model is defined as a particular case of the MRMT model in which $\psi(p) = 0$ in (3.17) and serves to compare the upscaled mass transfer model with a Fickian model. The structure of the discussion is as follows. First, we analyzed the reproduction of the ensemble average behavior of BTCs and its associated uncertainty with $A_T = 0$. This avoids mass transfer effects between blocks *Fernández-García et al.* (2007) and allows to focus on the longitudinal component of dispersive fluxes. Then, we discuss the effect of including $A_T \neq 0$ into the upscaled models.

3.5.1 Ensemble Average Behavior

We start by looking at the ensemble average behavior of the main features associated with the simulated BTCs, which we characterized by: (a) the early arrival time (the time at which 5% of the mass arrives at the x -location, denoted as T_{05}); (b) the maximum value of concentrations (peak); (c) the late-time slope of BTCs; and (d) the spreading of BTCs. The spreading of BTCs is measured by means of an effective longitudinal dispersivity coefficient estimated as

$$A^{eff}(x) = \frac{x}{2} \left\langle \frac{\mu_2(x)}{\mu_1^2(x)} \right\rangle \quad (3.25)$$

where the brackets denote the expected operator, x is the coordinate of the control plane in the mean flow direction, and μ_1' and μ_2 the first two temporal moments of BTCs, written as

$$\mu_1' = \frac{\int_0^\infty tC(t)dt}{\int_0^\infty C(t)dt} \quad (3.26)$$

$$\mu_2 = \frac{\int_0^\infty (t - \mu_1')^2 C(t)dt}{\int_0^\infty C(t)dt} = \frac{\int_0^\infty t^2 C(t)dt}{\int_0^\infty C(t)dt} - (\mu_1')^2 \quad (3.27)$$

where $C(t)$ denotes flux-concentrations. Figure 3.6 displays A^{eff} as a function of travel distance for the different upscaled models. Remarkably, we see that the inclusion of memory in the transport equation allows an accurate reproduction of effective spreading when either a discrete MRMT model with more than two immobile domains are considered or a continuous distribution of mass transfer rates is described with a truncated power-law.

This is in contrast with the macrodispersive model and the single-rate mass transfer model results which largely underestimate A^{eff} . The reason for this is that the memory function associated with these models are too simple to properly describe the heterogeneous processes taking place within a block. This is shown in Figure 3.7 which depicts the mean sum of square errors (SSE) associated with the calibrated model obtained after curve-fitting the block residence time distribution with the theoretical model. Note that the ultimate SSE values for the single-rate model are substantially larger than those associated with the truncated power-law and the double-rate model.

Spreading by itself does not provide enough information about the complete distribution of concentrations. The interest on the different characteristic behaviors of the BTC depends on the type of application. The early-time of BTCs usually displays a sharp rising limb and can be characterized by its early arrival time, T_{05} . In practice, this parameter is important for designing underground radioactive repositories. Figure 3.8 compares the simulated mean T_{05}

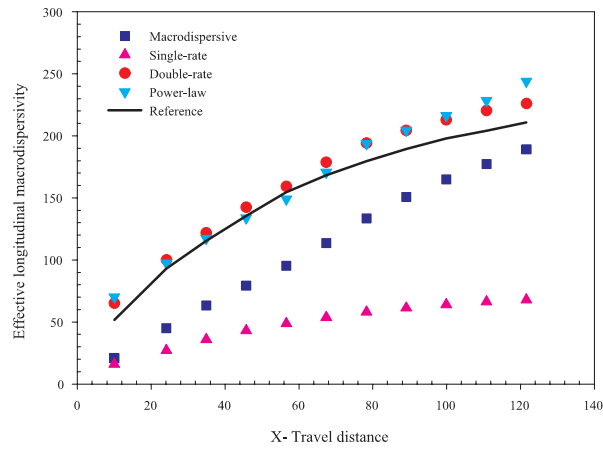


Figure 3.6: Evolution of the effective longitudinal dispersivity with travel distance .

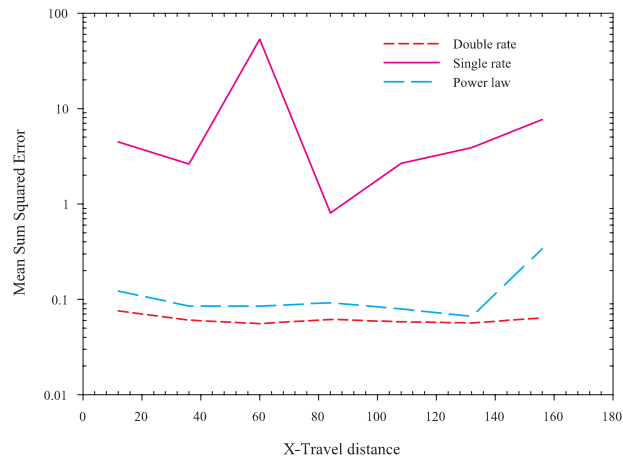


Figure 3.7: Evolution with travel distance of the mean sum of square error associated with the calibrated model obtained curve-fitting f_T with a theoretical model.

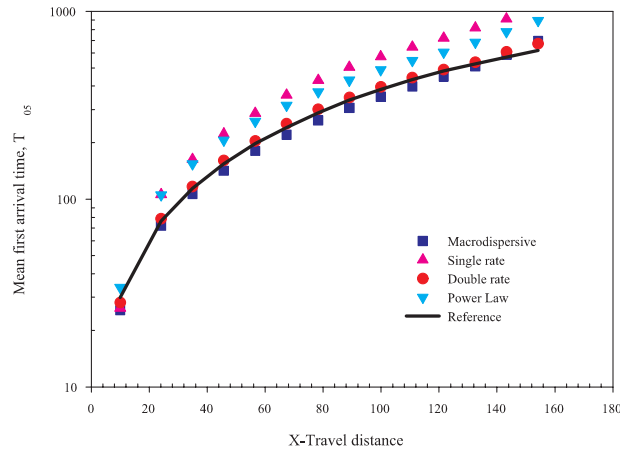


Figure 3.8: Evolution of the ensemble average first arrival of the BTC T_{05} with travel distance.

value obtained at the small support scale to its corresponding upscaled model solution. As expected, the upscaled advective model yields not conservative estimates of travel times, i.e., the upscaled model overestimates T_{05} . Most remarkably, in this case, even though the double-rate and the power-law model are described with the same number of parameters (degrees of freedom), the truncated power-law model can largely underestimate T_{05} .

A proper representation of the late-time behavior of BTCs has recently received much attention for being indicative of anomalous transport (e.g., *Haggerty et al.*, 2000; *Harvey and Gorelick*, 2000; *Salamon et al.*, 2007; *Riva et al.*, 2008; *Willmann et al.*, 2008). It also constitutes an important parameter for the calculation of clean-up times needed to remediate contaminated aquifers. Typically, BTCs are observed to behave as a power law at late times (i.e. $C(t) \sim t^{-m}$), where m is the slope of the BTC on double log-scale. The mechanisms by which the presence of slow and fast channels (heterogeneity) affects the slope m have been recently studied by *Willmann et al.* (2008), who found that, for conservative solutes moving in a heterogeneous medium, the slope mainly depends on "connectivity" rather than the classical statistical properties of the aquifer (variance of $\ln T$).

Here, we do not concentrate on the fundamental nature of the slope but we look at the capability of upscaled mass transfer models to reproduce tailing. In other words, we evaluate whether a proper description of residence times, f_τ , at each block of a numerical model assures the reproduction of the late-time behavior of BTCs. To do this, we concentrate on the simulated slope

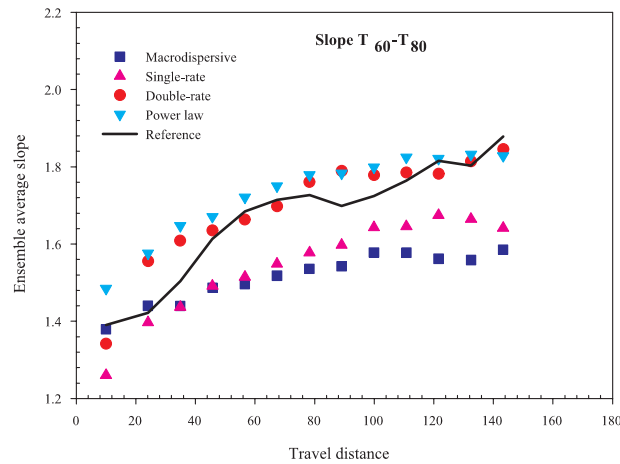


Figure 3.9: Evolution of the ensemble average slope $T_{60} - T_{80}$ with travel distance.

attained over two time intervals of the BTCs: (T_{60}, T_{80}) and (T_{80}, T_{95}) , where T_{60} denotes the time at which 60% of the mass passes through the observation location and so on. The slope was estimated by using least square regression of the corresponding BTC values plotted in a double log-scale. The ensemble average behavior of the slope as a function of travel distance is shown in Figures 3.9 and 3.10.

For all models and time scales, the slope slowly increases with travel distances and thus tends to a more Fickian-like behavior. As expected, the upscaled mass transfer models provide a better description of the late-time behavior of BTCs, being the macrodispersive model a less adequate model for this matter. In this context, we see that while the truncated power-law model can accurately simulate the late-time behavior of BTCs at all time scales (the two intervals of time), the double-rate model is only capable to describe the late-time behavior over the time interval (T_{60}, T_{80}) . This is consistent with theory, *Carrera et al.* (1998) demonstrated that the late-time behavior of BTCs associated with MRMT models is the result of an infinite superposition of single-rate mass transfer modes (*Carrera et al.*, 1998). Thus, a proper description beyond $t > T_{80}$ in this case requires a discrete mass transfer model with more than two modes.

Interestingly, the slope reproduced by the macrodispersive model is small compared to the reference solution. This points out an important conceptual limitations of the macrodispersive model, which is back-dispersion. Close to the source, where concentration gradients are usually higher, the macrodisper-

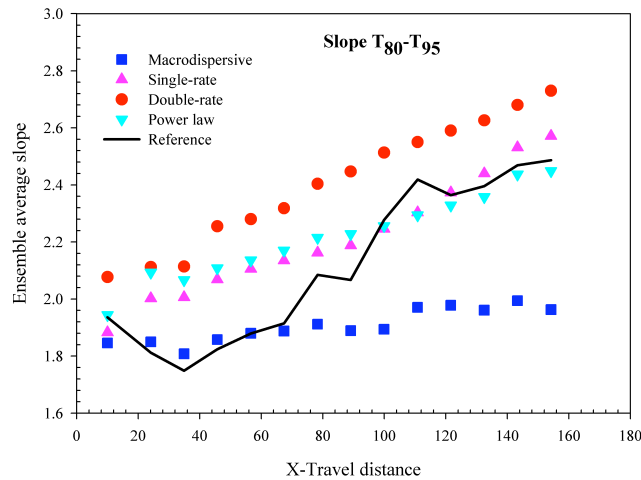


Figure 3.10: Evolution of the ensemble average slope $T_{80} - T_{95}$ with travel distance.

sive model creates dispersive mass fluxes oriented in the opposite direction to flow, which are not physically possible. Due to this mechanism, particles close to the source were susceptible to be trapped in low velocity regions during simulations, causing the presence of very slow particles.

Another important characteristic parameter of a BTC is the concentration peak. When groundwater is the source for drinking water, this water is required to meet certain drinking water standards. This standard is typically contrasted against a maximum concentration threshold. Figure 3.11 shows the performance of the upscaled models in terms of the peak of concentrations associated with the simulated BTCs. Now, we see that, albeit both models are described with the same number of degrees of freedom, a discrete MRMT model with only two modes provides a better description of the maximum value of concentrations than the the truncated power-law model.

3.5.2 Propagation of Uncertainty

The lack of complete knowledge of an aquifer on the one hand and the large spatial variability of the aquifer attributes on the other makes deterministic models to be highly inadequate for representing solute transport in heterogeneous media. Alternatively, multiple possible scenarios should be considered (see (Riva *et al.*, 2008) for an illustrative field example). In this context, the transfer of information from one scale to another by upscaling should also require the proper propagation of model uncertainty.

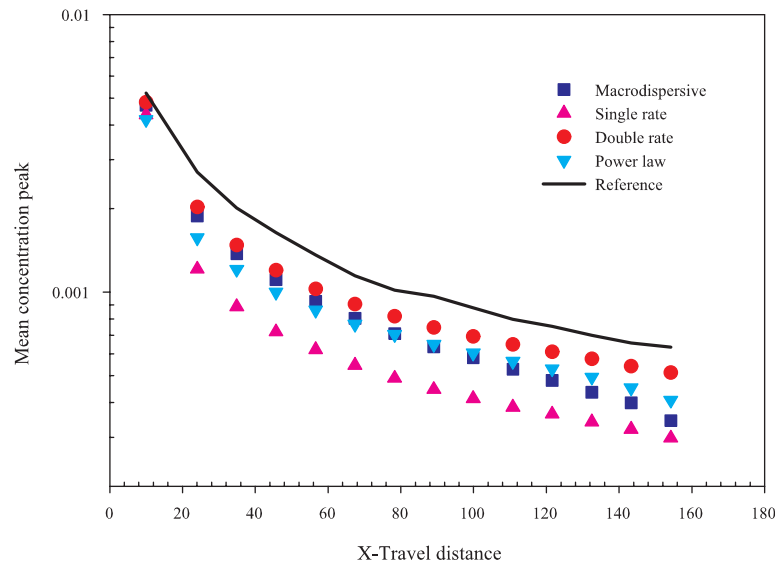


Figure 3.11: Evolution of the mean concentration peak with travel distance.

Here, we evaluate the reproduction of uncertainty by qualitatively examining the 95%-confidence interval associated with the ensemble of BTCs. Figures 3.12 and 3.13 compares the ensemble of Monte Carlo-based BTCs obtained using the reference transmissivity fields to those associated with each upscaled mass transfer model at two control planes ($x = 34$ units and $x = 110$ units). By comparing the ensemble of BTCs to the 95%-confidence interval associated with the fine-scale model, it is clear that all the upscaled mass transfer models exhibit a reduction of uncertainty to a certain degree. This reduction is more apparent for late times (slow particles) and small travel distances. The latter is shown in Figure 3.14, which displays the 95%-confidence intervals of the BTCs obtained at two different control planes.

A complete evaluation of uncertainty is provided by examining the cumulative frequency distribution function (CDF) of the main features associated with the BTCs obtained at a given control plane.

Figures ?? and 3.17 respectively show the CDF of the slope ($T_{60} - T_{80}$) and the first arrival (T_{05}) associated with the simulated BTCs obtained at $x = 34.9$ units and $x = 110.8$ units. Interestingly, at early times, when particles have still not pass through few blocks, the integrated BTC is simply the superposition of residence time distributions of all sample blocks, and therefore, for small travel distances, the CDF of the late-time slope associated with

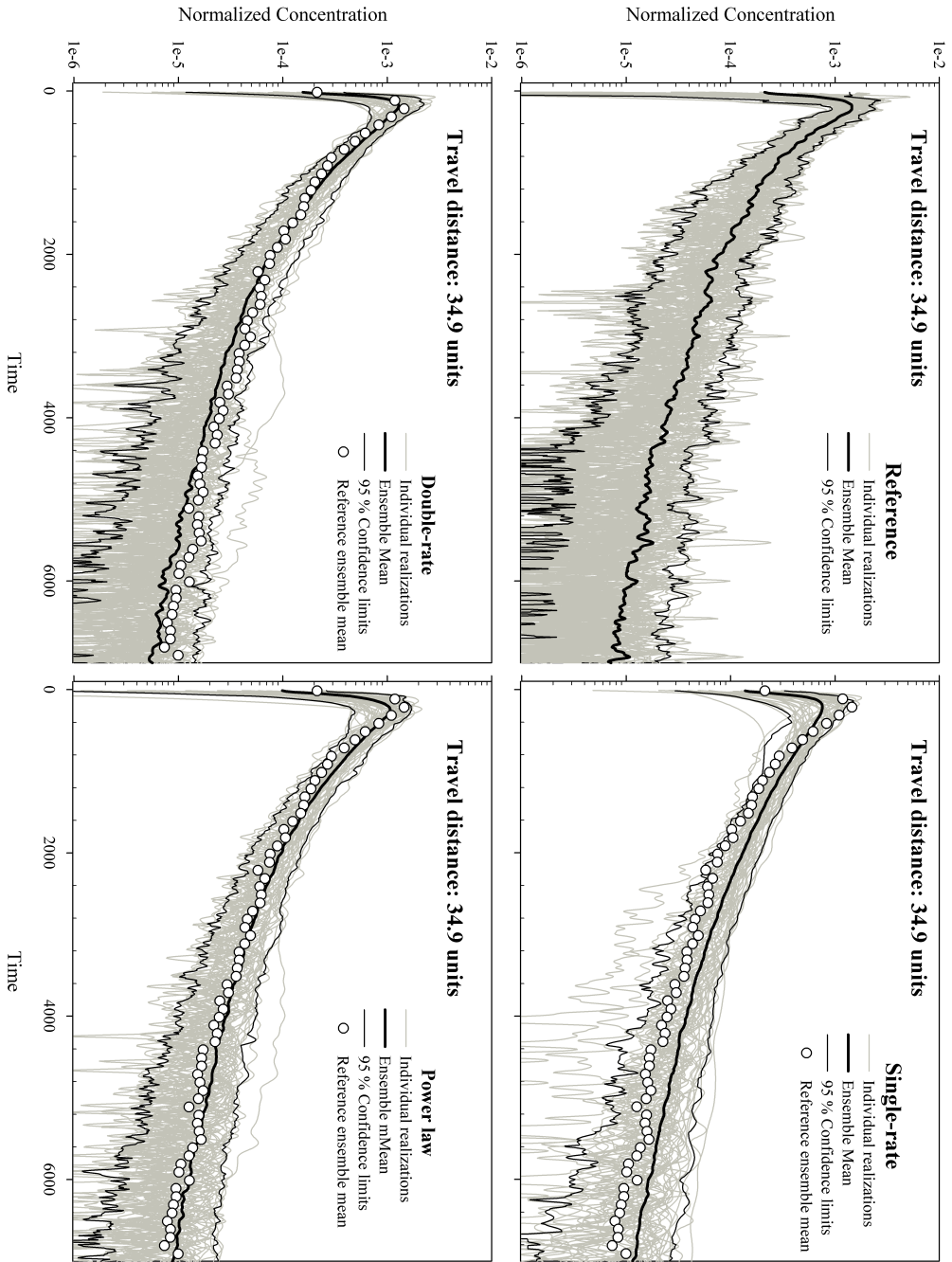


Figure 3.12: Ensemble of breakthrough curves obtained at $x = 34$ units for the different upscaled models contrasted against the reference solution. The 95% confidence interval refer to the ensemble of 50 realizations.

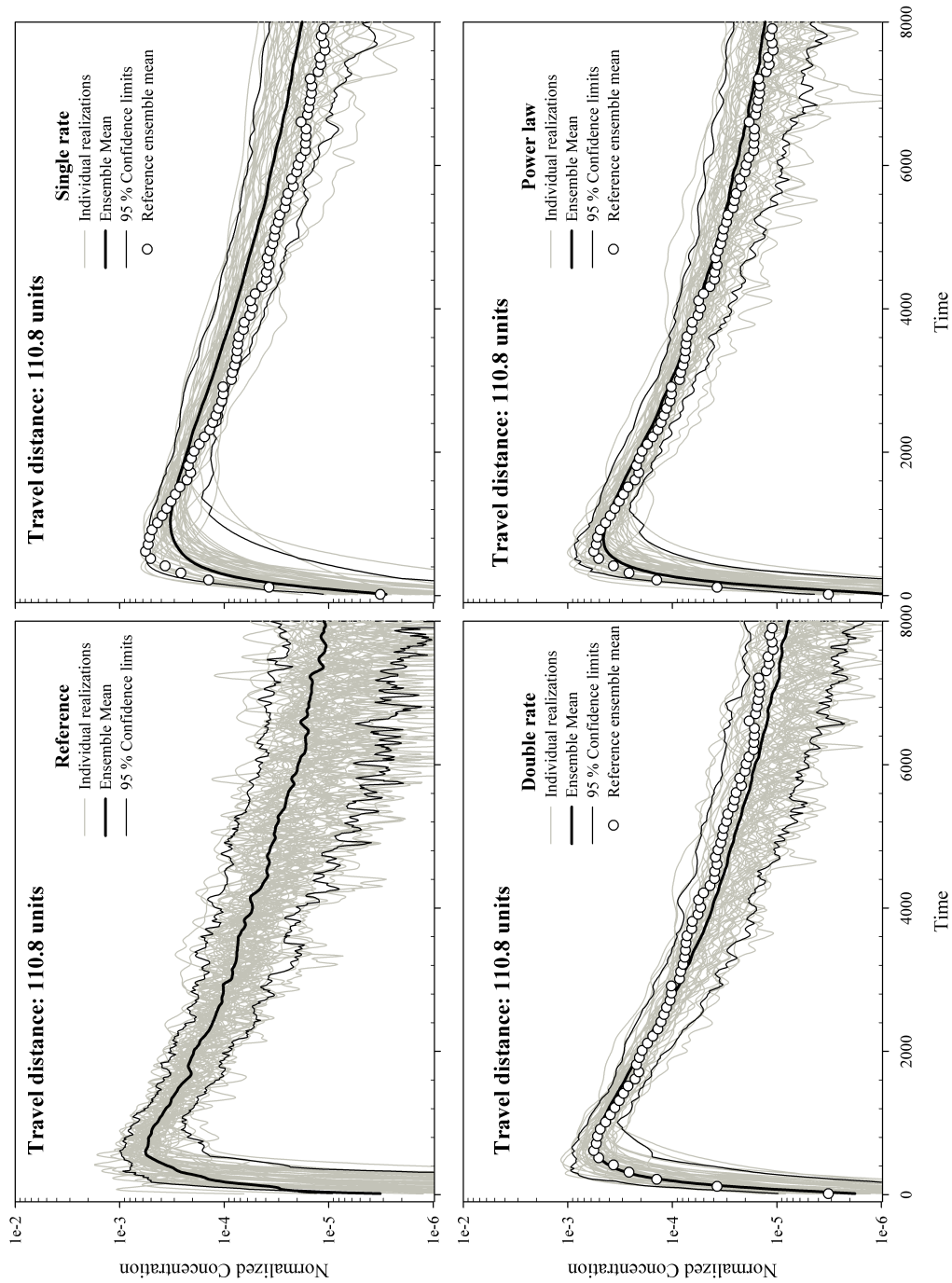


Figure 3.13: Ensemble of breakthrough curves obtained at $x = 110.8$ units for the different upscaled models contrasted against the reference solution. The 95% confidence interval refer to the ensemble of 50 realizations.

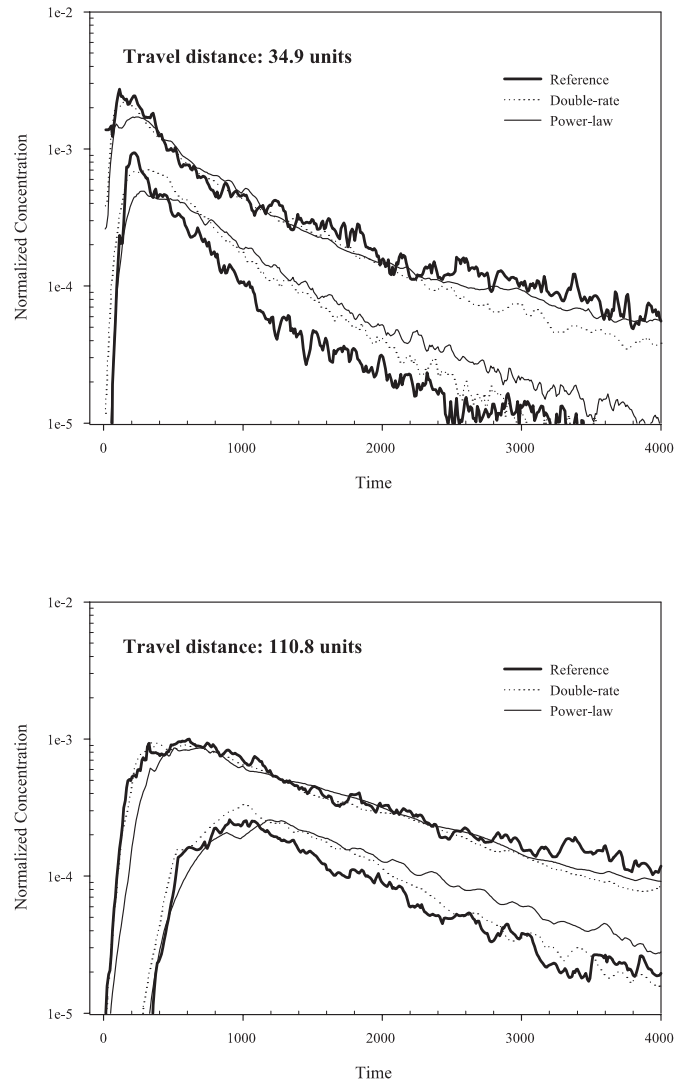


Figure 3.14: Propagation of uncertainty: Comparison of the reference confidence interval with those obtained using the upscaled models at two different control planes.

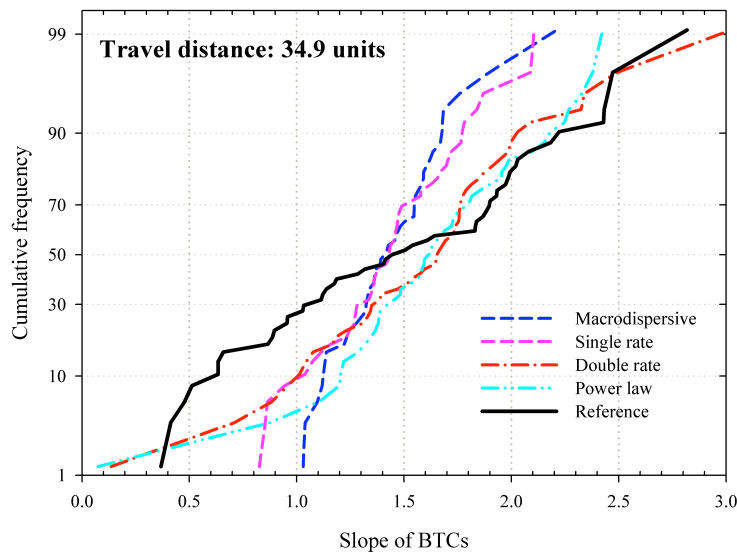


Figure 3.15: Cumulative frequency distribution of the late-time slope of BTCs for the different upscaled models. The late-time slope corresponds to the region of the BTCs comprised between the 60% and 80% of the BTC total mass obtained at $x = 34.9$ units.

the double-rate and the truncated power-law model is adequately reproduced. As soon as particles pass through few blocks, the CDF of the late-time slope associated with the upscaled mass transfer model largely underestimates the dispersion of the corresponding probability density function. This effect increases with distance.

In regards to the CDF associated with T_{05} , results show that only the double-rate model is able to properly describe uncertainty for all travel distances. In this case, the truncated power-law model provides a biased estimator of T_{05} , but still seems to properly capture the general trend depicted by the CDF.

Now, we examine the effect of including a macroscopic transverse dispersion into the upscaled model. This parameter describes the dispersive fluxes taking place in the transverse direction to the block-averaged flow based on a Fickian model. From Figure 3.18 we see that while accounting for transverse dispersive fluxes improves the reproduction of the late-time behavior of the BTCs, it causes an excess of dilution into the system (reduction of peak concentrations). Again, this is attributed to the Fickian assumption.

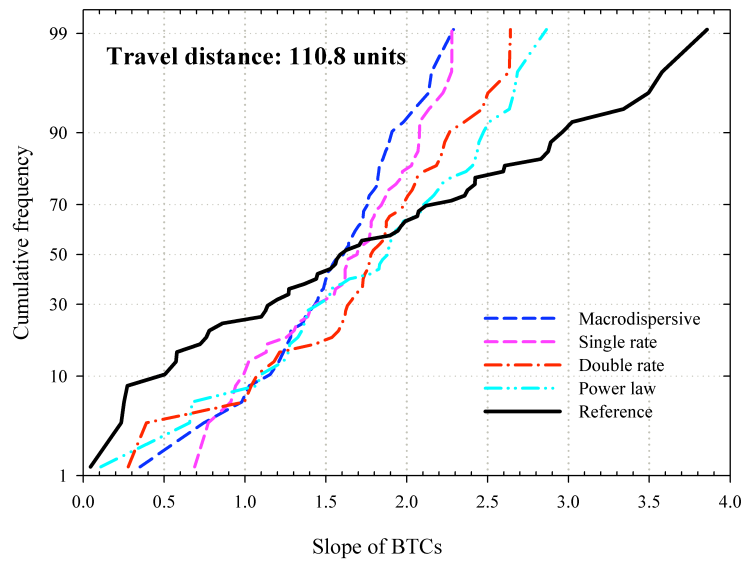


Figure 3.16: Cumulative frequency distribution of the late-time slope of BTCs for the different upscaled models. The late-time slope corresponds to the region of the BTCs comprised between the 60% and 80% of the BTC total mass obtained at $x = 110.8$ units.

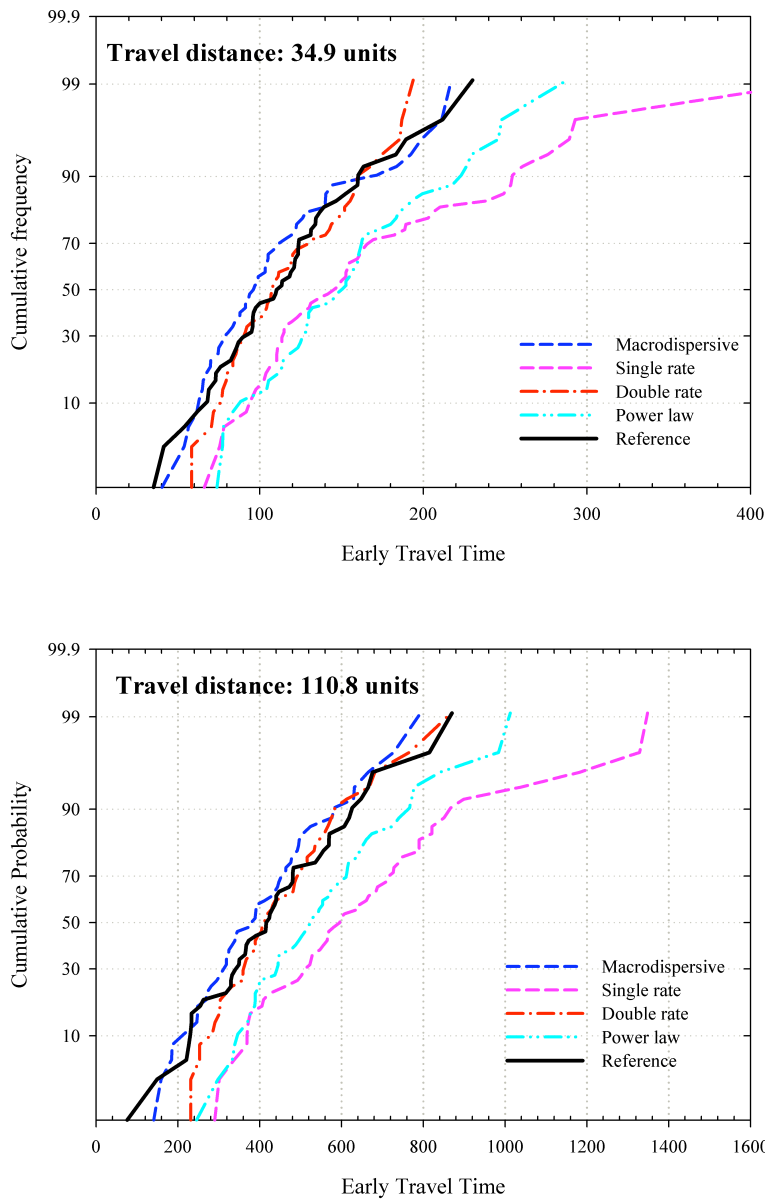


Figure 3.17: Cumulative frequency distribution of the early arrival time (T_{05}) of BTCs for the different upscaled models.

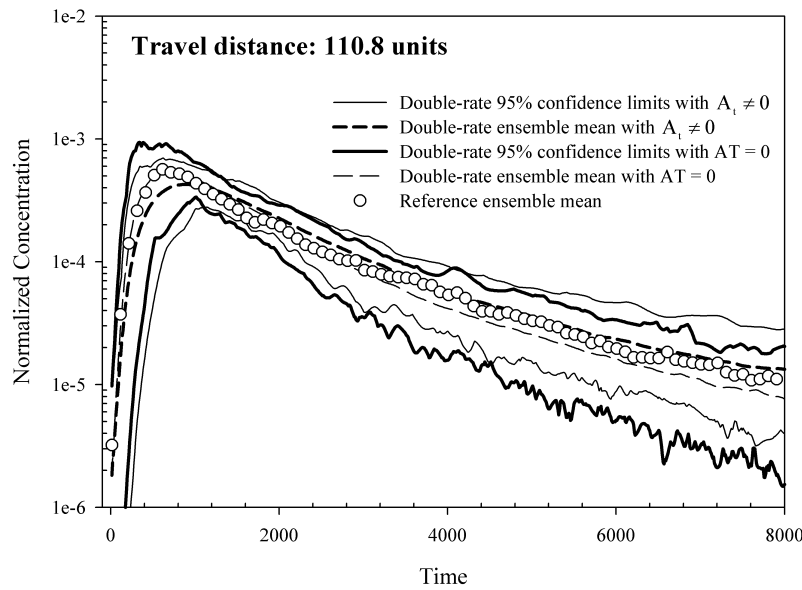


Figure 3.18: Comparison of the simulated ensemble of BTCs obtained with and without transverse macrodispersivity.

3.6 Summary and Conclusions

We have investigated the use of upscaled mass transfer models as a tool for upscaling solute transport in a general numerical modeling framework. This was achieved by comparing Monte Carlo simulations of solute transport at two different support scales. Transport phenomena at the computational scale was described by means of a multirate mass transfer model.

The performance of the upscaled models was evaluated from two different perspectives. First, we analyzed the reproduction of the ensemble mean behavior of the main features associated with the simulated BTCs. Importantly, results showed that an appropriate description of the residence time distribution for all blocks of the numerical model provides an upscaled transport model that is capable to reproduce the ensemble mean behavior of the BTCs. In particular, the truncated power-law model provided an excellent reproduction of the effective spreading as well as the ensemble mean slope of the BTCs for all time scales. Yet, it slightly underestimated the first arrival of mass particles at control planes as well as the maximum concentration of the BTCs. In this context, the double-rate mass transfer model, which involved the same number of degrees of freedom as the truncated power-law, gave more consistent estimates of the first arrival and the concentration peak. However,

as a drawback and consistent with theory, this model was found not able to properly describe the slope of the BTCs at all time scales ($t > T_{80}$). Remarkably, the single-rate model did not capture any of the main features of the BTCs, giving then a sign of caution to the use of this widely employed model in field applications.

Then, we examined the effect of upscaling on model uncertainty. We found that a complete reproduction of uncertainty was not provided by any of the up-scaled transport models, which substantially underestimated the uncertainty associated with the late-time behavior of BTCs and the peak of concentrations. Essentially, this was the result that a truthful reproduction of a BTC associated with an individual realization cannot in general be satisfied. The reason mostly lies on the poor description (lack of memory) of the dispersive mass fluxes transverse to the block-averaged flow direction. While using mass transfer models as a tool for upscaling can preserve the residence time distribution of mass particles in the system, the lack of memory in space prevents the model from reproducing mass fluxes in all directions. In particular, the reproduction of mass fluxes taking place at the interface between two blocks of the upscaled model are not satisfied by upscaling. Thus, results indicate that the lack of directionality involved in the memory term associated with mass transfer models prevents upscaling from reproducing uncertainty and mass fluxes at block interfaces. In this case, a proper description of the non-Fickian nature of dispersive mass fluxes should also be included into the constitutive transport equation.

Bibliography

- Adams, E. E., L. W. Gelhar (1992), Field study of dispersion in a heterogeneous aquifer 2. Spatial moment analysis, *Water Resources Research*, 28(12), 3293–3307.
- Benson, D. A., S. W. Wheatcrat, and M. M. Meerschaert (2000), Application of a fractional advection-dispersion equation, *Water Resources Research*, 36(6), 1403–1412.
- Berkowitz, B., and H. Scher (1998), Theory of anomalous chemical transport in fracture networks, *Physical Review E*, 57(5), 5858–5869.
- Berkowitz, B., J. Klafter, R. Metzler, and H. Scher (2002), Physical pictures of transport in heterogeneous media: Advection-dispersion, random-walk, and fractional derivative formulations, *Water Resources Research*, 38(10), 1191, doi:10.1029/2001WR001030.
- Berkowitz, B., A. Cortis, M. Dentz, and H. Scher (2006), Modeling non-fickian transport in geological formations as a continuous time random walk, *Reviews of Geophysics*, 44, RG2003, doi:10.1029/2005RG000178.
- Carrera, J., X. Sánchez-Vila, I. Benet, A. Medina, G. Galarza, and J. Guimerà (1998), On matrix diffusion: formulations, solution methods and qualitative effects, *Hydrogeology Journal*, 6, 178–190.
- Cushman, J. H., and T. R. Ginn (2000), Fractional advection-dispersion equation: A classical mass balance with convolution-Fickian flux, *Water Resources Research*, 36(12):3763–3766.
- Dentz, M., B. Berkowitz (2003), Transport behavior of a passive solute in continuous time random walks and multirate mass transfer, *Water Resources Research*, 39(5), 1111, doi: 10.1029/2001WR001163.
- Doherty, J. (2004), *Manual for PEST*, 5th edition, Brisbane, Australia: Watermark Numerical Computing.

- Feehley, C. E., C. Zheng, and F. J. Molz (2000), A dual-domain mass transfer approach for modeling solute transport in heterogeneous aquifers: Application to the Macrodispersion Experiment (MADE) site, *Water Resources Research*, 36(9), 2501–2515.
- Fernàndez-Garcia, D., T. H. Illangasekare, and H. Rajaram (2005a), Differences in the scale-dependence of dispersivity and retardation factors estimated from forced-gradient and uniform flow tracer tests in three-dimensional physically and chemically heterogeneous porous media, *Water Resources Research*, 41, W03012, doi:10.1029/2004WR003125.
- Fernàndez-Garcia, D., T. H. Illangasekare, and Harihar Rajaram (2005b), Differences in the scale dependence of dispersivity estimated from temporal and spatial moments in chemically and physically heterogeneous porous media, *Advances in Water Resources*, 28, 745–759.
- Fernàndez-Garcia, D., H. Rajaram, and T. H. Illangasekare (2005c), Assessment of the predictive capabilities of stochastic theories in a three-dimensional laboratory test aquifer: Effective hydraulic conductivity and temporal moments of breakthrough curves, *Water Resources Research*, 41, W04002, doi:10.1029/2004WR003523.
- Fernàndez-Garcia and Gómez-Hernández (2007), Impact of upscaling on solute transport: travel times, scale-dependence of dispersivity and uncertainty, *Water Resources Research*, 43, W02423, doi:10.1029/2005WR004727, 2007.
- Gómez-Hernández, J. J., and Srivastava R. M. (1990), ISIM3D: An ANSI-C three-dimensional multiple indicator conditional simulation program, *Computer and Geosciences*, 16(4), 395–440.
- Gómez-Hernández, J. J. (1991), A stochastic approach to the simulation of block conductivity fields conditioned upon data measured at a smaller scale, Ph.D. thesis, Stanford University, CA., 351 pp.
- Gómez-Hernández, J. J., and A. G. Journel (1993), Joint simulation of multi-Gaussian random variables. In: Soares A, editor. *Geostatistics Tróia’92*, vol. 1. Dordrecht, Kluwer, 85–94.
- Gouze, P., T. Le Borgne, R. Leprovost, G. Lods, T. Poidras, and P. Pezard (2008), Non-Fickian dispersion in porous media: Multiscale measurements using single-well injection withdrawal tracer tests, *Water Resources Research*, 44, W06426, doi:10.1029/2007WR006278.
- Guswa, A. J., and D. L. Freyberg (2002), On using the equivalent conductivity to characterize solute spreading in environments with

- low-permeability lenses, *Water Resources Research*, 38, (8), 1132, doi:10.1029/2001WR000528.
- Haggerty, R., and S. M. Gorelick (1995), Multiple-rate mass transfer for modeling diffusion and surface reactions in media with pore-scale heterogeneity, *Water Resources Research*, 31,(10), 2383–2400.
- Haggerty, R., S.A. McKenna, and L. C. Meigs (2000), On the late-time behaviour of tracer test breakthrough curves, *Water Resources Research*, 36, (12), 3467–3479.
- Haggerty, R., and P. Reeves (2002), STAMMT-L: Solute Transport and Multirate Mass Transfer, Version 1.0, User’s Manual, *ERMS#520308*, Sandia Natl. Lab., Albuquerque, N. M.
- Haggerty, R., C. F. Harvey, C. Freiherr von Schwerin, and L. C. Meigs (2004), What controls the apparent timescale of solute mass transfer in aquifers and soils? A comparison of experimental results, *Water Resources Research*, 40, W01510, doi:10.1029/2002WR001716.
- Harbaugh, A. W., Banta, E. R., Hill, M. C., and McDonald, M. G. MODFLOW-2000, The U.S. Geological Survey Modular Ground-Water Model-user guide to modularization concepts and the ground-water flow process, *Open-file Report 00-92*, 2000.
- Harvey, C., and S. M. Gorelick (2000), Rate-limited mass transfer or macrodispersion: Which dominates plume evolution at the Macrodispersion Experiment (MADE) site?, *Water Resources Research*, 36(3), 637–650.
- Hu, B. X., D.-W. Deng, and J.H. Cushman (1995), Nonlocal reactive transport with physical and chemical heterogeneity: Linear non-equilibrium sorption with random K_d , *Water Resources Research*, 31(9), 2239–2252.
- Koch, D. L., J. F. Brady (1985), Dispersion in fixed beds, *Journal of Fluid Mechanics*, 154, 399–427.
- Lawrence, A. E., X. Sanchez-Vila, and Y. Rubin, Conditional moments of the breakthrough curves of kinetically sorbing solute in heterogeneous porous media using multirate mass transfer models for sorption and desorption, *Water Resources Research*, 38(11), 1248, doi:10.1029/2001WR001006, 2002.
- Levy, M. and B. Berkowitz (2003). Measurement and analysis of non-Fickian dispersion in heterogeneous porous media, *Journal of Contaminant Hydrology*, 64(3-4), 203–226.

- Liu G., Ch. Zheng, and S. M. Gorelick (2004), Limits of applicability of the advection-dispersion model in aquifers containing connected high-conductivity channels, *Water Resources Research*, 40, W08308, doi: 10.1029/2003WR002735.
- Lu Z., and D. Zhang (2002), On stochastic modeling of flow in multimodal heterogeneous formations, *Water Resources Research*, 38(10), 1190, doi: 10.1029/2001WR001026.
- Mackay, D. M., D. L. Freyberg, P. B. Roberts, J. A. Cherry (1986), A natural gradient experiment on solute transport in a sand aquifer: 1. Approach and overview of plume movement, *Water Resources Research*, 22(13), 2017–2029.
- Meigs L. C., and R. L. Beauheim (2001), Tracer tests in fractured dolomite: 1. Experimental design and observed tracer recoveries, *Water Resources Research*, 37(5), 1113–1128, doi:10.1029/2000WR900335
- Morales-Casique, E., S. P. Neuman, A. Guadagnini (2006), Non-local and localized analyses of non-reactive solute transport in bounded randomly heterogeneous porous media: Theoretical framework, *Advances in Water Resources*, 29(9), 1399–1418.
- Neuman, S. P. (1993), Eulerian–Lagrangian theory of transport in spacetime nonstationary velocity fields: exact nonlocal formalism by conditional moments and weak approximation. *Water Resources Research*, 29(3), 633–645.
- Neuman, S. P., D. M. Tartakovsky (2008), Perspective on theories of non-Fickian transport in heterogeneous media, *Advances in Water Resources*, in press.
- Riva, M., L. Guadagnini, A. Guadagnini, T. Ptak, E. Martac (2006), Probabilistic study of well capture zones distribution at the Luswiesen field site. *Journal of Contaminant Hydrology*, 88, 92–118.
- Riva, M., A. Guadagnini, D. Fernández-García, X. Sanchez-Vila, T. Ptak (2008), Relative importance of geostatistical and transport models in describing heavily tailed breakthrough curves at the Lauswiesen site, *Journal of Contaminant Hydrology*, 101, 1–13.
- Rubin, Y., and A. G. Journel (1991), Simulation of non-Gaussian space random functions for modeling transport in groundwater, *Water Resources Research*, 27(7), 1711–1721.
- Rubin, Y. (1995), Flow and transport in bimodal heterogeneous formations, *Water Resources Research*, 31(10), 2461–2468.

- Salamon, P., D. Fernàndez-Garcia, and J. J. Gómez-Hernández (2006a), A review and numerical assessment of the random walk particle tracking method, *Journal of Contaminant Hydrology*, 87, 277–305.
- Salamon, P., D. Fernàndez-Garcia, and J. J. Gómez-Hernández (2006b), Modeling mass transfer processes using random walk particle tracking, *Water Resources Research.*, VOL. 42, W11417, doi:10.1029/2006WR004927,2006.
- Salamon, P., Fernàndez-Garcia, D., J. J. Gómez-Hernández (2007), Modeling tracer transport at the MADE site: The importance of heterogeneity, *Water Resources. Research.*, 43, W08404, doi:10.1029/2006WR005522.
- Sánchez-Vila, X., J. P. Girardi, and J. Carrera (1995), A synthesis of approaches to upscaling of hydraulic conductivities, *Water Resources. Research.*, 31(4), 867–882.
- Sanchez-Vila, X., A. Guadagnini, and J. Carrera (2006), Representative hydraulic conductivities in saturated groundwater flow, *Reviews of Geophysics*, 44, RG3002, doi:10.1029/2005RG000169.
- Wen, X. H., and J. J. Gómez-Hernández (1996), The constant displacement scheme for tracking particles in heterogeneous aquifers, *Ground Water*, 34(1), 135–142.
- Wen, X.-H., and J. J. Gómez-Hernández (1996), Upscaling hydraulic conductivities in heterogeneous media: An overview, *Journal of Hydrology*, 183 (1–2), ix–xxxii.
- Willmann, M., J. Carrera, and X. Sanchez-Vila (2008), Transport upscaling in heterogeneous aquifers: What physical parameters control memory functions?, *Water Resources Research*, doi:10.1029/2007WR006531, in press.
- Wood, B. D., F. Cherblan, M. Quintard, and S. Whitaker (2003), Volume averaging for determining the effective dispersion tensor: Closure using periodic unit cells and comparison with ensemble averaging, *Water Resources Research*, 39(8), 1210, doi:10.1029/2002WR001723.
- Zheng, C., and P. P. Wang, *MT3DMS: A Modular Three-Dimensional Multi-Species Model for Simulation of Advection, Dispersion, and Chemical Reactions of Contaminants in Groundwater Systems: Documentation and User’s Guide*, SERDP-99-1, U. S. Army Engineer Research and Development Center, Vicksburg, MS, 1999.
- Zinn, B., and Ch. F. Harvey (2003), When good statistical models of aquifer heterogeneity go bad: A comparison of flow, dispersion, and mass transfer

in connected and multivariate Gaussian hydraulic conductivity fields, *Water Resources Research*, 39(3), 1051, doi:10.1029/2001WR001146.

4

Modeling solute transport at large scale in heterogeneous media

Abstract

We evaluate the use of (multi-rate) mass transfer as the constitutive transport model at large scale in heterogeneous media. The non-Fickian transport usually observed in field, manifested by peaked concentration profiles with pronounced tailing, has questioned the use of the classical advection-dispersion equation to simulate solute transport at large scale with a numerical model. In this framework, performance assessment of the alternative transport equations is achieved by comparing transport simulations of non-reactive solute plume at two different support scales. The solutions are illustrated in a complex geological environment formed by highly conductive conducts embedded in an otherwise well behaving Gaussian heterogeneous medium. For modeling solute transport at large scale, the numerical transport model consists in a phenomenological model based on memory functions that are used to represent the unresolved process taking place within each homogenized block of the numerical models. The parameters values associated with memory functions are determined by transferring the small scale information on aquifer properties into the computational scale defined by the numerical model discretization. The numerical results demonstrated that upscaled transport models based on

memory functions can yield a good prediction of the large scale main features associated with mass plume in comparison to a macrodispersion model.

4.1 Introduction

Hydrogeologic properties in an aquifer vary in space and time, which means the characterization of the spatial variation of the properties are needed to predict the behavior of flow and solute transport. Geostatistics provides the ability to characterize the spatial variation of hydrogeologic properties with a high resolution. However, in hydrogeology practice modeling flow with such resolution is most frequently unfeasible. Traditionally, the flow and hydraulic head are simulated using equivalent hydraulic parameter values obtained by the analysis of aquifer tests, these parameters are assigned over various grid-blocks formed big homogeneous zones in the model. During the calibration process, these equivalent parameters are adjusted at computational block scale to reproduce the historical field measurements. But, to simulate solute transport, the aquifer models must capture the heterogeneity of hydrogeologic properties at small scale, however a representation of high definition of the architecture hydrogeology of the aquifer is not feasible, so that effects that control the spacial-temporal evolution of transport must be capture with an upscaled model (*Fernàndez-García et al.*, 2007; *Guswa and Freyberg*, 2002).

In the literature there are a lot of work about the upscaling of hydraulic conductivity (*Wen and Gómez-Hernández*, 1996; *Renard and de Marsily*, 1993; *Sánchez et al.*, 2006). *Scheibe and Yabusaki* (1998) showed that upscaling of conductivity is effective for reproduction of flow behaviour, but do not necessary lead the best reproduction of transport behaviour. Since the values of conductivity obtained through upscaling does not contain information about the attribute heterogeneity that control solute transport.

Much attention has been devoted in recent years to the development of methodologies for the characterization of heterogeneity of the hydrogeologic properties (*Carrera*, 1993; *de Marsily et al.*, 2005; *Gómez-Hernández*, 2006), and important theories have been developed in area of stochastic and/or deterministic hydrogeology to describe the flow and solute transport through aquifer.

The effect of the hydrogeology heterogeneity that produces an anomalous (non-Fickian) transport behaviour, such as plumes asymmetry and breakthrough curves with large tails has been revealed through experimental data from field (*Boggs et al.*, 1992; *Adams and Gelhar*, 1992; *Feehley et al.*, 2000; *Salamon et al.*, 2007; *Riva et al.*, 2008) and from laboratory (*Bajracharya and Barry*, 1997; *Fernàndez-García et al.*, 2005c; *Levy and Berkowitz*, 2003).

The high contrast between high and low conductivities zones makes the mass solute to travel quickly in the direction of preferential flow paths, whereas that in low conductivities areas the solute moves slowly along the velocity creating tailing that cannot be reproduced by the classical advection dispersion equation (ADE) (*Adams and Gelhar, 1992; Feehley et al., 2000; Guswa and Freyberg, 2000; Zinn and Harvey, 2003; Berkowitz et al., 2006; Fernández-García et al., 2007; Riva et al., 2008*). Furthermore, ADE has been shown not to be adequate to model solute transport at scale larger than the scale of heterogeneity.

Various numerical experiment using synthetic models *Guswa and Freyberg (2000); Zinn and Harvey (2003); Liu et al. (2004); Carrera et al. (1998); Willmann et al. (2008)*, have demonstrated that the quality of solute transport predictions, in particular the late-time behavior of breakthrough curves, is significantly improved when the mass transfer equations are added to the ADE.

Alternative transport formulations based on the ADE have been proposed in the literature for modeling solute transport (*Haggerty and Gorelick, 1995; Carrera et al., 1998*). *Carrera et al. (1998)* proposed to add a sink/source term to ADE to account for the exchange of solute mass between high and low conductivity zones producing anomalous behaviors. This is formally represented by decomposing the domain into a mobile zone, where the transport phenomena include advection and dispersion, and an immobile zone where advection is negligible (*Haggerty and Gorelick, 1995; Carrera et al., 1998; Haggerty et al., 2000*). The mass flux between mobile and immobile zones is modeled by linear mass exchange process controlled by a source/sink term. This term can be expressed as a convolution product of a memory function. The memory function represents the mass flux to the immobile zones per unit volume of aquifer, for a unit change in concentration in the mobile zones (*Haggerty et al., 2000; Carrera et al., 1998*). The formulation of this term depends on the geometry of the immobile zones and on the variability of mass transfer or diffusion rates (*Haggerty et al., 2000*). This type of model is commonly referred to as multirate mass transfer models (MRMT).

Similarly, models to better represent the anomalous transport behaviour observed in heterogeneous aquifers at the computational scale have been developed in recent years. In this context, *Berkowitz and Scher (1998); Berkowitz et al. (2000)* presented a model based on the framework of continuous time random walk (CTRW). In this models particle transport in heterogeneous aquifer is represented as a random walk in space and time (*Berkowitz and Scher, 1998; Dentz and Berkowitz, 2003; Dentz et al., 2004*). *Dentz and Berkowitz (2003)* demonstrated that the mathematical formulation of MRMT is a special case of CTRW.

Neuman and Tartakovsky (2008); Berkowitz et al. (2006) present extensive review of the developed approaches to describe the evolution of the solute transport in porous media.

An interesting real case in which to evaluate these concepts is the MADE experimental site (*Adams and Gelhar, 1992*). Some transport models have been developed used a fine grid-cells entire domain to capture the aquifer heterogeneity. For example, *Salamon et al. (2007)* improved a geostatistical interpretation of the flowmeter data, and concluded that the ADE model is capable of describe the extensive tracer spreading, when small-scale variability of hydraulic conductivity is modeled at the flowmeter measurement support scale. *Barlebo et al. (2004)* using inverse flow and transport modeling obtained the same results, however the effective hydraulic conductivities product of the calibration phase were 5 times higher than the measured in the field using the flowmeter. *Harvey and Gorelick (2000); Feehley et al. (2000)* used the dual-domain mass transfer model to explain the solute transport at the MADE site. Both work compare the mass transfer model with ADE.

Feehley et al. (2000) used the ordinary kriging and conditional simulation based on fractional Brownian motion to represent the hydraulic conductivity, and calibrating the mass transfer coefficient and the immobile porosity reproduced the shape of mass plume. *Harvey and Gorelick (2000)* developed a transport model to recreate one-dimensional concentration profiles observed using ADE and an analytical homogeneous solution of mass transfer model. Results of both work indicate that including mass transfer effects can largely improve the performance of solute transport in comparison with the macrodispersive model.

Another approach used to simulate the anomalous transport behavior at MADE site is continuous time random walk model (*Berkowitz and Scher, 1998*). This model was able to reproduce the anomalous breakthrough curves and the non-Gaussian shape of tracer plume observed in the complex geological environment of MADE site.

Riva et al. (2008) analyzed the solute transport at the Lauswiesen forced-gradient trace test experiment. This study consists of a stochastic Monte Carlo analysis to evaluate the structure the heterogeneity of the aquifer and the application of the numerical transport models to represent the advective, advection-dispersion and mass transfer process to recreate the tailed multilevel breakthrough curves, and conclude the same as *Salamon et al. (2007)* on the fact that the ADE can describe the behaviour transport anomalous at a small support scale combined with a high-resolution description of heterogeneity.

In a practical application of flow and solute transport we used models that employ coarse computational grid and large effective transport coefficients obtained from the interpretation of a tracer test or compute some spatial average of the concentration field that are distributed uniformly over the entire domain

or assigned homogeneous zones of aquifer. In this context various researchers [e.g. (*Guswa and Freyberg, 2002; Carrera et al., 1998; Zinn and Harvey, 2003; Liu et al., 2004; Willmann et al., 2008; Riva et al., 2008*)] have shown that the description of behaviour of non-reactive solute transport observed in heterogeneous medium is better simulated at large scale using upscaled mass transfer models. In this framework, the scope of this work is to evaluate the use of MRMT as the constitutive transport model to simulate the large scale behavior of solute transport within a given area. Performance assessment of the alternative transport equation is achieved by comparing transport simulations of a non-reactive solute plume at two different support scales.

We simulated the solute transport at smallest scale to obtain a representative set of the reference solutions, in this case the transport solution is defined on the basis of a local ADE. At coarse scale we use as alternative transport model based on the form of the memory function of a discrete series of mass transfer rate with two immobile domains (double-rate).

Solute transport at large scale consists of a phenomenological model based on the memory functions that are used to represent the unresolved processes taking place within each homogenized block of the numerical model. The parameters associated with the memory functions are determined by transferring the small scale information on aquifer attribute into the computational scale defined by the numerical model discretization.

In this work, the numerical simulation at large scale the aquifer domain is discretized into computational scale and assigned of parameters associated with the memory function to each of these blocks. Then, to simulate solute transport the aquifer at large scale is not completely homogenized as other studies about solute transport upscaling reported in the literature (e.g., *Harvey and Gorelick, 2000; Zinn and Harvey, 2003; Willmann et al., 2008*)

4.2 Solute transport experiments

4.2.1 Experimental Design

We consider a synthetic case to simulate a typical field tracer test, where the mass of solute is introduced instantaneously into a steady-state flow field at an injection point. The flow domain in two-dimension has an extension of 240 units in each side. The aquifer is confined and under steady-state flow and uniform flow. No-flow boundary conditions were fixed on the top and bottom limits while constant head boundaries on the other sides imposed a mean hydraulic gradient equal to 0.01 along x .

The aquifer is heterogeneous with respect to transmissivity T , and represented considering $\ln T = G(\mathbf{x})$. $G(\mathbf{x})$ is assumed isotropic at the small support scale and is represented with a resolution of 240 x 240 pixels of 1 unit

size. The transport experimental consist in a realization of transport simulation obtained by generating unconditional stochastic realization of $G(\mathbf{x})$.

Here, two different sizes of upscaled block were defined in the spatial discretization of domain at coarse scale. Hence, the upscaling process consist in transferring from fine-scale information (240 x 240 cells) to regular computational grid of 48 x 48 and 16 x 16 regular homogeneous blocks, corresponding a size of square block of 5 and 15 cells, respectively.

The antilog of $G(\mathbf{x})$ at coarse scale is represented by a diagonal tensor T^v . We applied the Simple Laplacian with skin to compute T^v (Gómez-Hernández, 1991; Wen and Gómez-Hernández, 1996). Essentiality, for a given realization of $G(x)$, the grid-block being upscaled is isolated from the rest of the blocks in the aquifer. This area comprises the grid-block plus a skin region. The skin is used to represented approximately the realistic boundary conditions on the grid-block without having to solve the flow problem for the entire domain. Wen and Gómez-Hernández (1996); Renard and de Marsily (1993); Sánchez et al. (2006) presented a extensive review of the different methods for hydraulic conductivity upscaling.

In this study the skin was arbitrarily set to 12 units in each direction of the block. In each numerical experimental we considerate at local scale the simulate the simple process transport purely advective.

4.2.2 Reference transmissivity field

The performance of upscaled models are compared for three different environment scenarios test. We simulate flow and transport through an aquifer complex geological formed by high or low conductive lenses embedded into a heterogeneous background material. Among the 3 scenarios, the material M_1 and M_2 represents background material and a lenses family, respectively. In different scenarios, we vary the background material and the value of transmissivity assigned to M_2 . The orientation of the lenses family we have chosen to align to the head gradient with the x axe in the simulations.

The lenses family was obtained employing a binary random function. The binary function is defined as

$$I(\mathbf{x}) = \begin{cases} 1 & \mathbf{x} \in M_2 \\ 0 & \text{otherwise} \end{cases} \quad (4.1)$$

The volumetric proportion of material M_2 , denoted as p_2 , defines the mean and variance of the indicator random variable, respectively written as $\langle I(\mathbf{x}) \rangle = p_2$ and $\sigma_I^2 = p_2 p_1$, where p_1 is the volumetric proportion of M_1 ($p_1 = 1 - p_2$). We consider that the lenses family (material M_2) occupies 20% of the domain, i.e., $p_2 = 0.2$ and $p_1 = 0.8$. The indicator variable was further characterized with an anisotropic covariance function,

$$C_I(|\mathbf{r}|) = \sigma_I^2 \exp \left(-\sqrt{\left(\frac{r_x}{\lambda_x^I}\right)^2 + \left(\frac{r_y}{\lambda_y^I}\right)^2} \right) \quad (4.2)$$

where λ_x^I and λ_y^I are the longitudinal and transverse correlation scales of the indicator variable set to 16 units and 1 unit, respectively.

The background fields $G_1(\mathbf{x})$ were generated using a sequential Gaussian simulation program, GCOSIM3D (Gómez-Hernández and Journel, 1993), whereas the lenses family $I(\mathbf{x})$ generated using an indicator sequential simulation program ISIM3D (Gómez-Hernández and Srivastava, 1990).

The stochastic generation of $G_1(\mathbf{x})$ and $I(\mathbf{x})$ was performed independently, assuming $G_1(\mathbf{x})$ and $I(\mathbf{x})$ are not correlated. The composite media is finally obtained from $Y(\mathbf{x}) = (1 - I(\mathbf{x}))G_1(\mathbf{x}) + I(\mathbf{x})G_2$. Figure 4.1 illustrates the steps involved in the stochastic generation of the composite random field for a given realization of $G(\mathbf{x})$ in each case.

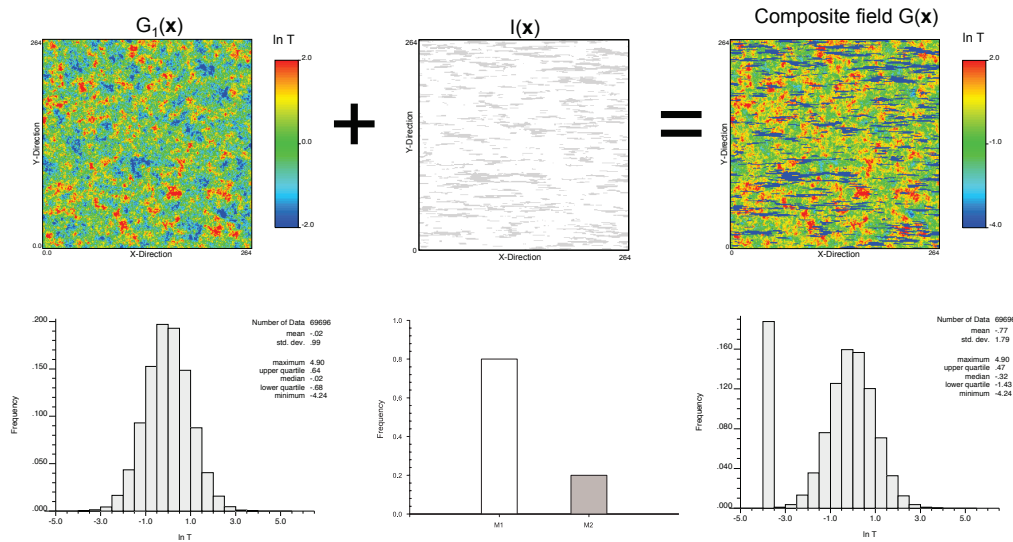


Figure 4.1: Representation of the steps involved in the stochastic generation of composite transmissivity field.

All background fields have the same geometric mean of one. The first field of background material M_1 is heterogeneous and described by a transmissivity characterized with a multi-Gaussian distribution following an anisotropy exponential covariance function.

$$C_{G_1}(|\mathbf{r}|) = \sigma_{G_1}^2 \exp \left(-\sqrt{\left(\frac{r_x}{\lambda_x^{G_1}}\right)^2 + \left(\frac{r_y}{\lambda_y^{G_1}}\right)^2} \right) \quad (4.3)$$

where $\mathbf{r} = (r_x, r_y)$ is the separation vector between two points of the aquifer, $\sigma_{Y_1}^2$ is the variance of $G_1(\mathbf{x}) = \ln T_1(\mathbf{x})$ assumed as 9, and $\lambda_x^{G_1}$ and $\lambda_y^{G_1}$ are the longitudinal and transverse correlation scales set to 40 and 4 units, respectively. Figure 4.2 display the realization of $G_1(\mathbf{x})$ for first scenario of M_1 .

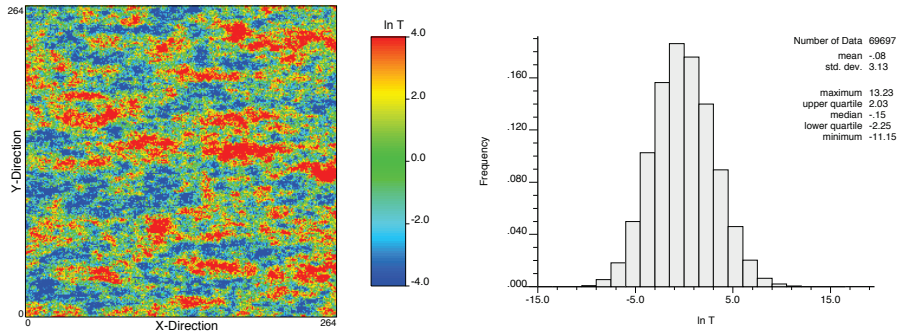


Figure 4.2: Illustration of the realization of the reference natural log of transmissivity $G_1(\mathbf{x})$ of M_1 of the first environment

The second field of $G_1(\mathbf{x})$ associated to M_1 is characterized with a multi-Gaussian distribution following an isotropic exponential covariance function.

$$C_{G_1}(|\mathbf{r}|) = \sigma_{G_1}^2 \exp \left(-\frac{|\mathbf{r}|}{\lambda} \right) \quad (4.4)$$

where the correlation scale set to 4 units. $G_1(\mathbf{x})$ of M_1 . The field exhibit a mean of zero and a variance of one as shown in the figure 4.3.

In all environment scenarios test we considered that the variation within G_2 is of minor importance compared with the contrast between G_1 and G_2 , and we therefore assigned a constant log transmissivity value to M_2 of 2.0 and -4.0 in the scenarios 1 and 2 respectively. Figure 4.4 is shown the composite random field for first scenario considered in this work. The frequency distribution and univariate statistical of the values set are provides in the image of the histogram plotted on the right side. The semivariogram of $\ln T$ for the x and y directions are illustrated in figure 4.5. For reference the first composite field the integral scale in the x and y directions are $\lambda_x^G = 32.8$ units and $\lambda_y^G = 3.2$ units for the anisotropic exponential model fit.

Figure 4.6 illustrates the comparison of the cumulative breakthrough curves obtained at given x - control plane using the realization of composite random

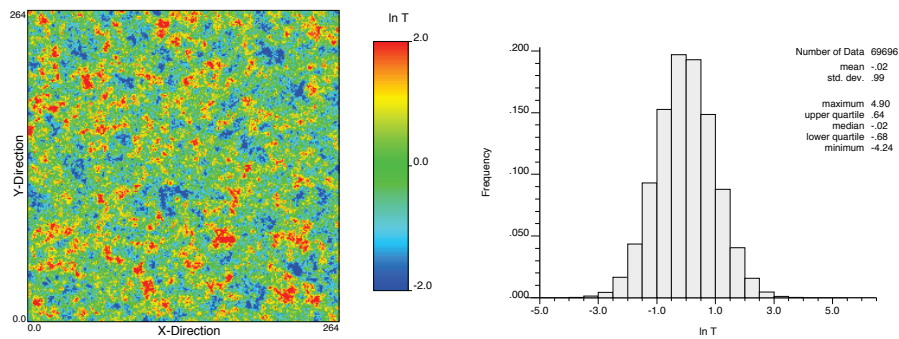


Figure 4.3: Illustration of the realization of the reference natural log of transmissivity $G_1(\mathbf{x})$ of M_1 of the second environment

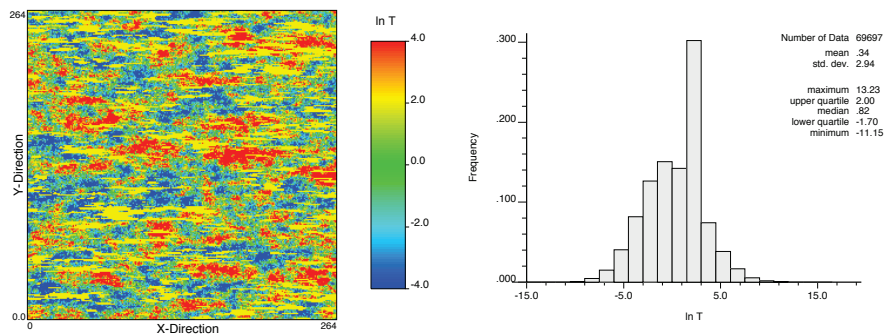


Figure 4.4: Transmissivity structure and histogram for the first composite field.

field $G(\mathbf{x})$ and $G_1(\mathbf{x})$ for the scenario 1. We observed that the the solute transport behaviour for $G_1(\mathbf{x})$ is clearly different than that the observed for $G(\mathbf{x})$. Note different substantial between the slope late-time behavior observed for both cases.

The second composite transmissivity field considered in this work is shown in figure 4.7. The field exhibit a mean of -0.77 and a variance of 3.2 . The semivariogram of $\ln T$ for the x and y direction are illustrated in figure 4.8. The integral scale in the x and y directions are $\lambda_x^G = 7.0$ units and $\lambda_y^G = 2.0$ units for the anisotropic exponential model fit.

Cumulative mass flux breakthrough curves obtained using the realization of $G_1(\mathbf{x})$ is compared with those obtained with the associated second composite transmissivity field in figure 4.9 for travel distance of $x = 159.9$ units. Note the big different between transport behaviour observed for $G_1(\mathbf{x})$ and $G(\mathbf{x})$

A third field test was build by transformation of the second field. The transformation consist in multiplying by -1.0 the values of $\ln T$ that form the

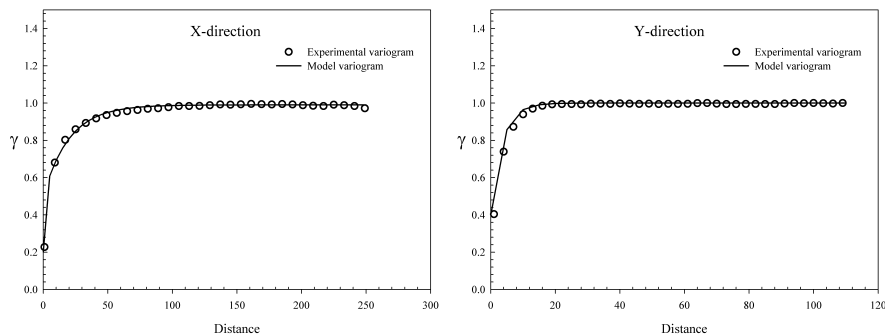


Figure 4.5: Experimental variogram and model variogram as inferred from to realization of the first scenario for the x and y directions.

second composite random field. The field is shown in figure 4.7. The integral scale in the x and y directions for field 3 are the same that its associated field 2. Figure 4.11 provide examples of the cumulative mass flux breakthrough curves obtained at a given x-control plane ($x = 159.90$ units) using second and third composite fields. For field 3, where the solute particles is traveling faster than through field 2, this reflect that high values of transmissivity are connected.

The crucial point about the composite transmissivity fields is, that they present different hydrogeologic character, which is important in order to illustrated the influence of high and low conductivity zones features and how they can be captured by the block equivalent parameters associated to the upscaled models.

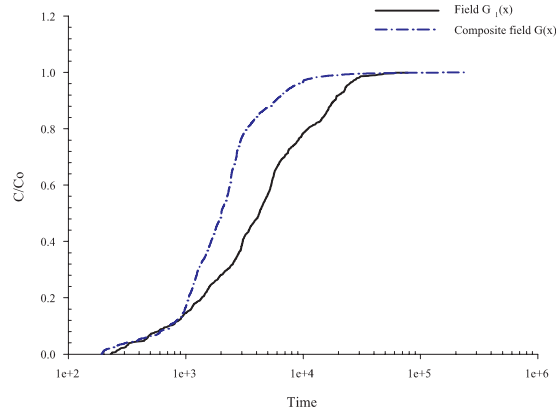


Figure 4.6: Cumulative mass flux breakthrough curves obtained at a given x -control plane ($x = 159.9$ units) using the realization of the transmissivity field $G_1(\mathbf{x})$ and its associated the first composite medium $G(\mathbf{x})$

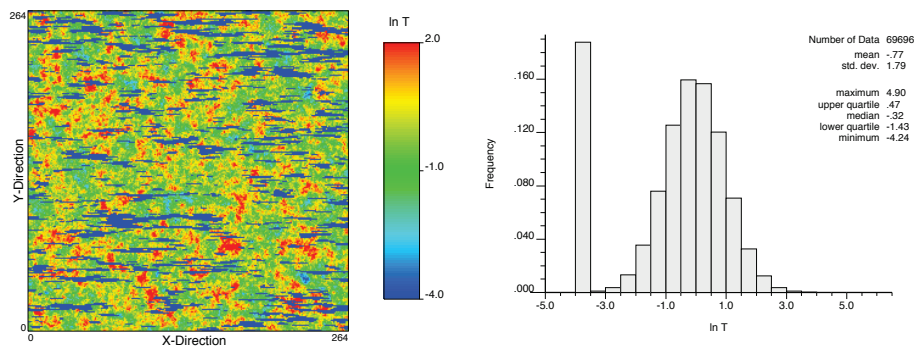


Figure 4.7: Transmissivity structure and histogram for the second composite field.

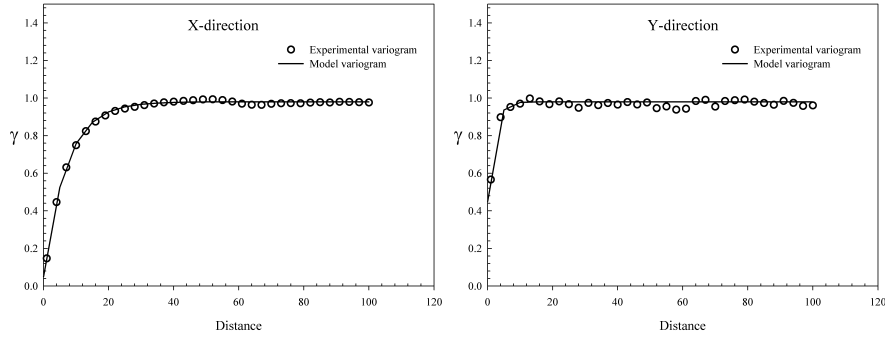


Figure 4.8: Experimental variogram and model variogram as inferred from to realization of the second composite field for the x and y directions.

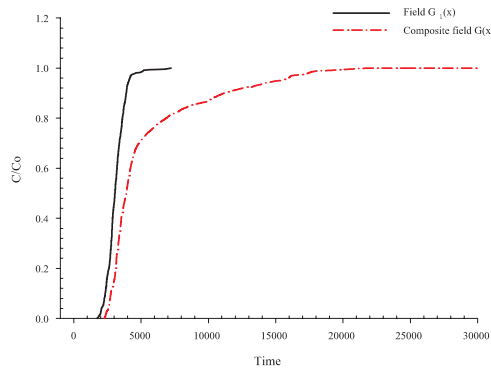


Figure 4.9: Cumulative mass flux breakthrough curves obtained at a given x -control plane ($x = 159.9$ units) using the realization of the transmissivity field $G_1(\mathbf{x})$ and its associated second composite medium $G(\mathbf{x})$ for field 2.

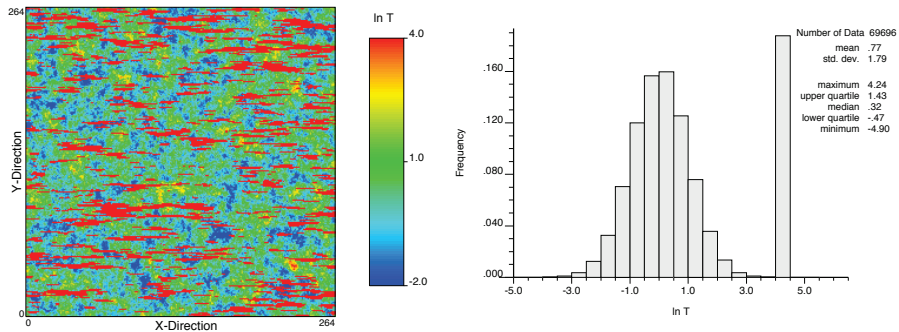


Figure 4.10: Transmissivity structure and histogram for the third composite field.

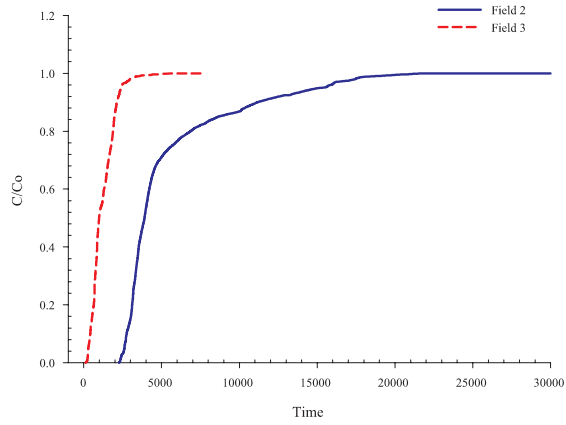


Figure 4.11: Cumulative mass flux breakthrough curves obtained at a given x -control plane ($x = 159.9$ units) using the realization of the transmissivity composite field 2 and its associated composite field 3.

4.2.3 Flow and transport solution

Three type of numerical grids are used to simulate the flow and solute transport: a fine grid with 1 unit side square cells that provides the reference solution and two coarse grid with 5, and 15 units side square grid-blocks respectively that are used to model transport at large scale using upscaled mass transfer model (see figure 4.12). The fine-grid is designed on the basis of the discretization of the spacial distribution of transmissivities.

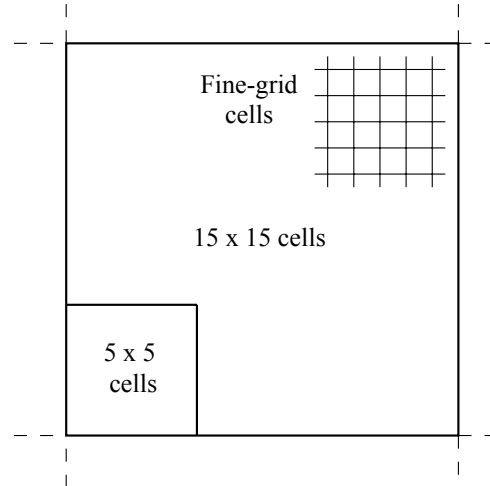


Figure 4.12: Different size of blocks used to change of scale of the reference $G(\mathbf{x})$ field

The flow problem was solved with MODFLOW2000 (*Harbaugh et al.*, 2000) at both scale. The solute transport was solved with random walk particle tracking code RW3D (*Fernández-García et al.*, 2005a,b; *Salamon et al.*, 2006). RW3D was used to simulate either conservative solute transport needed to obtain the reference solutions or solute transport coupled with multirate mass transfer to obtain the corresponding solution at large scale.

Simulation of solute transport with mass transfer is based on the particle tracking methodology presented by *Salamon et al.* (2007). Basically, transport is simulated by injecting a large number of mass particles into the system, each particle representing a small portion of the plume solute. Advection is simulated by moving particles along flowlines, whereas dispersion is emulated by a Brownian motion. Mass-transfer process are efficiently incorporated by switching the state of the particles between mobile/immobile states according to appropriate transition probabilities.

In each case we simulated the behaviour of the released solute for a period of time, $t = 3000$. For this purpose 40,000 particles, where each particle was

assigned the same mass, and were uniformly distributed over the 15 x 150 units rectangular source area is indicated in the figure 4.13. For each movement, the time step was adapted based on a grid Courant number of 0.01 (*Wen and Gómez-Hernández, 1996*).

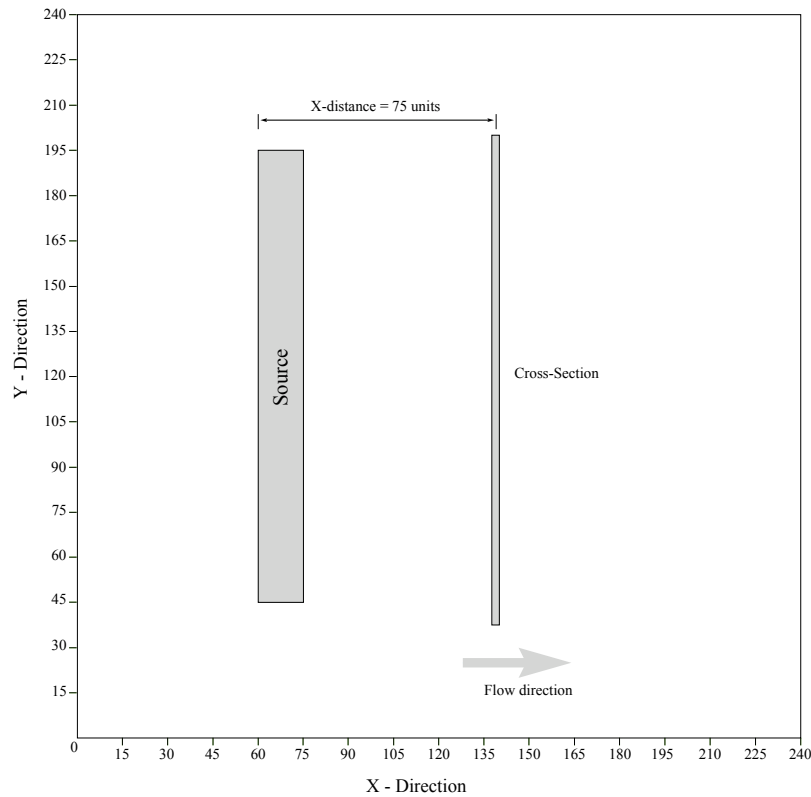


Figure 4.13: Plan view of the location of source and a transverse cross section. Cross-section indicate the location used to display temporal evolution of mass profiles at x-distance 75 units from injection point.

4.2.4 Flow and transport parameters

Transport parameter values to each grid-block are obtained with the upscaling technique presented in chapter 3. The new technique consist in replacing each block with heterogeneous transmissivity by a homogeneous block, in which the parameters associated to the memory function are used to represent the unresolved mass exchange between highly mobile and less mobile zones occurring within each block. Block transport parameters are estimated through the interpretation of the residence time distribution of particles passing through a given block using fine-scale simulations.

4.3 Results and discussion

4.3.1 Overview of plume behavior

The spatial distribution of solute mass obtained at $t = 300$ after the release for the upscaled models using the size of block of 5×5 and 15×15 cells are presented in figures 4.14 and 4.15, respectively. They show the same solute plume discretized on two different scales. The reference corresponds "true" plume obtained at fine scale, and the coarser grid to some large-scale representation of the same plume simulated by upscaled models. The representation of solute plume at coarse scale and fine scale were obtained by accounting over a fine grid with 1 unit side square cells. Then the tracer mass for each cell was calculated a total of particles, where each particle was assigned the same mass, was allocated according to the total amount of mass in each cell.

For completeness, the double rate mass transfer models is contrasted against the standard macrodispersive transport models. The macrodispersive model is determined by simply using the macrodispersion coefficient in equation alternative of transport without mass transfer process.

Since the solution of transport in either of these examples test is purely advective at local scale, the solute spreading is due entirely to the heterogeneity in the composite transmissivity fields. One can see after the release the solute mass display that behavior of the transport solute is non-Fickian at local scale for the three composite fields test. The solute mass travel through preferential zones narrow paths, which are controlled by the attribute of heterogeneity causing the variations of velocity. Another characteristic of plume at local scale is that display a shape highly asymmetric. Note, the solute plume associated to the second field present a shape regular.

The solute plume simulated with the upscaled models are smoothing and display more spreading in comparison than reference solution. Note, for all test case, the plume simulated by upscaled models exhibit larger spreading that the reference solution. In general, the fine structure of aquifer heterogeneity, that generated velocity fluctuations at small scale, are explicitly included in the upscaled models. Note, however, that the velocity variations cause by those fine structure for the reference solution are seen in the upscaled models results when the size of block used is 5×5 cells, whereas that the results associated with the size of block of 15×15 cells, the solute plume displays a greater dilution.

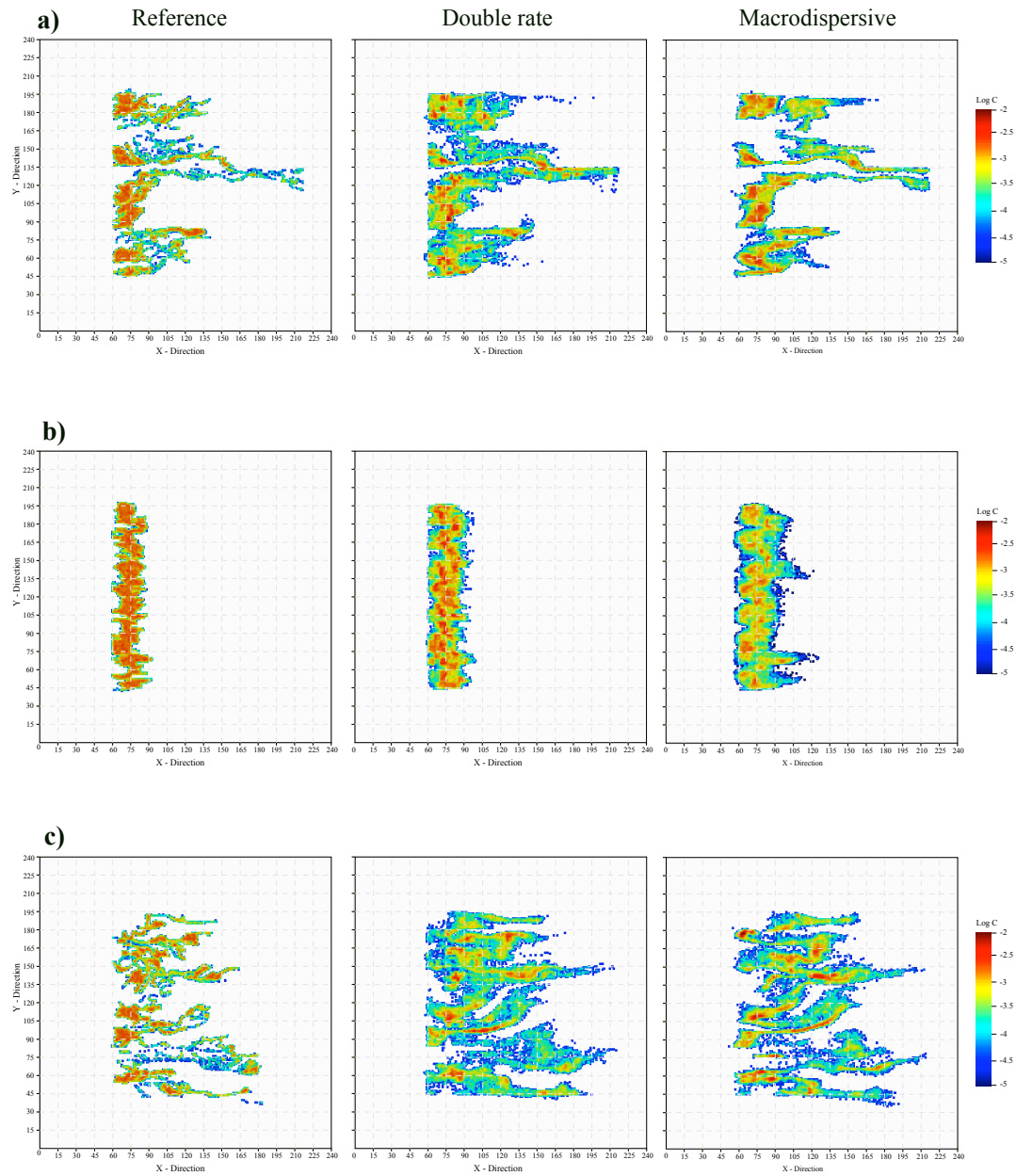


Figure 4.14: Solute log concentration plume simulated for different upscaled models at $t = 300$ using a size of block 5 cells and corresponding the reference solution for the three cases of composite field. (a) case of the first scenario, (b) case of the second scenario and (c) case of the third scenario.

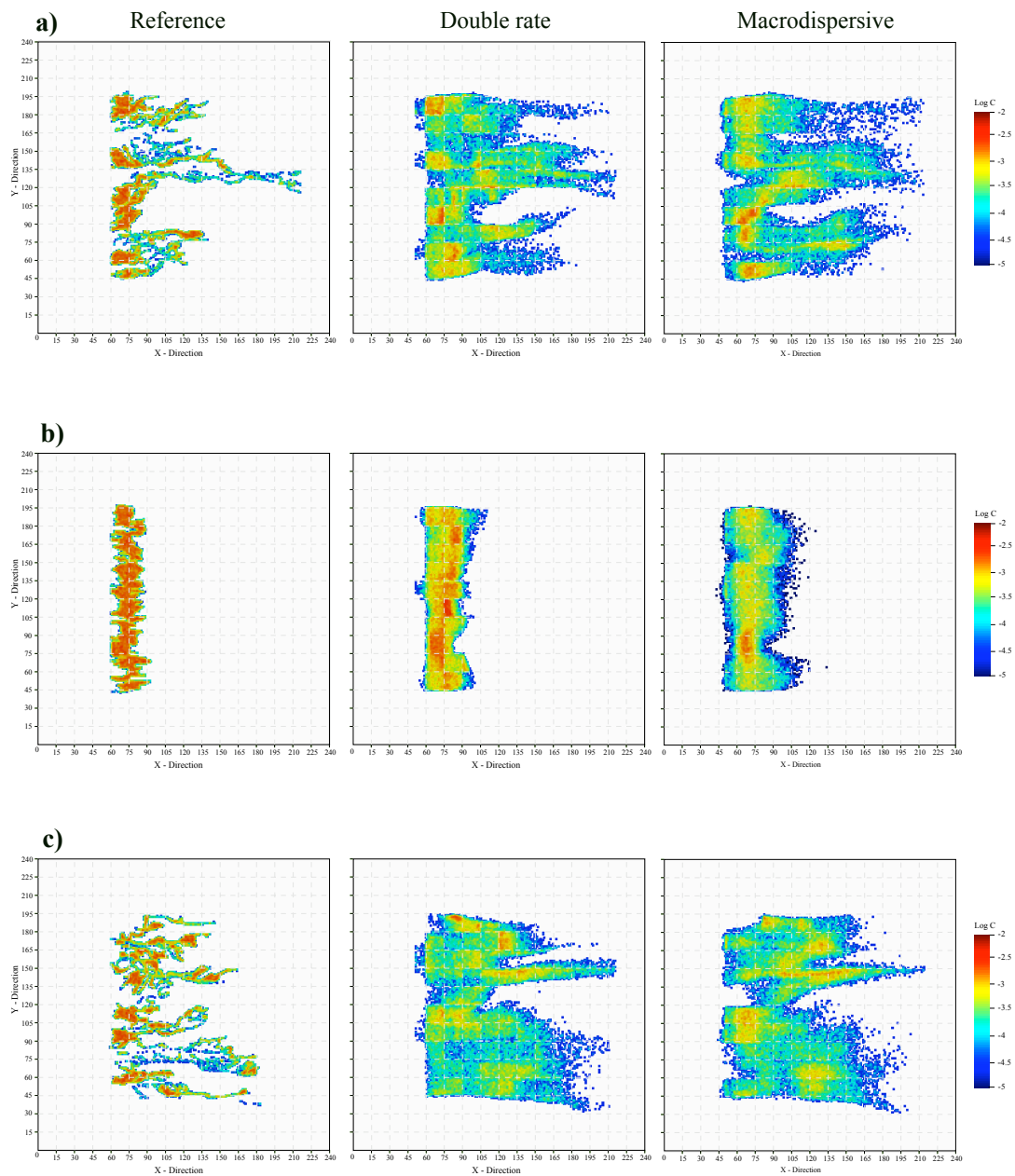


Figure 4.15: Solute log concentration plume simulated for different upscaled models at $t = 300$ using a size of block 15 cells and corresponding the reference solution for the three cases of composite field. (a) case of the first scenario, (b) case of the second scenario and (c) case of the third scenario

Applying the concept of relative entropy we measure the performance of upscaled models. The relative entropy is a measure of the difference between two distribution p and q over the same space (Kullback, 1959). For a set of n blocks the relative entropy (**RE**) between two distribution of particles is defined

$$\mathbf{RE}(t) = \sum_{i=1}^n p_i \ln \frac{p_i}{q_i} \quad (4.5)$$

where the frequencies q_i and p_i are computed from the sample number particles located within of a block n_i associated with each plume outcomes as $q_i = n_i/N_p$, N_p is the total number of particles found within the system flow at a given time, i.e. a snapshot. **RE** is zero only when two distribution of particles are identical.

RE computed for each of the three cases test are presented in figure 4.16 for two size of blocks used in the spatial discretization at coarse scale. In each case, **RE** is estimated based on the representation of solute plume at coarse scale and fine scale were obtained by accounting over a square fine-grid formed by 240 x 240 blocks of 1 unit side.

In the first and third cases, the comparison of the temporal evolution of **RE** associated double rate and macrodispersion shows in figure 4.16. Since, **RE** is a measure of the lack of fit, a value of **RE** close to zero implies that the fit is perfect. This plot indicates that the representation solute plume at coarse scale through double rate or macrodispersion predict the same results when the size of block used is 15 x 15 cells. However, from these figure one can see that, in the first case macrodispersion is better than double rate, whereas in third case double rate does as well, when the size of block is 5 x 5 cells.

In the second case, the temporal evolution of **RE** shows that the fit of the double rate to the reference solution is better than observed for the macrodispersion model for two size of blocks. This indicates the coarse grid representation of the behaviour of the solute mass plume with double rate for this case is accept as an well description some scale.

The examples of composite test are characterized by large, eccentric, very low or high conductivity lenses oriented in direction to the flow mean direction. The models given comparable results in case of the first and third scenario, because the nature of behaviour transport around the lenses produce spreading that the macrodispersion and double rate can reproduces at large scale. However, in the case of second scenario the transport is controlled the low transmissivity values gives rise behaviour that is describe well by double rate.

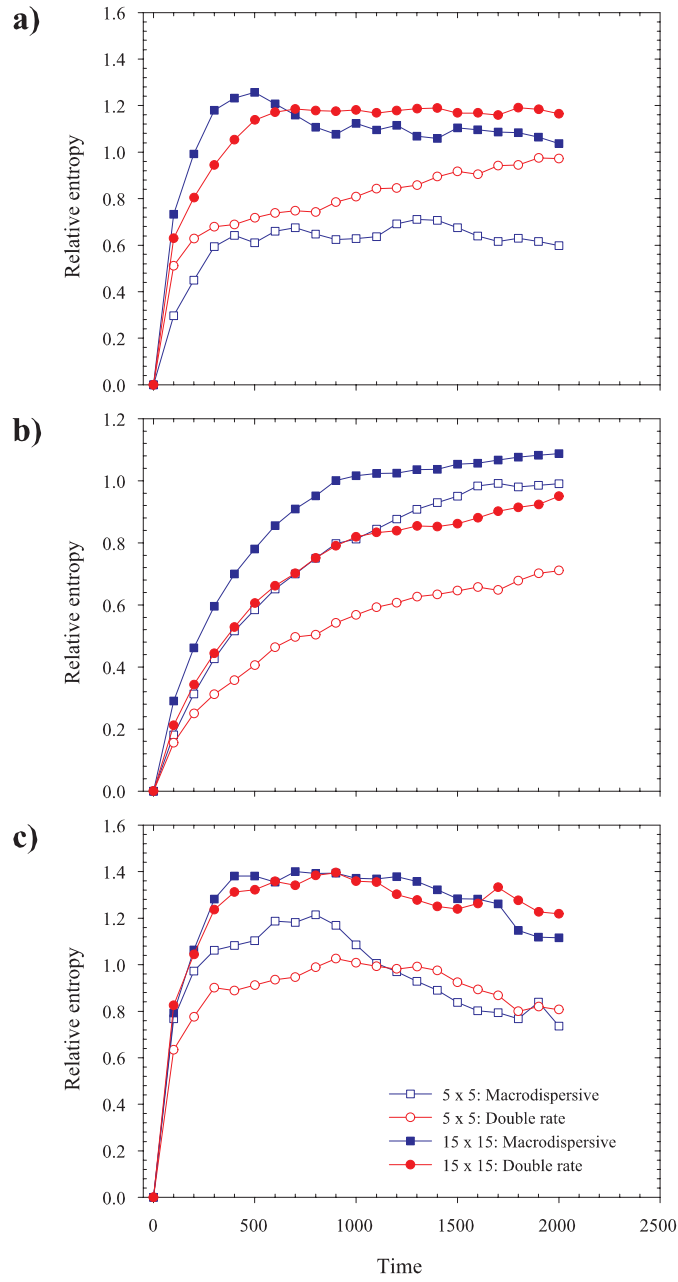


Figure 4.16: Comparison of the temporal evolution of relative entropy of double rate and macrodispersion models for the three cases test.

4.3.2 Longitudinal distribution mass profile

In the following section, longitudinal mass profiles of the reference solution and the simulated plumes by upscaled models at two elapsed times after injection are compared. In each case the mass profile was obtained by integrating the mass of 240 equally step sizes each of 1 unit of width along Y - direction and normalizing it by the total injected mass.

Figures 4.17 and 4.18 plots the longitudinal mass distribution profiles at times $t = 300$ and $t = 600$ after the release for two different support scale. These plots represent the value obtained from the simulations with transport realizations of each model. From these graphics we can see that the shape of the mass profiles of the reference solution at both times is better reproduced by the upscaled models associated to double rate in comparison to macrodispersive as shown in figure of the case of the second scenario, where the mass profile of reference is described well by the double rate. The profile calculated by the macrodispersive model display a back dispersion, which is not physically possible, since the particles displace opposite to flow direction.

Figure 4.19 shows the performance of upscaled models in term of the temporal evolution of mass profiles sampled from a cross sections to the mean flow direction and located at x -distance = 75 units from the injection point. In each case the mass profile was obtained by integrating the normalized mass cross the section a given time, i.e. a shapshot..

The results shown in figure 4.19 illustrated that upscaled models represent by double rate provide a better description of the temporal evolution of mass profile of reference at cross sections. Note, however, the peak and tails are not matched exactly. We see that mass profiles obtained from the results of macrodispersive model for case the second scenario present very little solute passes over the period of simulation through the fraction of the domain of sampled. Indicating that the plume simulated by macrodispersive model with macrodispersion coefficient assigned in big homogeneous blocks to describe the spreading effects of aquifer heterogeneity gives rise a retardation greater that in case of the double rate model.

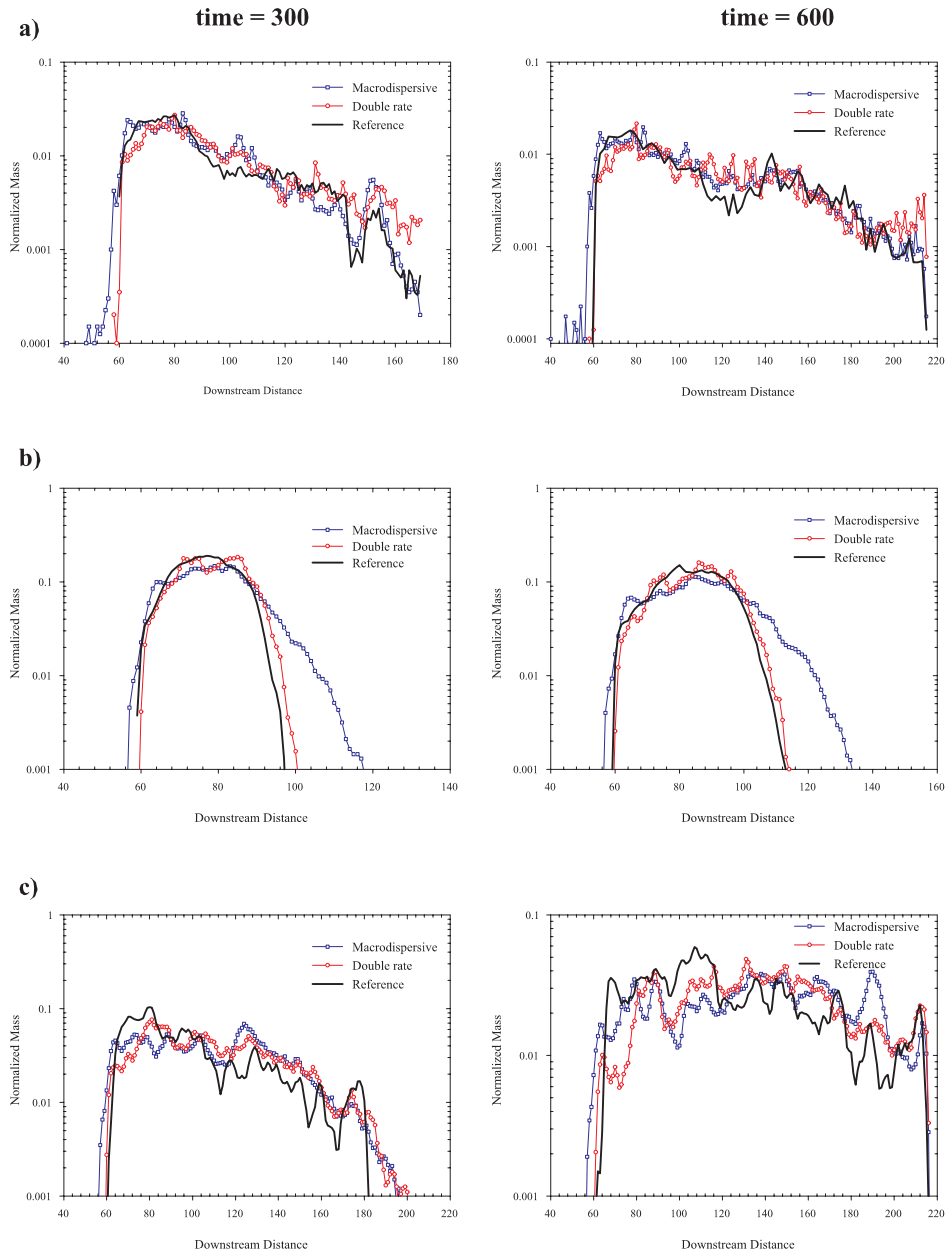
4.3.3 Dilution Index

Here, we analyzed the relative aquifer volume occupied by the solute plume. The dilution index is a quantitative measure of the plume structure, which can help us to evaluate the capability of upscaled models.

The dilution index is proposed by (*Kitanidis*, 1994) and it is expressed by

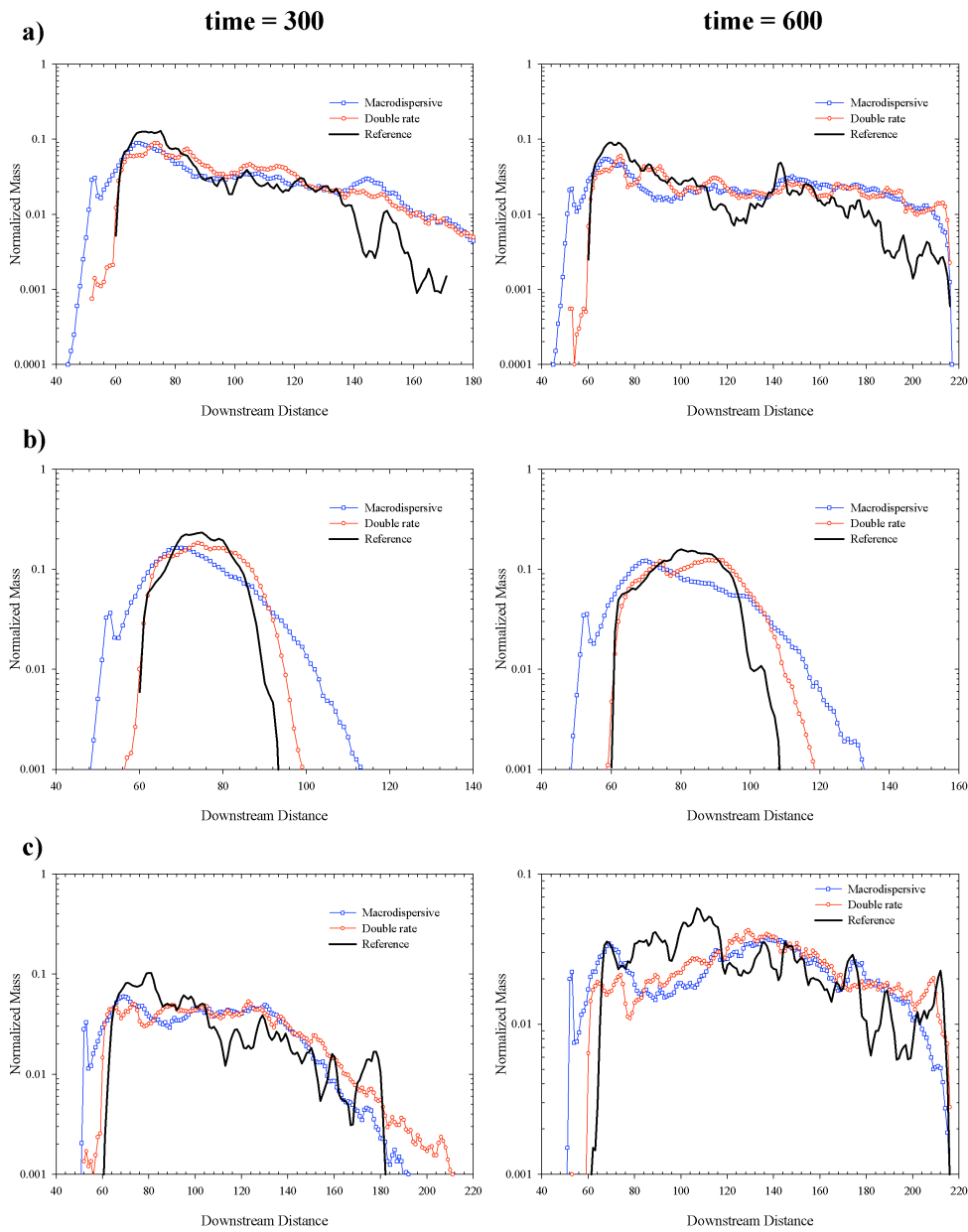
$$I = \frac{E(t)}{E_{max}} \quad (4.6)$$

where $E(t)$ for a set of m blocks is expressed as



Size of block: 5 cells

Figure 4.17: Longitudinal mass distribution profiles of the reference solution and predictions using double rate with those associated with macrodispersive models corresponding at time $t = 300$ (left column) and $t = 600$ (right column). Row a), b) and c) corresponding to the 5×5 upscaled case 1, case 2 and case 3 of the scenarios of composite field test, respectively. Injection point at $x = 60$ units



Size of block: 15 cells

Figure 4.18: Longitudinal mass distribution profiles of the reference solution and predictions using double rate with those associated with macrodispersive models corresponding at time $t = 300$ (left column) and $t = 600$ (right column). Row a), b) and c) corresponding to the 15 x 15 upscaled case 1, case 2 and case 3 of the scenarios of composite field test, respectively. Injection point at $x = 60$ units

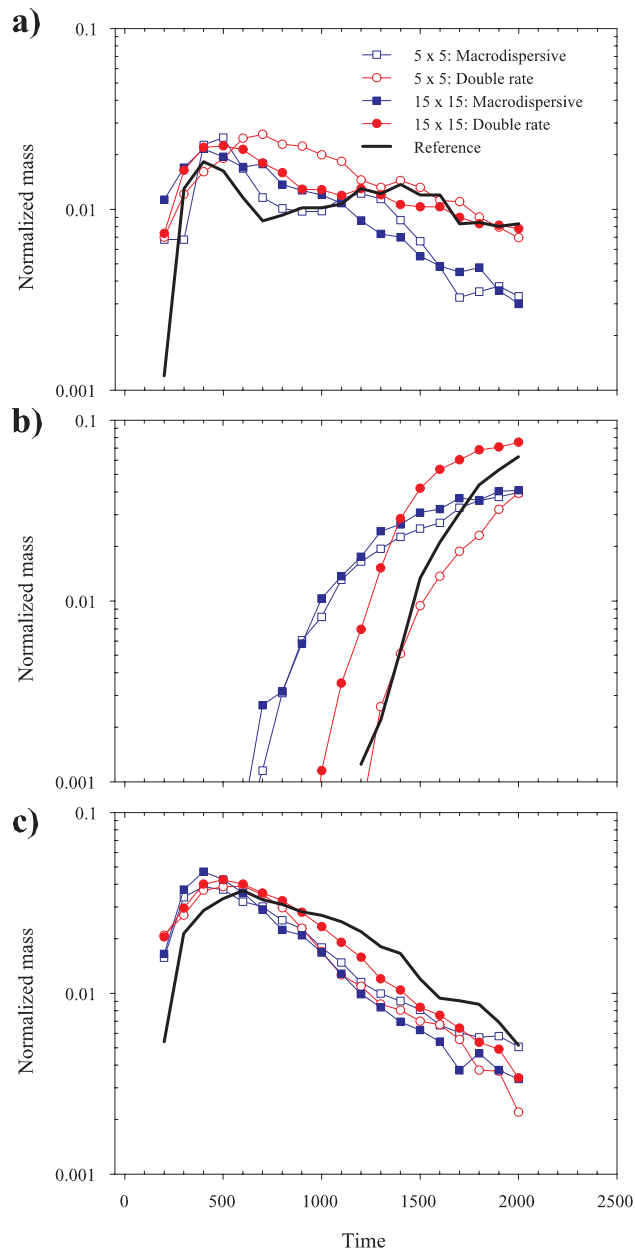


Figure 4.19: Comparison of the temporal evolution of normalized mass at a given location downstream from the injection point $x = 75$ units for double rate with those associated with macrodispersive models versus the reference solution: (a) case of the first scenario, (b) case of the second scenario, and (c) case of the third scenario of composite field test.

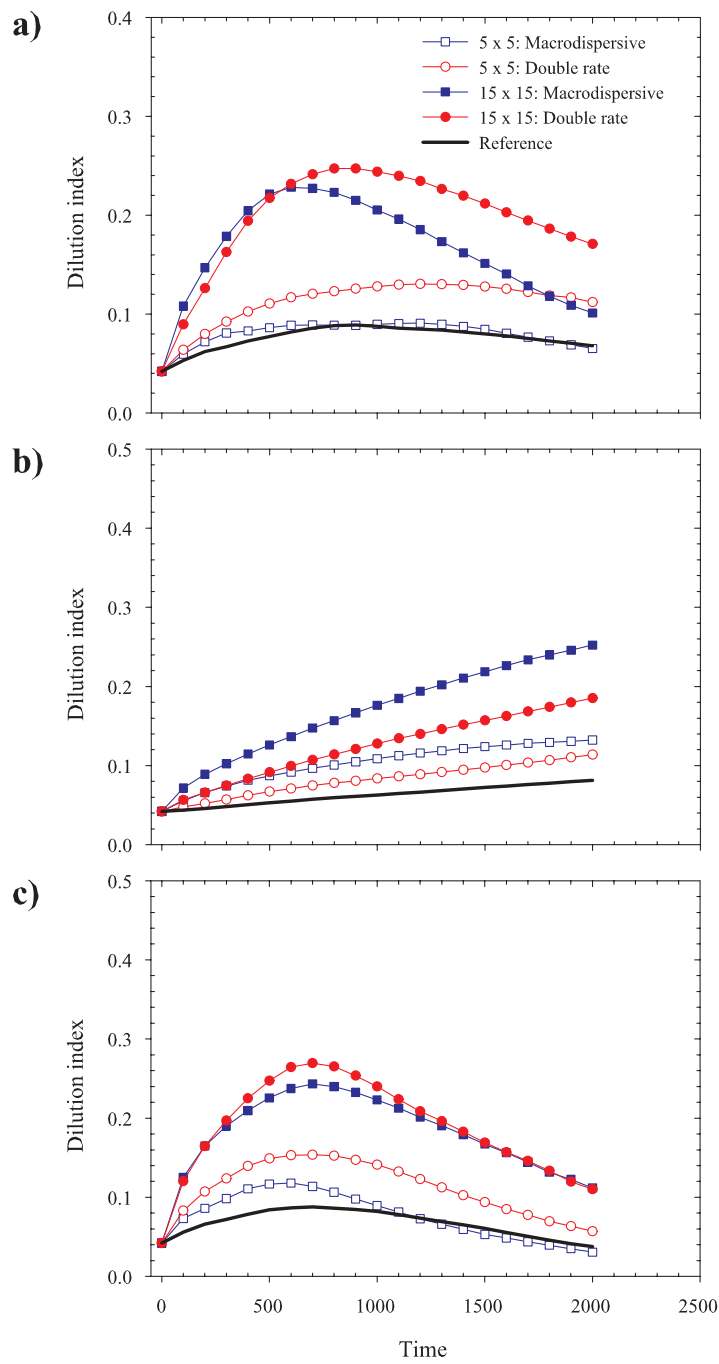


Figure 4.20: Comparison of the temporal evolution of the dilution index

$$E(t) = \Delta V \exp \left[- \sum_{k=1}^m P_k(t) \ln(P_k(t)) \right] \quad (4.7)$$

where $P_k(t)$ is the ratio of the mass of solute in a region volume ΔV of the system to total mass of solute in the aquifer at time t . In a practical point view I expressed the ratio of volume occupied by the mass solute in a region to the total aquifer volume at time t . Thus, values of I near 1 indicate complete dilution, whereas values near 0 that the mass solute is nonuniform distributed in the porous media.

Figure 4.20 displays the behaviour of I as function of time for double rate and macrodispersive models. These I values plots in the figure, I obtained from the simulations of transport realizations in each case. In each case the dilution index was obtained using a square grid with a resolution of 240 x 240 cells of 1 unit size.

We can see that the mean value associated with the reference solution is less than 0,15, and at larger times decreases to values near to 0.1, since part of the solute mass is out of system. In contrast the solute mass simulated by upscaled models display larger dilution in comparison to reference solution, and this behaviour reflect that the plume simulated at large scale displays greater dispersion due to partial homogenization of the attribute of the aquifer heterogeneity. Also, so far, the dilution increases with the scale over which local solute concentration fluctuate.

4.4 Summary and conclusions

We developed a numerical experiment to evaluate the ability of upscaled mass transfer models to reproduce the solute behaviour at large scale. The results of upscaled models were evaluated using simulations of solute transport considering three cases of scenarios of a complex geological system formed by high or low conductivity lenses embedded into an anisotropic and an isotropic back field. In particular, the solute plume simulated at local scale in each scenario has specific features due to aquifer heterogeneity.

Performance assessment of upscaled models is done by comparing transport simulations of non-reactive solute plume at two different different support scales. First, we simulated the solute transport at a smallest scale to obtain a set of reference solutions. At large scale, the formulation double rate of mass transfer model is evaluated as an alternative transport model. For completeness, the double rate mass transfer models is contrasted against the standard macrodispersive transport models.

In order to examine the performance of upscaled models we analyzed the results from two different perspectives. Diagnostic of performance of upscaled

models is provided by comparing of the behavior the solute mass plume at times after the releases in a single realization transport. The solute plume simulated in each case of scenarios investigated in this work, have traveled sufficiently far to sample a wide range of aquifer heterogeneity, both at fine scale and large scale. We have observed that the transport simulation with upscaled models do not accurately recreated the asymmetric shape of the spatial distribution of solute mass observed at smallest scale. Note, however, in the cases of the second scenario, double rate can describe well the main features associate with solute plume of reference solution.

Otherwise, the results showed that representation of solute transport at computational scale with upscaled models based on the memory functions that is used to represent the unresolved process yielded a good prediction of the description of the behaviour solute plume in comparison to macrodispersive model. However, a part of our numerical experiment shown that the effects of small scale aquifer heterogeneity can captured both double rate and macrodispersion models, at least if there is no large scale variability (scenario 1 and 3) In the first models a sink term to account for exchange of solute between mobile and immobile phases to describe the solute spreading, whereas the second model a macrodispersion coefficient accounts for the effect of aquifer heterogeneity on the solute spreading.

We observed that solute plume predictions using upscaled models presents greater dilution than the reference solution. Dilution at coarse scale is affected by sub-grid heterogeneity, then due to partial homogenization of the attribute of the aquifer heterogeneity the upscale model fail to reproduce some key features, especially the dilution of a plume. In general, large-scale features of a solute plume can not be reproduced by any upscaled transport model investigated in this work. The reason is that albeit the parameters associated to memory function are calibrated to replicate the residence time distribution of mass particles during the upscaling process the models at large scale present a lack of memory in space that caused the inability of reproduction of mass fluxes taking place at interface between two homogeneous block of upscaled model.

Bibliography

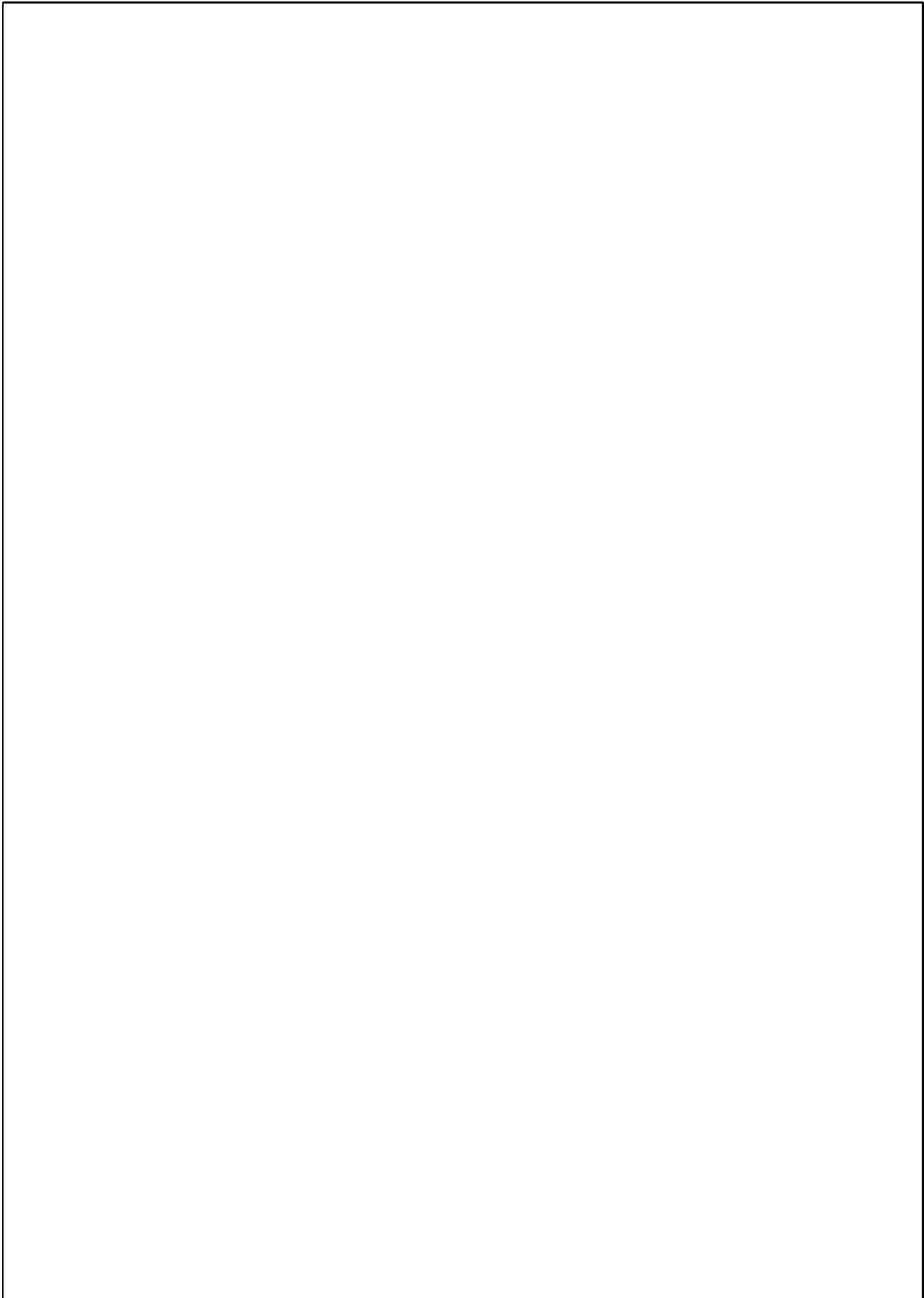
- Adams, E. E., L. W. Gelhar (1992), Field study of dispersion in a heterogeneous aquifer 2. Spatial moment analysis, *Water Resources Research*, 28(12), 3293–3307.
- Bajracharya, K., and D. A. Barry (1997), Nonequilibrium solute transport parameters and their physical significance: numerical and experimental results, *Journal of Contaminant Hydrology*, 24, 185–204.
- Barbelo, H. C., M. C. Hill, and D. Rosbjerg (2004), Investigating the Macrodispersion Experiment (MADE) site in Columbus, Mississippi, using a three-dimensional inverse flow and transport model, *Water Resources Research*, 40, W04211m doi:10.1029/2002WR001935.
- Berkowitz, B. and H. Scher (1998), Theory of anomalous chemical transport in random fracture networks, *Physical Review E*, 57(5) 5858–5869.
- Berkowitz, B. , H. Scher, and S.E. Silliman (2000), Anomalous transport in laboratory-scale, heterogeneous porous media, *Water Resources Research*, 36(1), 149–158.
- Berkowitz, B., A. Cortis, M. Dentz, and H. Scher (2006), Modeling non-fickian transport in geological formations as a continuous time random walk, *Reviews of Geophysics*, 44, RG2003, doi:10.1029/2005RG000178.
- Boggs, J. M., S. C. Young, and L. M. Beard (1992), Field study of dispersion in a heterogeneous aquifer 1. Overview and site description, *Water Resources Research*, 28(12), 3281–3291.
- Carrera, J, An Overview of uncertainties in modeling groundwater solute transport, *Journal of Contaminant Hydrology*, 13, 23–48.
- Carrera, J., X. Sánchez-Vila, I. Benet, A. Medina, G. Galarza, and J. Guimerà (1998), On matrix diffusion: formulations, solution methods and qualitative effects, *Hydrogeology Journal*, 6, 178–190.

- Cushman, J. H., and T. R. Ginn (2000), Fractional advection-dispersion equation: A classical mass balance with convolution-Fickian flux, *Water Resources Research*, 36(12), 3763–3766.
- de Marsily, G., F. Delay, J. Gol  sal  s, P. Renard, V. Teles, and S. Violette (2005), Dealing with spatial heterogeneity, *Hydrogeology journal*, 13, 161–183.
- Dentz, M., and B. Berkowitz (2003), Transport behavior of a passive solute in continuous time random walks and multirate mass transfer, *Water Resources Research*, 39(5), 1111, doi:10.1029/2001WR001163.
- Dentz, M., A. Cortis, H. Scher, and B. Berkowitz (2004), Transport behavior of solute transport in heterogeneous media: transition from anomalous to normal transport, *Advances in Water Resources*, 27, 155–173.
- Doherty, J. (2004), *Manual for PEST*, 5th edition, Brisbane, Australia: Watermark Numerical Computing.
- Feehley, C. E., C. Zheng, and F. J. Molz(2000), A dual-domain mass transfer approach for modeling solute transport in heterogeneous aquifer: Application to the Macrodispersion Experiment (MADE) site, *Water Resources Research*, 36(9), 2501–2515.
- Fern  ndez-Garcia, D., T. H. Illangasekare, and H. Rajaram (2005a), Differences in the scale-dependence of dispersivity and retardation factors estimated from forced-gradient and uniform flow tracer tests in three-dimensional physically and chemically heterogeneous porous media, *Water Resources Research*, 41, W03012, doi:10.1029/2004WR003125.
- Fern  ndez-Garcia, D., T. H. Illangasekare, and Harihar Rajaram (2005b), Differences in the scale dependence of dispersivity estimated from temporal and spatial moments in chemically and physically heterogeneous porous media, *Advances in Water Resources*, 28, 745–759.
- Fern  ndez-Garcia, D., H. Rajaram, and T. H. Illangasekare (2005c), Assessment of the predictive capabilities of stochastic theories in a three-dimensional laboratory test aquifer: Effective hydraulic conductivity and temporal moments of breakthrough curves, *Water Resources Research*, 41, W04002, doi:10.1029/2004WR003523.
- Fern  ndez-Garcia and G  mez-Hern  ndez (2007), Impact of upscaling on solute transport: travel times, scale-dependence of dispersivity and uncertainty, *Water Resources Research*, 43, W02423, doi:10.1029/2005WR004727, 2007.

- Gómez-Hernández, J. J., and Srivastava R. M. (1990), ISIM3D: An ANSI-C three-dimensional multiple indicator conditional simulation program, *Computer and Geosciences*, 16(4), 395–440.
- Gómez-Hernández, J. J. (1991), A stochastic approach to the simulation of block conductivity fields conditioned upon data measured at a smaller scale, Ph.D. thesis, Stanford University, CA., 351 pp.
- Gómez-Hernández, J. J., and A. G. Journel (1993), Joint sequential simulation of multi-Gaussian fields, in *Geostatistics Troia '92*, edited by A. Soares, vol. 1, 85–94, Kluwer.
- Gómez-Hernández, J. J. (2006), Complexity *Ground Water*, 44(6), 782–785.
- Guswa, A. J., and D. L. Freyberg (2002), On using the equivalent conductivity to characterize solute spreading in environments with low-permeability lenses, *Water Resources Research*, 38(8), 1132, doi:10.1029/2001WR000528.
- Guswa, A. J., and D. L. Freyberg (2000), Slow advection and diffusion through low permeability inclusions, *Journal of Contaminant Hydrology*, (46), 205–232.
- Haggerty, R., and S. M. Gorelick (1995), Multiple-rate mass transfer for modeling diffusion and surface reactions in media with pore-scale heterogeneity, *Water Resources Research*, 31(10) 2383–2400.
- Haggerty, R., S.A. McKenna, and L. C. Meigs (2000), On the late-time behaviour of tracer test breakthrough curves, *Water Resources Research*, 36(12), 3467–3479.
- Haggerty, R., and P. Reeves (2002), STAMMT-L: Solute Transport and Multirate Mass Transfer, Version 1.0, User’s Manual, *ERMS#520308*, Sandia Natl. Lab., Albuquerque, N. M.
- Harbaugh, A. W., Banta, E. R., Hill, M. C., and McDonald, M. G. MODFLOW-2000, The U.S. Geological Survey Modular Ground-Water Model-user guide to modularization concepts and the ground-water flow process, *Open-file Report 00-92*, 2000.
- Harvey, C., and S. M. Gorelick (2000), Rate-limited mass transfer or macrodispersion: Which dominates plume evolution at the Macrodispersion Experiment (MADE) site?., *Water Resources Research*, 36(3), 637–650.
- Herr M., G. Schafer, K. Spitz K. (1989), Experimental studies of transport in porous media with local heterogeneities, *Journal of Contaminant Hydrology*, 4, 113–205.

- Kullback, S. (1959), *Information of Theory and Statistics*. Wiley, New York.
- Kitanidis, P. K. (1994), The concept of the dilution index, *Water Resources Research*, 37(7), 2011–2026.
- Levy M. and Brian Berkowitz (2003), Measurement and analysis of non-Fickian dispersion in heterogeneous porous media, *Journal of Contaminant Hydrology*, 64, 203–226.
- Liu, G., C. Zheng, and S. M. Gorelick (2004), Limits of applicability of the advection-dispersion model in aquifers containing connected high-conductivity channels, *Water Resources Research*, 40, W08308, doi:10.1029/2003WR002735.
- Lu Z., and D. Zhang (2002), On stochastic modeling of flow in multimodal heterogeneous formations, *Water Resources Research*, 38(10), 1190, doi:10.1029/2001WR001026.
- Metzler, R. and J. Klafter (2000), The random walk’s guide to anomalous diffusion: A fractional dynamics approach, *Physical reports*, 339, 1–77.
- McLaughlin, D. and F. Raun, Macrodispersivity and large-scale hydrogeologic variability, *Transport in porous media*, 42(1-2), 133–144.
- Morales-Casique, E., S. P. Neuman, A. Guadagnini (2006), Non-local and localized analyses of non-reactive solute transport in bounded randomly heterogeneous porous media: Theoretical framework, *Advances in Water Resources*, 29(9), 1399–1418.
- Neuman, S. P. (1993), Eulerian-Lagrangian theory of transport in spacetime nonstationary velocity fields: exact nonlocal formalism by conditional moments and weak approximation, *Water Resources Research*, 29(3), 633–645.
- Neuman, S. P., D. M. Tartakovsky (2008), Perspective on theories of non-Fickian transport in heterogeneous media, *Advances Water Resources*, in press.
- Salamon, P., D. Fernàndez-Garcia, and Gómez-Hernández,(2007), A review and numerical assessment of the random walk particle tracking method, *Journal of Contaminant Hydrology*, 87(3-4), 277–305.
- Salamon, P., D. Fernàndez-Garcia, and Gómez-Hernández,(2007), Modelig tracer transport at the MADE site: The importance of the heterogeneity, *Water Resources Research*, 43, W08404, doi:10.1029/2006WRR005522.

- Sánchez-Vila, X., J. P. Girardi, and J. Carrera (1995), A synthesis of approaches to upscaling of hydraulic conductivities, *Water Resources Research*, 31(4), 867–882.
- Sánchez-Vila, X., A. Guadagnini, and J. Carrera (2006), Representative Hydraulic conductivities in saturated groundwater flow, *Rev. Geophys*, 44, RG3002, doi:10.1029/2005WRR000169.
- Sheibe TD, and S. Yabusaki (1998) Scaling of flow and transport behaviour in heterogeneous groundwater systems, *Advances in Water Resources*, 22(3),223–238.
- Renard P., and G. de Marsily (1997), Calculating equivalent permeability: A review, *Advances in Water Resources*, 20(5-6), 253–278
- Riva, M., A. Guadagnini, D. Fernández-García, X. Sánchez-Vila, T. Ptak (2008), Relative importance of geostatistical and transport models in describing heavily tailed breakthrough curves at the Lauswiesen site, *Journal of Contaminant Hydrology*, 101, 1–13.
- Rubin, Y., and A. G. Journel (1991), Simulation of non-Gaussian space random functions for modeling transport in groundwater, *Water Resources Research*, 27(7), 1711–1721.
- Rubin, Y. (1995), Flow and transport in bimodal heterogeneous formations, *Water Resources Research*, 31(10), 2461–2468.
- Wen, X. H., and J. J. Gómez-Hernández (1996), The constant displacement scheme for tracking particles in heterogeneous aquifers, *Ground Water*, 34(1), 135–142.
- Wen, X.-H., and J. J. Gómez-Hernández (1996), Upscaling hydraulic conductivities in heterogeneous media: An overview, *Journal of Hydrology*, 183 (1–2), ix–xxxii.
- Willmann, M., J. Carrera, and X. Sánchez-Vila (2008), Transport upscaling in heterogeneous aquifers: What physical parameters control memory functions?, *Water Resource Research*, doi:10.1029/2007WR006531.
- Zinn, B., and C. F. Harvey (2003), When good statistical models of aquifer heterogeneity go bad: A comparison of flow, dispersion, and mass transfer in connected and multivariate Gaussian hydraulic conductivity fields, *Water Resources Research*, 39(3), 1051, doi:10.1029/2001WR0



5

Conclusions and future research

5.1 General Conclusion

The hydrogeologic properties of an aquifer often exhibit high degree of spatial variability over the range of scales because of the heterogeneous nature of geologic formations. This means that to predict the behavior of flow and transport the characterization of the spatial variability is needed. Geostatistics provides the ability to characterize the spatial variation of hydrogeologic properties with high resolution. However, in hydrogeologic practice modeling, due to the high computational demands when running flow and transport at such resolution it is often necessary to reduce the dimensions of the problem. Traditionally, the flow and hydraulic head are simulated using equivalent hydraulic parameter values obtained from the analysis of aquifer tests, these parameters are assigned over various grid-blocks forming large homogeneous zones in the model. During the calibration process, these equivalent parameters are adjusted at computational block scale to reproduce the historical field measurements. In contrast, to simulate solute transport, there is a need to introduce additional equivalent parameters such as block macrodispersion, in order to reproduce the solute behaviour. We analyze different methods for solute upscaling.

The effect of the hydrogeology heterogeneity that produces an anomalous (non-Fickian) behavior, such as asymmetric plume and breakthrough curves

with large tails has been revealed through experimental data from field. In other words, transport phenomena by groundwater is very much effected by the existence the high and low water velocity zones, where the contaminant can travel quickly in direction preferential flow path or get stagnant. For this reason, the use of the classical advection-disperion equation (ADE) has questioned to model transport solute at the usual computational scale. In this framework, trying of reproduce the transport behaviour observed in the upscaled model may be impossible if only ADE is used to represent the same controlling transport mechanics at small scale.

For the reasons exposed above in Chapter 2 the task was to review the main alternatives transport approach has been proposed in the hydrogeologic literature. We focus our attention on four approach that are: Multirate mass transfer (MRMT), Time-Depend Macrodispersive (TDM), Continuous time random walk (CTRW) and Fractional Advection-Dispersion Transport (FADT). We start presenting the theoretical framework of ADE. The emphasis of this review has been place on the theoretical framework of each approach. These models provide new ways to quantify contaminant transport. However, transport problem generally requires a greater detail of heterogeneity than the flow problems.

The important issues to represent solute transport is to capture aquifer heterogeneity. The question of how to assign appropriate transport parameter values to each element or block in the numerical model has not been completely resolved. A way to resolve this issue is to use upscaling. So, the main objective in chapter 3 the developed a methodology to performance upscaling of non-reactive solute transport.

The proposed scale-up technique is based on multirate mass transfer model. Each block with heterogeneous transmissivities is replaced by a homogeneous block in which the parameters associated to a memory functions are used to represent the unresolved mass exchange between highly mobile and less mobile zones occurring within each block. Upscaling of the transmissivity is based on the Simple Laplacian with skin, whereas block transport parameters are estimated through the interpretation of the residence time distribution of particles passing through a given block during fine-scale simulations.

The new upscaling technique is evaluated using the upscaled models as a tool for upscaling solute transport in a general numerical modeling framework (chapter 3 and 4). This was achieved by comparing Monte Carlo simulations of solute transport at two different support scales. Importantly, results showed that an appropriate description of the residence time distribution for all blocks of the numerical model provides an upscaled transport model that is capable to reproduce the ensemble mean behavior of the BTCs, and also that a complete reproduction of uncertainty and dilution of plume was not provided by any of the upscaled transport models. The major drawback of the proposed

method, from practical point of view, is that it is specific to each case can be computational expensive because it requires to solve flow and transport at fine scale. This is only is possibly when running complex upscaled model to simulate a more computational demanding problem (e.g., reactive transport with many species and reactions).

5.2 Future researches

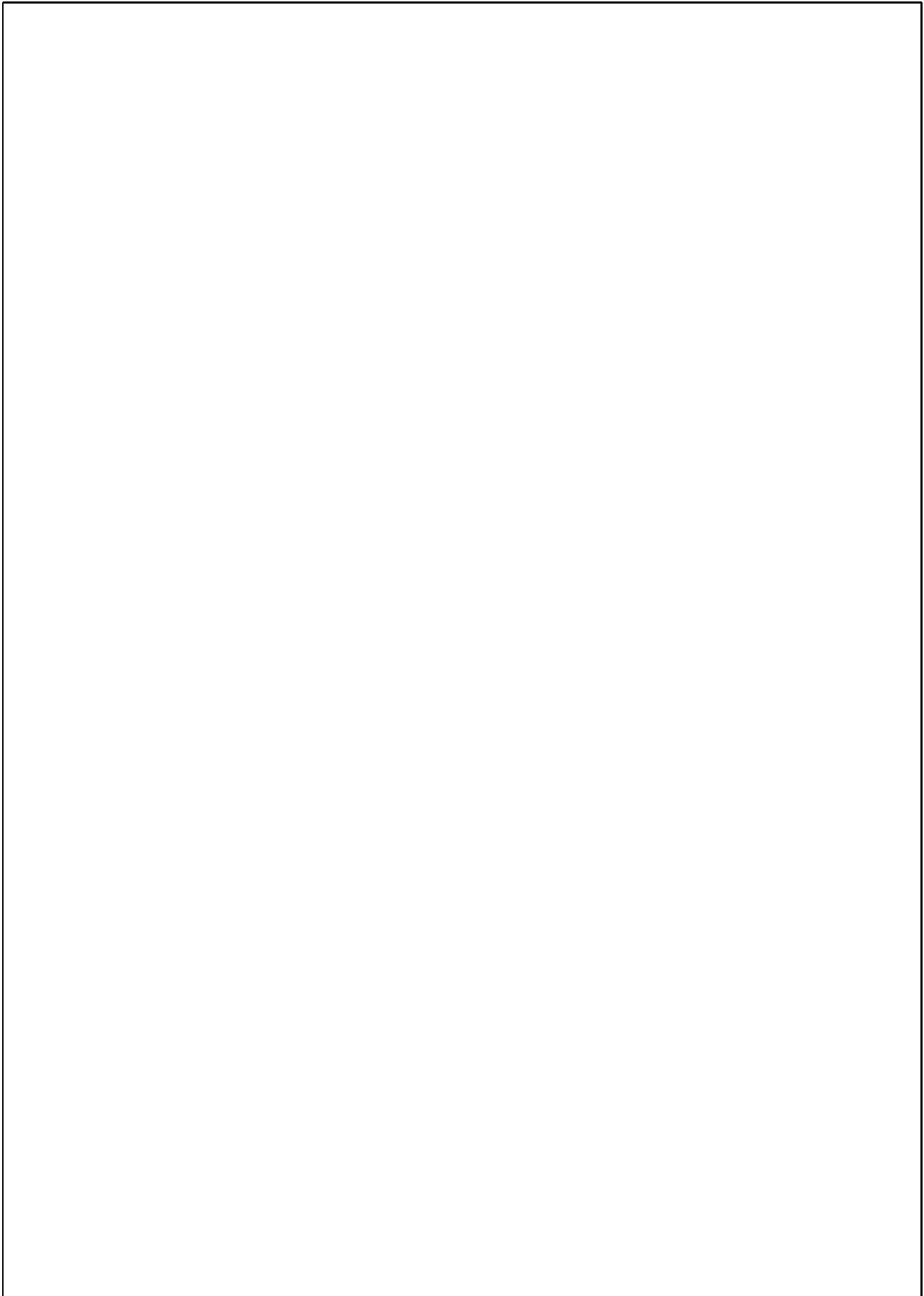
As product of task developed within this dissertation, following future studies are suggested:

The extension of the methodology to three dimension is also a important research issue. Hence, it is important to consider the possibility of improving the scale-up technique without consider the entire flow and transport solution at fine scale. To avoid solving the transport problem for the entire domain, the equations can be iteratively solved for each block over smaller support volume, which contain the block plus a "skin" region. The skin should be used to approximately reproduce flow and transport boundary conditions on the block without having to solve the transport problem for the entire domain. Further research should be carried in order to determine how large the skin should be so that resulting estimates of upscaled models are close to the calculating that would have been obtained considering the entire aquifer been used as skin. In order to account for spatiotemporal memory effects on transport, the injection of particles should be performed in the skin region. In this way particles passing through the block have already sampled the heterogeneous system nearby. Furthermore, evaluate the alternative type of injection of particles. One possibility is introduced the particles along a line proportional to fluid flux, as proposed by *Desbarats* (1990).

Furthermore, it is important to test the methodology in a real-case study. Existing well-studied tracer test that are readily available, for example, Air Force Base in Mississippi.

Bibliography

Desbarats, A. J. Macrodistribution in sand–shale sequences, *Water Resources Research*, 26(1), 153–163.



A

Calibration of Mass Transfer Parameters

This appendix describes the numerical details involved in the calibration process of mass transfer parameters. The objective function minimized by PEST included the estimates of the distribution function obtained at different times as well as the low-order temporal moments of $f_\tau(\tau)$, formally written as

$$J(\mathbf{P}) = \sum_{i=1}^{N_{obs}} \omega_i [F_\tau(t_i) - F_{\tau,m}(t_i; \mathbf{P})]^2 + \lambda_1 [\bar{\tau} - \bar{\tau}_m(\mathbf{P})]^2 + \lambda_2 [\sigma_\tau^2 - \sigma_{\tau,m}^2(\mathbf{P})]^2 \quad (\text{A.1})$$

where \mathbf{P} is a vector of parameters (see Table 3.1), N_{obs} is the number of time observations, $F_\tau(t_i)$ is the sample cumulative distribution function of residence times at time t_i . $F_{\tau,m}$ is the analytical solution (3.17), $\bar{\tau}$ and σ_τ^2 are the sample mean and variance of the residence time distribution, $\bar{\tau}_m$ and $\sigma_{\tau,m}^2$ are the analytical solutions of the mean and variance of the residence time distribution, and $\{\omega_i, \lambda_1, \lambda_2\}$ are the weights of the observations, mean and variance of the residence time. The number of estimated parameters depends on the selected upscaled mass transfer model. The analytical solution of the mean and variance of the residence time distribution can be easily obtained from (3.17) as

$$\bar{\tau}_m(\mathbf{P}) = - \lim_{p \rightarrow 0} \frac{d\bar{f}_\tau(p)}{dp} = \frac{L_b}{v_m} (1 + \beta) \quad (\text{A.2})$$

$$\sigma_{\tau,m}^2(\mathbf{P}) = \lim_{p \rightarrow 0} \frac{d^2 \ln \bar{f}_\tau(p)}{dp^2} = \frac{2A_\ell}{v_m^2} (1 + \beta)^2 L_b + \frac{2L_b}{v_m} \beta \int_0^\infty \frac{f(\alpha)}{\alpha} d\alpha \quad (\text{A.3})$$

These results are consistent with the temporal moment analysis conducted by *Lawrence et al.* (2006).

Bibliography

Lawrence, A. E., X. Sanchez-Vila, and Y. Rubin, Conditional moments of the breakthrough curves of kinetically sorbing solute in heterogeneous porous media using multirate mass transfer models for sorption and desorption, *Water Resources Research*, 38(11), 1248, doi:10.1029/2001WR001006, 2002.

